The Electronic Structure of Distorted Porphyrins and Cobalt Schiff Base Derivatives as Novel Enzyme Inhibitors

Thesis

Submitted by

Toshihiko Takeuchi

In Partial Fulfillment of the Requirements

for the Degree of Doctor of Philosophy in Chemistry

Division of Chemistry and Chemical Engineering

California Institute of Technology

Pasadena, California

1996

(Submitted January 19, 1996)

Acknowledgments

I am most grateful for the freedom that I was given by my advisors, Harry Gray, Bill Goddard, and Tom Meade, to pursue the research that was of interest to me. The guidance and training given to me by my advisors has instilled a sense of confidence in my future scientific pursuits. I would have accomplished little in my graduate career without the assistance of Rick Muller, Julia Hodge, Maureen Hughes, Faiz Kayyem, Gary Mines, and Jack Mizoguchi. These people have been wonderful teachers and have been patient with me while I asked numerous questions regarding the research that I was performing. I'd like to thank Arnd Böttcher and Kevin Hoke who have been extremely helpful and fun to work with on the Redox project. I have had many fruitful collaborations and would like to thank Mel Simon, Siddharth Dasgupta, John Shellnut, Cather Simpson, David Christianson, Laura Scolnick, and the SURFs that I've been associated with for all the helpful discussions and assistance with my work. I also give my thanks to Mary Flowers for all of her help in keeping the Meade and Fraser laboratories running smoothly. I would like to thank the DOD, Redox Pharmaceuticals, Sun, and the DOE for funding.

Outside of the laboratory, my life was not standing still, and I gratefully acknowledge the guidance of Alan Gross, Delores Bing, Paul Stein, and Ron Chapman for helping me become a better musician and person. I have had many wonderful times playing tennis, and I am grateful for the friendship and company of Don Low, my long standing doubles partner, Jack Mizoguchi, Mark McCluskey, Eva Birnbaum, Wayne Larson, Eric Stemp, Jay Labinger, and Harry Gray, whose kindness and generosity is unsurpassed. I thank Jerome Claverie, my musical partner in chamber music, Dian Buchness, Jamie Schlessman, Tracey Fu, Dan Hall, Bob Gutzmann, Karl Irikura,

Kazunori Yasuda, Jeff Aragaki, Jordan Kaplan, Rob Knopp, Geoff Burr, Natalia Colocci, Sabrina Yadzpour, and Julian Chen for all of the wonderful times we've had in making music. I've had lots of fun on the softball field with Rudy Rico and Tim Herzog, who were also great roomates, Tom Meade, whose friendship and gall bladder will always be remembered, Gary Mines, Kara Bren, Bill Connick, Debbie Wuttke, Jim Bailey, Julia Hodge, Maureen Hughes, Andy Kiely, Brent Flatt, Vinny Miskowski, Jorge Colon, Jay Winkler, Mike Hill, Torbjorn Pascher, Kevin Hoke, Arnd Böettcher, Hans Nikol, Mark Grinstaff, Ben Ramirez, Elizabeth Krider, Bob Terbuggen, Ai-Ching Lim, Suzanne Lin, Tim Johann, and Michelle Arkin. I thank Rick Muller, Erik Bierwagon, Jason Perry, Hiroshi Yamamoto, Kevin Plaxco, KT Lim, Terry Coley, Jamil Tahir-Kheli, and Abner Mintz for wonderful times with the Goddard group. I thank Faiz Kayyem, Rex Moats, Andrea Staubli, Angie Louie, Ofer Blum, and Tom Welch in the Meade group for their friendship and support. I thank my parents for all of their support throughout the years. I appreciate all the sacrifices that were made to further my education. Finally, I am grateful for all the love and encouragement that Yonchu Jenkins has given me.

Abstract

Halogenated porphyrins, which are catalysts for the oxidation of alkanes, were studied by semiempirical AM1 calculations. The calculations predicted the effects of halogenation of the porphyrin ring on UV-visible absorption spectra and electrochemical data. Predictions regarding the stability of catalysts were made, and have been experimentally verified. INDO/S semiempirical calculations were performed on a series of porphyrins to understand the effects of a highly disfavored distortion that is conserved in cytochromes *c*. The highest occupied molecular orbitals were destabilized, and the orbital energy of the metal and the lowest unoccupied orbitals change, causing a shift in the redox potential of the heme and a change in the electron transfer properties of cytochromes *c*.

In order to delineate the anti-enzymatic properties of Co(acacen) derivatives, which are potent inhibitors of the herpes virus, carbonic anhydrase (CA), thermolysin (TL), and thrombin (TH) were chosen as targets. Inhibition of CA occurs upon incubation with the novel water-soluble Co(II)hydroxypropylacacen (Co(II)hpr) but not with $[Co(III)hpr(NH_3)_2]^+(OAc)^-$. The difference in reactivity of the species is a consequence of the steric limitations imposed by the axial ligands bound to the Co(III) complex. $[Co(III)acacen(NH_3)_2]^+$ irreversibly inhibits TL, and this inhibition was prevented by binding a strong reversible inhibitor to the active site of the enzyme before addition of the cobalt species, suggesting that cobalt-acacen derivatives can inhibit enzymes by binding to active site histidines. In an effort to develop more potent and selective enzyme inhibitors, active site-directed peptides were coupled via a peptide bond through a carboxylic acid, which is part of the acacen ligand framework. The peptide coupled derivatives rapidly and irreversibly inhibited TH, and the potency of inhibition was over an order of magnitude better than the uncoupled components.

Table of Contents

List of Figures

List of Tables

Chapter 1. Introduction to the UV-visible Spectroscopy of Porphyrins and the Chemistry of Co(III) Schiff Base Complexes

Introduction to Porphyrin UV-visible Spectroscopy

Porphyrins are remarkable in that they are involved in a wide variety of catalytic reactions, including light harvesting by chlorophyll, electron carrying in photosynthesis and respiration by cytochromes, oxygen transport by hemoglobin/myoglobin, and mediation of the transformation of dioxygen to water by cytochrome-oxidase.[1] Porphyrins are able to display this wide range of reactivity because the electronic properties of the porphyrin can be easily varied. These properties are altered by changing the substituents at the periphery of the ring, incorporating a different metal into the core of the porphyrin, and changing the axial ligands bound to the metal. Figure 1.1 shows a generic metalloporphyrin.

Another means of modulating the electronic properties of porphyrins is through distortion of the macrocycle from the planar geometry. Ring distortion can occur in order to relieve unfavorable steric interactions between the substituents of the porphryin periphery, but the distortion also disrupts the extended p-conjugation throughout the porphyrin macrocycle, causing a change in the electronic structure of these porphyrins. Two main classes of porphyrin distortion will be discussed: saddling distortions and ruffling distortions. Saddling distortions are porphyrin distortions that occur along the pyrrole groups, whereas ruffling distortions occur along the *meso* positions of the porphyrin (Figure 1.2).

One class of porphyrins that are known to undergo saddling distortions are the β-halogenated porphyrins. These β-halogenated porphyrins are of great interest due to their ability to catalyze the oxygenation of alkanes.[2] For example, chloro[tetrakis(pentafluorophenyl)-β-octabromoporphyrinato]iron (III) (denoted $ClFeTFPPBr_8$) catalyzes the room temperature conversion of isobutane to *tert*-butyl alchohol in the presence of oxygen at a rate of 190 moles of product per mole catalyst per

Figure 1.1. A Generic Metalloporphyrin. B represents a β-pyrrole substituent, m represents a *meso* substituent, and M represents the metal.

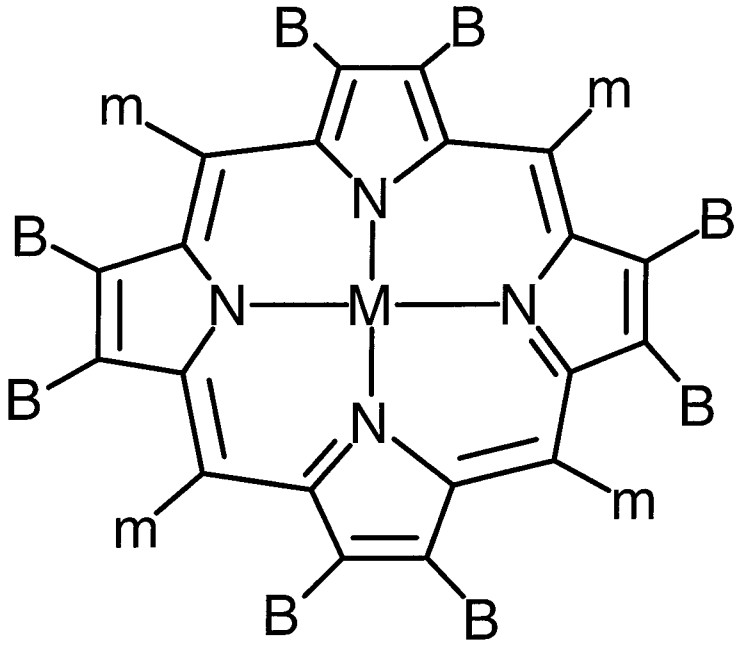

Figure 1.2. Porphryin Distortions. Porphyrins with bulky pyrrole substituents will tend to saddle, while porphyrins with bulky *meso* substituents will ruffle. Pictured below is a molecular model from the crystal structure of Ni(II)β-octabromo-tetrakis(pentafluorophenyl)porphyrin (saddled structure) and a representation of Ni(II)*meso*-tetra(*tert*-butyl)porphyrin (ruffled structure) based on molecular modeling calculations.

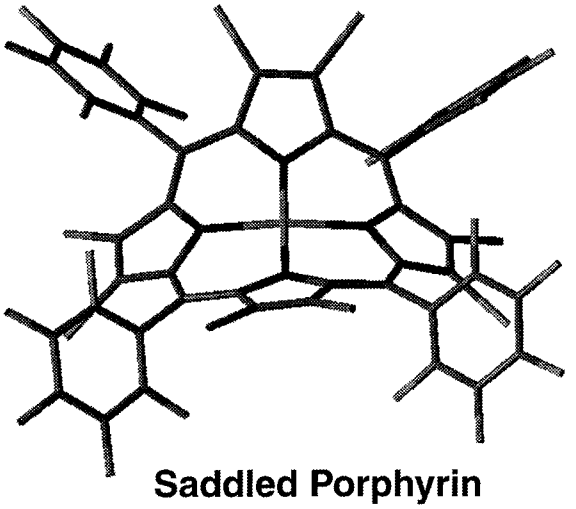

Saddled Porphyrin

Ruffled Porphyrin

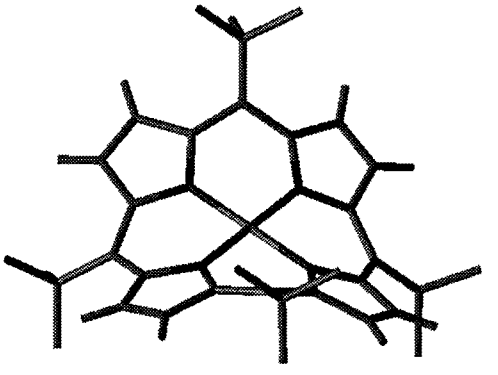

hour with over 90% selectivity to the alcohol. Remarkably, this activity is unchanged after 74 hours.[2c]

Because there is a general correlation of catalytic activity with halogen content, Lyons and Ellis suggested that electron withdrawal from the ring enhances the reactivity of these iron porphyrins.[2c] Halogenation causes large changes in both the *geometric structure* (leading to highly non-planar porphyrins) and in the *electronic structure* (shifts in both the Q and Soret absorption bands). Understanding the nature of these changes in geometric and electronic structure may give insight into the reactivity and catalytic activity of these halogenated porphryins, guiding the synthesis of future generations of catalytic porphryins.

Ruffling distortions are highly conserved among a wide variety of mitochondrial cytochromes *c*,[3] despite the fact that this distortion is energetically unfavorable.[4] Since these nonplanar distortions can alter the chemical and photophysical properties of porphyrins, it is possible that protein-controlled ruffling of the heme in cytochrome *c* provides a mechanism by which the tertiary structure of the surrounding protein can regulate heme reduction potentials. Nickel (II) *meso*-tetrasubstituted porphyrins become increasingly ruffled as the size of the *meso* substituents increase. These increasingly ruffled porphryins can serve as a useful model system for characterizing the changes in the electronic structure of porphyrins as ruffling occurs.

Probing Changes in Porphyrin Electronic Structure

In order to probe the changes in electronic structure caused by changes in the porphyrin geometry, the nature of the frontier orbitals, which include the highest occupied molecular orbital (HOMO) and the lowest unoccupied molecular orbital (LUMO), must be understood, since these are the orbitals through which the porphyrin displays its reactivity. An understanding of the frontier orbitals will necessarily give a firm foundation for understanding porphyrin reactivity.

One of the best experimental probes of the frontier orbitals is through absorption spectra. At the simplest level, absorption spectra consist of transitions from the HOMO to the LUMO, HOMO to the SLUMO (S=second), SHOMO to the LUMO, etc. Since absorption spectra involve transitions among the frontier orbitals, understanding the absorption spectra would assist in understanding the electronic structure, and thus, the reactivity of the molecule. Typical porphyrin spectra are shown in Figure 1.3.

Understanding Porphyrin Absorption Spectra

The standard model for the interpretation of porphyrin spectra is the Four Orbital Model (FOM) proposed by M. Gouterman in 1961.[5] This model is a method of correlating the orbitals derived from simple Hückel calculations. Changes in the porphyrin absorption spectra with respect to substitution are rationalized with respect to changes in these four orbitals. This model involves two nearly degenerate MOs (b1 and b2 with b_{1u} and a_u symmetries in D_{2h}) occupied in the ground state (HOMOs) and two nearly degenerate MOs (c1 and c2 with b_{3g} and b_{2g} symmetries in D_{2h}) unoccupied in the ground state (LUMOs). These four orbitals are shown in Figure 1.4 for the simplest porphyrin porphine.

Thus the ground state $(b1)^2(b2)^2$ and the excited states are defined in terms of the transitions:

$$\left.\begin{matrix} Q_x \\ B_x \end{matrix}\right\} = [(b1c2)\pm(b2c1)] \qquad (1)$$

$$\left.\begin{matrix} Q_y \\ B_y \end{matrix}\right\} = [(b1c1)\pm(b2c2)] \qquad (2)$$

where Q_x, Q_y correspond to the visible bands and B_x, B_y correspond to the Soret bands (See Figure 1.3).

Figure 1.3. Typical Porphyrin UV-visible Absorption Spectra. The UV-visible absorption spectra of tetra(pentafluorophenyl)porphine is shown in spectrum a). The two bands at lower energy are the Q_x and Q_y bands, and the band at higher energy is the Soret band. The spectra of zinc(II)(tetra(pentafluorophenyl)porphyrin) is shown in spectrum b). The Q_x and Q_y bands are degenerate, so only one band at lower energy is seen.

a)

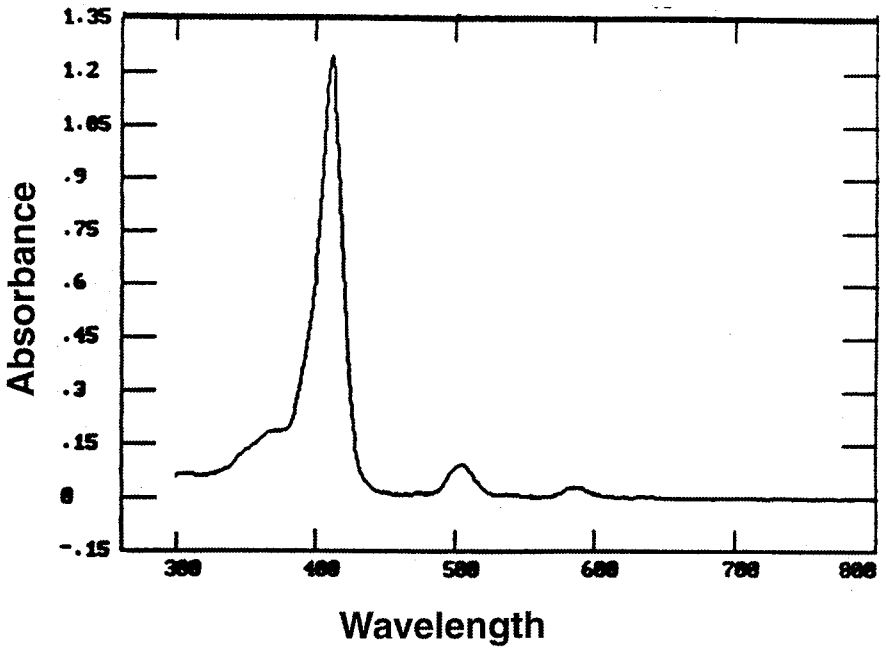
1.35
1.2
1.05
.9
.75
.6
.45
.3
.15
0
-.15
Absorbance
300
400
500
600
700
800
Wavelength

b)

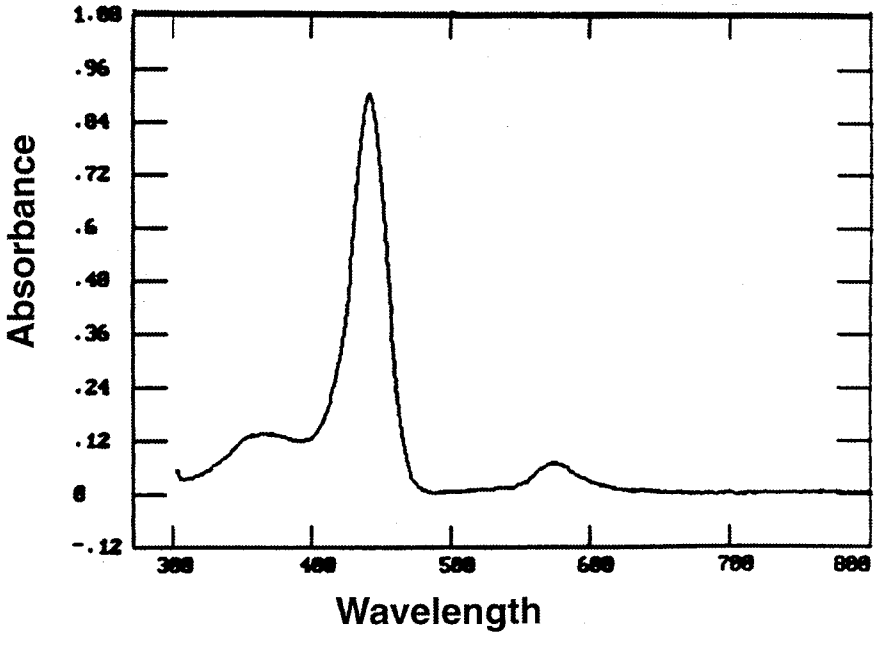
1.08
.96
.84
.72
.6
.48
.36
.24
.12
0
-.12
Absorbance
300
400
500
600
700
800
Wavelength

Figure 1.4. The Four Orbitals of Porphine.

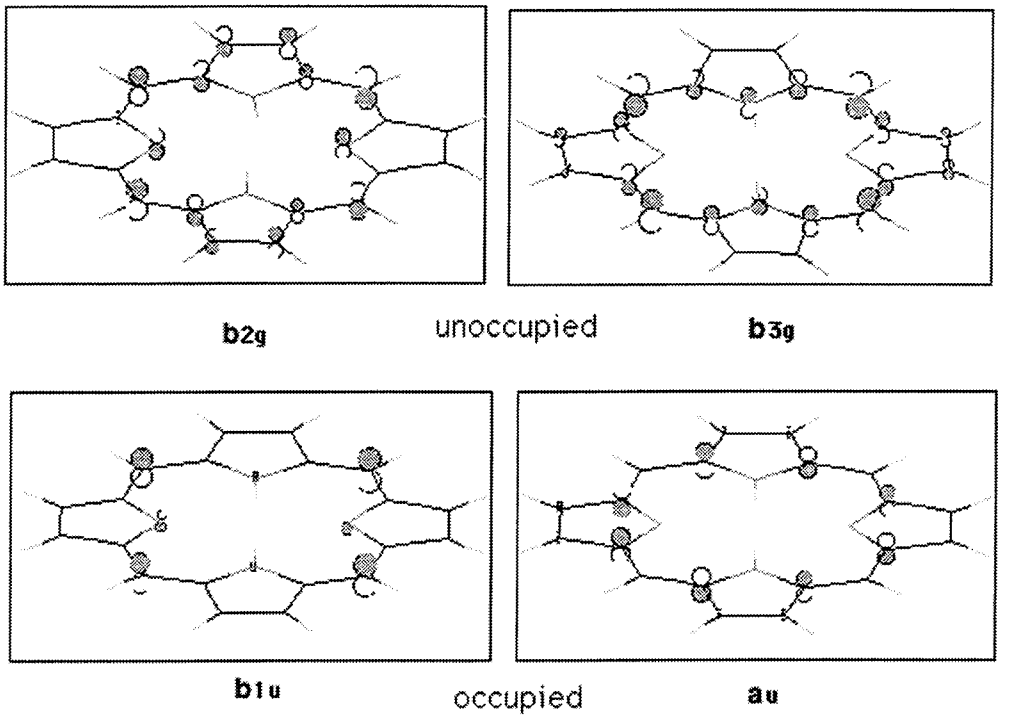

The porphyrin absorption spectra can be determined experimentally using UV-visible spectroscopy, and these absorption spectra can also be predicted using calculational techniques. Semiempirical molecular orbital methods are well suited for studying porphyrins, since the large size of the porphyrin framework makes it less tractable for more rigorous *ab initio* calculational methods. The use of AM1 and INDO/S semiempirical calculations and UV-visible spectroscopy for the characterization of highly distorted ruffled and saddled porphyrins will be described in chapters 2 and 3.

Introduction to the Chemistry of Cobalt Schiff Base Chelate Complexes

One of the major problems with the use of inorganic compounds as pharmaceuticals is the toxicity of metals. Heavy metals such as mercury and lead are notorious for their toxicity, and other metals such as nickel, chromium, and cadmium are known to be carcinogenic in humans and in animals. Even essential elements such as iron are toxic in higher dosages; the accidental ingestion of iron supplemental tablets by children is a common cause of poisoning. This problem in toxicity has left most of the attention focused on the development of organic compounds as drugs.[6]

Despite these deleterious effects of metals, there are several cases in which inorganic compounds have been successful in the treatment of disease. For example, Ehrlich's 606th arsenic compound provided a treatment for syphilis, gold cyanide was effective for tuberculosis, and antimony compounds are effective in treating the parasitic disease leishmaniasis.[7] Other examples include the use of zinc to promote healing of wounds, the use of silver to prevent infection in burn patients, and the use of copper carboxylate complexes as anti-inflammatory, antiulcer, and analgesic agents.[6] Two of the most successful drugs based on metals are platinum-based cisplatin, and gold-based auranofin shown in Figure (1.5). Cisplatin is used to treat genitourinary and head and neck tumors, while auranofin is used to treat rheumatoid arthritis.

Figure 1.5. Structures of Cisplatin and Auranofin. Cisplatin a) is used to treat genitourinary and head and neck tumors, while auranofin b) is used to treat rheumatoid arthritis. These two compounds are the most successful metal-based drugs.

a)

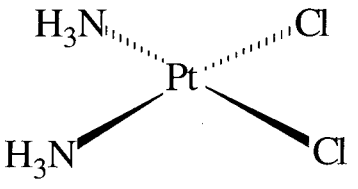

b)

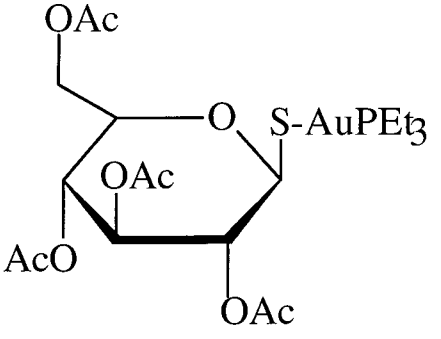

Cisplatin (Figure 1.5) is a paradigm for metal-based pharmaceuticals. The use of cisplatin results in long term survival for more than 90 percent of testicular cancer patients. Extensive mechanistic work suggests that the mode of action is the binding of these platinum complexes to DNA, causing a kinking in the DNA helix. This kinking of the DNA by the platinum compounds is not repaired by enzymes in tumor cells, resulting in an inhibition of cell replication. Detailed understanding of the mechanism of the anticancer activity is leading towards new generations of platinum drugs that show greater activity, decreased toxicity, and improved drug delivery.[13]

Unfortunately cisplatin is the exception among inorganic drugs, and relatively little is known about the mechanism of action or the targets for most of the other metallopharmaceuticals. For example, gold compounds have been used since 1929 for the treatment of rheumatoid arthritis, but the mode of action is still largely unknown. If a greater understanding of the mechanism and target sites of inorganic drugs is achieved, then progress may be made in the rational development of more potent and less toxic metal-based drugs.

It was recently discovered that cobalt (III) complexes of N,N'-ethylenebis(acetylacetoneimine) [acacen] (Figure 1.6) are effective antiviral agents against the herpes simplex virus type 1 (HSV-1) when applied to severe cases of epithelial and stromal keratitis in the rabbit.[8] Although the mechanism for the antiviral activity of these complexes is not yet known, these cobalt complexes may be inhibiting an enzyme that is crucial to the replication of the virus; if the mechanism is anti-enzymatic, then these cobalt compounds may be generally applicable towards a wide variety of problems.

One possible mechanism for the inactivation of enzymes with cobalt(III)acacen derivatives would be the binding of these complexes to active site residues that are crucial to enzyme activity. Since these cobalt complexes have an affinity for strong nitrogenous

Figure 1.6. Structure of Cobalt(III) Complexes of Acacen Derivatives. Complexes of [Co(III)(acacen)X_2]Y (A = methyl, B = H, X = NH_3, 2-methylimidazole, Y = Cl^-) were found to be effective inhibitors of the herpes simplex virus.

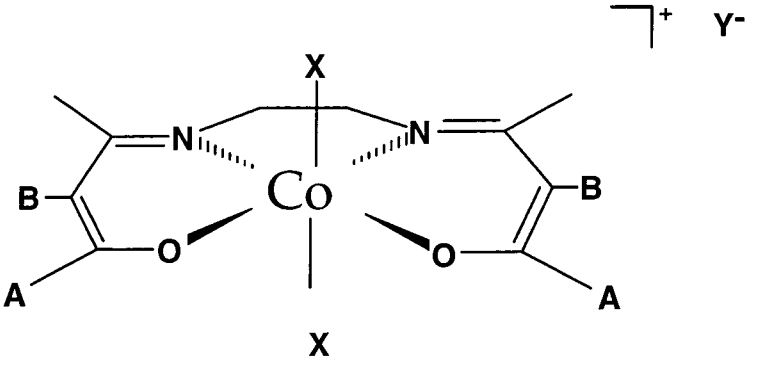

donors, they should irreversibly bind to the imidazole moiety of histidine residues. Free histidines are essential to the catalytic activity of a variety of enzymes such as serine proteases, cysteine proteases, and RNases,[9] and so the Co(III)acacen derivatives should bind to active site histidines and inhibit the catalytic activity of these enzymes. The second part of the thesis focuses on defining the inhibition of enzymes containing active site histidines. In these initial studies, carbonic anhydrase, thermolysin, and thrombin have been chosen as target enzymes for the Co(acacen) complexes.

Ligand Substitution Processes

Since the coordination sphere about $[Co(III)(acacen)L_2]^+$ is saturated, in order to achieve binding of the species to a target enzyme, it is necessary for a ligand exchange process to occur. Substitution reactions are generally classified as having a dissociative or associative mechanism. For the dissociative mechanism, the rate determining step is the loss of a ligand, forming a transient five-coordinate complex, followed by rapid binding of the incoming ligand. For the associative mechanism, the rate determining step is the association of the incoming ligand, forming a seven-coordinate species, with rapid loss of the leaving group to form the six-coordinate product. The associative mechanism is unfavored in octahedral complexes due to the steric crowding about the coordination sphere and lack of suitable orbitals for the bonding of incoming ligands. Indeed, most of the data available for the ligand exchange of octahedral complexes is consistent with the dissociative mechanism.[10] One mechanism of enzyme inhibition is the dissociation of an axial ligand to form a five coordinate intermediate, followed by binding to an enzyme active site ligand (Figure 1.7).

Although cobalt (III) complexes are generally inert to ligand substitution,[9] previous work by Fujii[11] has shown that Co (III) acacen complexes can be formed with amino acids as axial ligands (aliphatic amino acids and phenylalanine were studied), and these amino

Figure 1.7. Proposed Ligand Substitution Mechanism for Enzyme Inhibition. The first step in the proposed mechanism involves the loss of one axial ligand via a dissociative mechanism in order to form a five-coordinate intermediate. This intermediate can irreversibly bind to an enzyme histidine; if the histidine is essential to the catalytic activity of the enzyme, then inhibition of enzyme activity should occur.

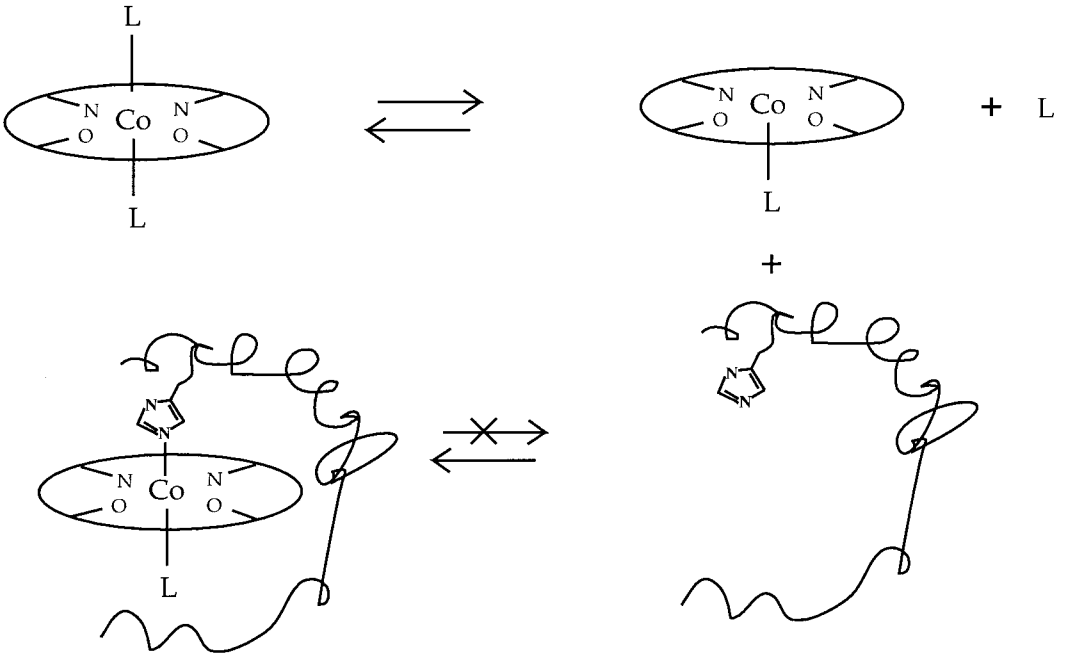

acids bind exclusively through the amine and not the carboxylate. Fujii further showed that ligand exchange of these amine complexes were facile and easily observable using NMR, which showed the presence of free amino acids and other equilibrium mixtures of the amino acid-cobalt acacen complexes. Although amine dissociation is a facile process, the interaction of the cobalt complex with imidazoles and histidines is much more inert to substitution. Previous studies have shown that $[Co(acacen)(NH_3)_2]^+$ binds to apomyoglobin and metmyoglobin at a stoichiometry of 6:1; NMR and UV-visible spectroscopic data suggest that this binding occurs to enzyme histidines.[12] This thesis extends this work by focusing on the binding to histidines as a means of inhibiting enzymes.

Redox Triggered Ligand Loss

Although axial ligand substitution in cobalt (III) acacen complexes is relatively slow, this exchange process is greatly labilized upon reduction to the corresponding cobalt (II) complex. The loss of axial ligands frees up two coordination sites and greatly reduces the steric bulk of the complex, since Co(II)acacen is essentially planar. Furthermore, the Co(II)acacen complex becomes much more hydrophobic and may readily target the lipophilic interior of enzymes due to the loss of charge. ($[Co(III)(acacen)(NH_3)_2]^+$ is positively charged, whereas the corresponding [Co(II)(acacen)] is neutral.) These differences in the properties of the cobalt(III) versus cobalt(II) complexes should allow the targeting and inhibition of certain enzymes with the cobalt(II) complex, while no inhibition is observed with the corresponding cobalt(III) complex. These ideas are summarized in Figure 1.8. The work with carbonic anhydrase (CA) as a model enzyme is presented later in this thesis. In that section it is shown that a Co(II) acacen derivative can target CA, while the corresponding $[Co(III)(acacen)(NH_3)_2]^+$ derivative does not affect CA.

Figure 1.8. Scheme for Redox Triggered Enzyme Inhibition. a) The initial cobalt (III) complex is sterically bulky due to the slow exchange of axial ligands, preventing the binding to the enzyme active site. b) Reduction to cobalt (II) greatly labilizes the ligand substitution process, resulting in a complex that is essentially planar. The increased hydrophobicity due to the neutralization of charge coupled with the loss of steric bulk allows the cobalt complex to target the enzyme active site. c) Binding to enzyme histidines results a large shift in the redox potential, facilitating oxidation to a very stable, irreversibly bound cobalt (III) complex.

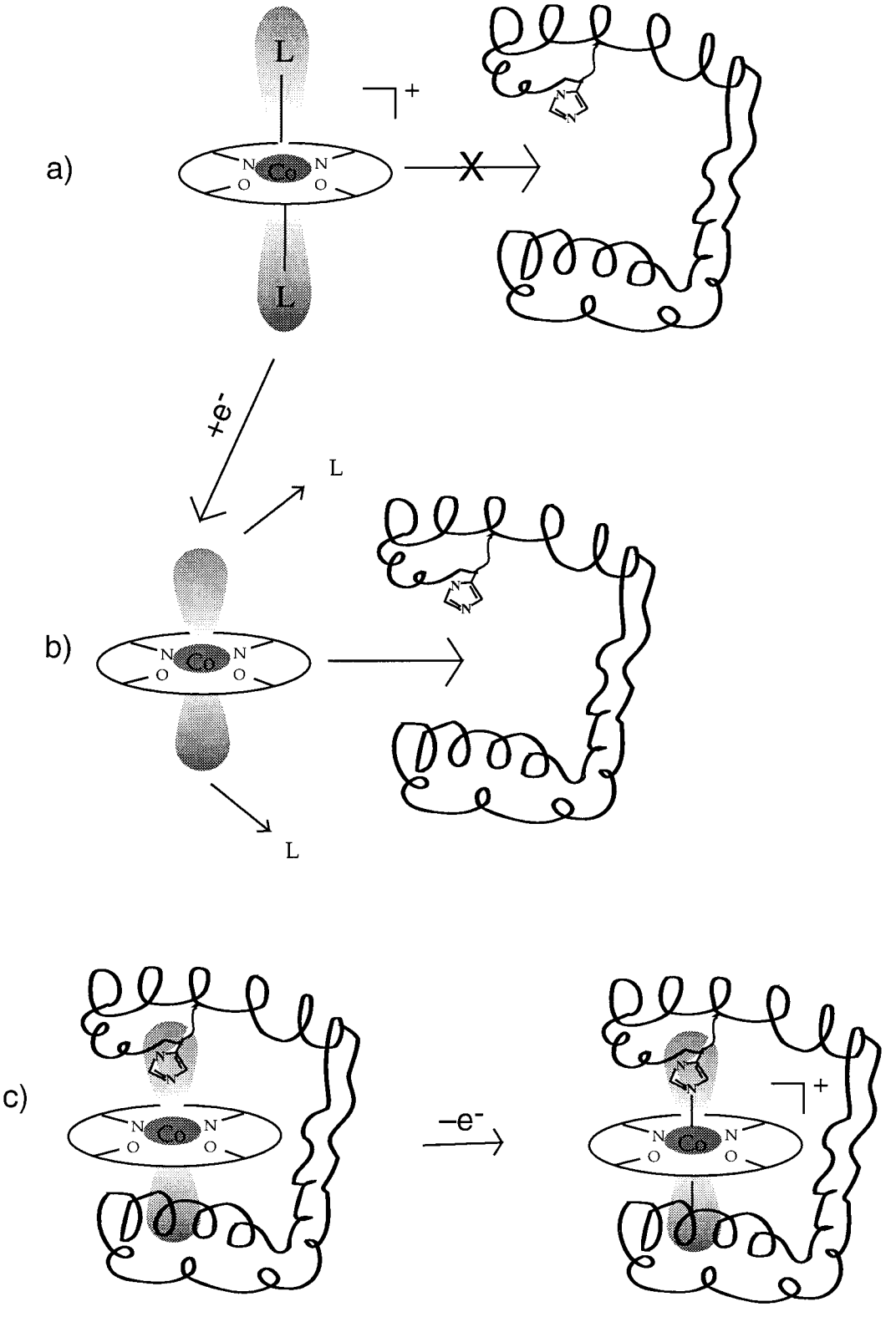
a)
L
Co
N
O
L
+
+e-
L
b)
L
c)
−e-
+

UV-visible Spectroscopy of [Co(III)(acacen)X_2]Y Complexes

In order to understand the reactivity and the changes in electronic structure that occur through the change in the axial ligand and changes in the periphery of the acacen ligand, it is important to have a firm understanding of the UV-visible spectroscopy and the electrochemistry, which is presented in the following section. Although systematic investigations of UV-visible spectra of [Co(III)(acacen)X_2]Y have not been carried out in great detail, there are reports of UV-visible solution spectra for some Co(III) acacen complexes (Marcu *et al.*, 1989; Abdel Salam El Absy *et al.*, 1982; Costa, G. *et al.*, 1966).[13,14] The free ligand H_2acacen shows an intense band with two maxima at 305 and 323 nm (ε = 30000 $M^{-1}cm^{-1}$),[12c] which is split due to the electrostatic coupling of two interacting chromophores (Larsen, 1969).[15] A transition at higher energy occurs at 196 nm (ε = 7800 $M^{-1}cm^{-1}$). The bands at lower energy can be attributed to π-π^* transitions within the azomethine chromophore, while the band at higher energy arises from transitions within the extended conjugated system of the ligand.

The electronic absorption spectra of the cobalt(III) complexes are red-shifted about 30 to 50 nm with respect to the free ligand. Intense intraligand transitions of the conjugated ligand system occur between 218 and 260 nm (ε = 15000-30000 $M^{-1}cm^{-1}$). Some of the observed bands are partially superimposed by π-π^* transitions of the aromatic systems of complexes containing either pyridine or imidazole derivatives as axial ligands. The most prominent feature of the studied Co(III) complexes in the visible region is the band with a maximum between 340 and 378 nm (ε = 6500 to 16600 $M^{-1}cm^{-1}$) in acetonitrile solution. In aqueous solution this band is shifted to higher energies by about 5 to 12 nm. This band can be assigned to the first π-π^* intraligand transition of the complexes. The axial ligand does not have significant influence on the position of this band, but it is greatly influenced by the substitution pattern on the equatorial ligand. Substitution of H by Cl in position B of

the complexes (see Figure 1.6) shifts the band to higher wavelengths. These shifts in energy further support the assignment as a ligand-based transition.

There is also a band between 400 to 450 nm, which generally appears as a shoulder in most of the complexes, that is significantly influenced by the axial ligands X. The energy of this transition decreases in the order NH_3 > Im > N-MeIm > 2-MeIm > py (A=Me). The great influence of the axial ligand upon the transition energies suggest that these transitions are d-d bands. The shift in the energy of this transition can be used to monitor the exchange of axial ligands from X = NH_3 to X = Im, as an example. Since monitoring the exchange of ammonia to imidazole models the binding of [Co(acacen)$(NH_3)_2$]Cl to enzyme histidines, understanding the kinetics of the ligand substitution process in the model X = NH_3 to X = Im system will help in the interpretation of enzyme inhibition kinetics. The absorption spectra of [Co(acacen)$(NH_3)_2$]Cl and [Co(acacen)$(Im)_2$]Cl are shown in Figure 1.9.

Electrochemical Investigations of Co(acacen) Derivatives

Since it is possible to target enzymes with Co(II) acacen derivatives where Co(III) acacen derivatives have no effect, the reduction of Co(III) complexes to Co(II) complexes may serve as a redox trigger for the activation of enzyme inhibitors. This trigger may be exploited within tumor cells, which are often lacking in oxygen due to high metabolism and low blood supply within the tumor. This lack of oxygen can make reductive reactions more favorable in tumor cells compared with normal, healthy cells.[16] If the potential of the Co(III/II) redox couple is tuned to a region where reduction to the Co(II) complex occurs only in tumor cells and not in healthy cells, then these cobalt complexes could be used as a drug for the selective targeting of tumor cells. However, before this trigger can be exploited within tumor cells, it is necessary to obtain a thorough understanding of the redox properties of Co(acacen) derivatives.[13]

Figure 1.9. UV-visible Absorption Spectra of [Co(acacen)(NH_3)$_2$]Cl and [Co(acacen)(Im)$_2$]Cl. Changing the ligand from ammonia (NH_3) to imidazole (Im) has little effect upon the absorption band at ~338 nm. However, there is an increase in the absorption at 420 nm. This increase in absorption can be used to monitor the change in axial ligand from NH_3 to Im in model studies of the ligand substitution process.

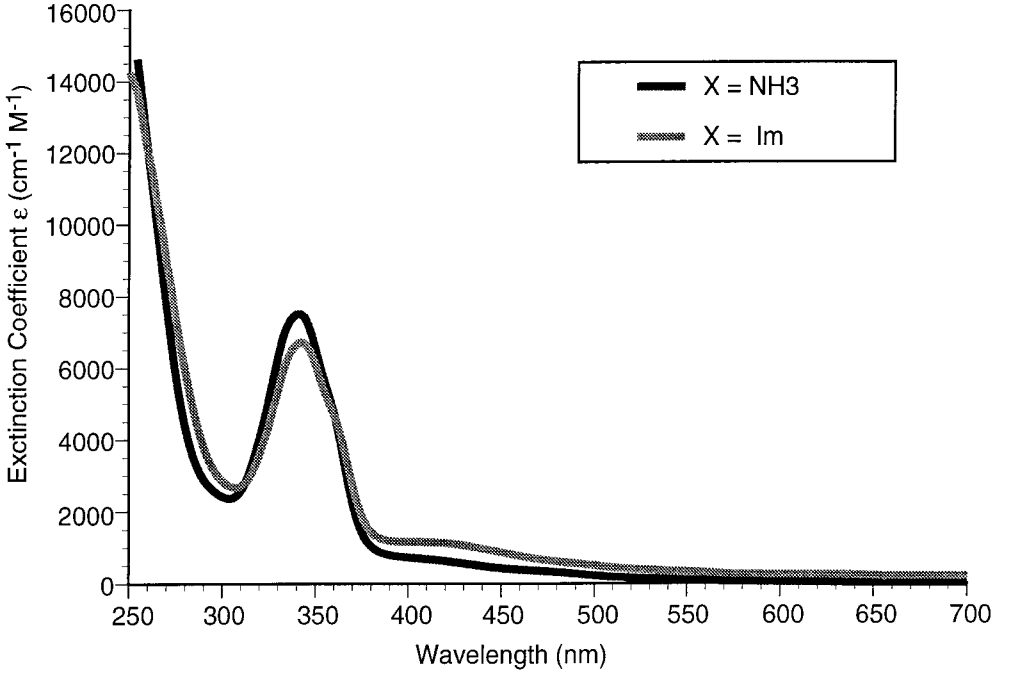

Although there are electrochemical studies on several Co(II)acacen derivatives[17] and Co(III)acacen complexes in strong donor solvents (e.g., pyridine),[18] the electrochemistry of the corresponding Co(III) analogues in weakly coordinating solvents and the relationship between the redox chemistry and axial and equatorial ligand substitution effects has been studied only recently in greater detail.[13]

Figure 1.10 shows a typical cyclic voltammogram of a Co(III)acacen complex in the potential range from + 0.7 to - 2.1 V (vs. Ag/AgCl) in acetonitrile solution. A scan initiated in the negative direction at 0.0 V reveals a first irreversible reduction wave at ca. - 0.8 V, which is due to the process $[Co(III)L(X)_2]^+ + e^- \longrightarrow [Co(II)L] + 2\ X$. Upon reduction, the Co complex loses its axial ligands in weakly coordinating solvents, since the electron is added to the antibonding dz^2 orbital perpendicular to the equatorial ligand plane.[19] Upon further reduction a second, well defined reversible process at ca. - 1.6 V is observed with about unit ratio of anodic to cathodic peak currents (i_{pa}/i_{pc}), corresponding to the simple one-electron process $[Co(II)L] \Leftrightarrow [Co(I)L]^-$.

After reversal of the scan direction, the Co(II) complex is reoxidized to Co(III) at much higher potential (ca. + 0.2 V). This oxidation is more difficult because there is no strong axial ligand available in sufficient amount at the electrode to form a species [Co(II)(L)X]. This leads to a decrease in the electron density on the metal and an increase in the oxidation potential. After oxidation, the hexacoordinate species $[Co(III)L(X)_2]^+$ is formed again in a fast consecutive reaction, since upon scan reversal and repetition of the cycle, reduction occurs at the same potential as observed in the first cycle. Multiple scans result in nearly superimposable cyclic voltammograms, which indicates the marked stability of the three oxidation states of cobalt observed in the study. These studies show that reduction of the cobalt(III) complex results in the rapid loss of ligands, which could be a viable mechanism for the activation of inert Co(III) complexes as described in Figure 1.9.

Figure 1.10. Cyclic Voltammogram of [Co(3-Cl-acacen)$(NH_3)_2$]Cl. The cyclic voltammogram was performed in acetonitrile at 293 K using v = 100 mV/s.

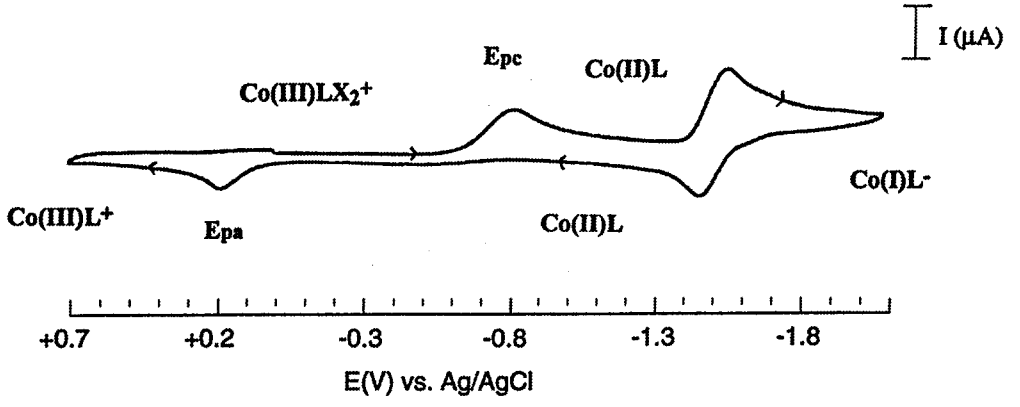

Furthermore, the electrochemical experiments suggest that the cobalt complexes are robust and stable and will not degrade after multiple cycles of reduction and oxidation.

Since the redox chemistry of $[Co(III)(acacen)X_2]^+$ is not in the physiological range, it is important to obtain an understanding of the shifts in the Co(II/III) couple upon substitution of the acacen framework and changes in the axial ligand. The reduction potentials obtained for a variety of acacen derivatives are shown in Table 1.1. The observed anodic peak potentials I_{pa} for the reduction process Co(III) —> Co(II) differ by almost 400 mV depending upon the nature of the axial ligand. This redox potential is qualitatively related to the ligand field strength (σ-donor strength, Lewis basicity) of the axial ligand; the electron affinity of the Co(III) complex decreases with increasing pK_a of the Lewis base in the axial positions.[20] The more positive potential of the complex with X = 2-MeIm (complex 12) compared with X = Im (complex 7) with the less basic axial ligand can be explained by the steric hindrance exerted by the methyl group of the former ligand, which probably results in longer metal-N distances and therefore less electron density on the cobalt center. This is consistent with the idea that ligand exchange should be much more rapid with the 2-MeIm compared with Im, since the electrochemical data suggest that the interaction of the 2-MeIm with the cobalt atom is restricted due to steric hindrance. The rate of ligand exchange is increased because of stabilization of the transition state due to relief of steric strain.

Substitution of the ligand framework with electron withdrawing substituents cause a significant effect upon the observed reduction peak potentials. For example, complexes with B = Cl are less cathodic than those with B = H by 225 mV in the case of A = Me and $X = NH_3$. The effects of equatorial ligand substitution are generally smaller than those induced by different axial ligands. This large change in potential is consistent with the addition of the electron to the dz^2 orbital, which is perpendicular to the in-plane ligand (i.e.,

Table 1.1. Reduction Potentials of Complexes [Co(acacen)$(X)_2$]Y in Acetonitrile.[a]

Complex	A	B	X	Y	E_{pa} (II→III)[b]	E_{pc} (III→II)[c]	$E_{1/2}$ (II↔I)[d]
1	Me	H	NH_3	Cl	0.150	-1.040	-1.77
2	Ph	H	NH_3	Cl	0.240	-0.970	-1.57
3	Me	Cl	NH_3	Cl	0.145	-0.815	-1.51
4	Ph	Cl	NH_3	Br	0.340	-0.830	-1.39
5	Me	H	py	Br	0.185	-0.710	-1.78
6	Ph	H	py	Br	0.220	-0.670	-1.58
7	Me	H	Im	Cl	0.230	-0.975	-1.78
8	*p*-ClPh	H	NH_3	Br	0.210	-0.880	-1.54
9	*p*-FPh	H	NH_3	PF_6	0.240	-0.910	-1.57
10	*p*-MeOPh	H	NH_3	Br	0.195	-0.940	-1.63
11	Me	H	N-MeIm	Br	0.125	-1.075	-1.78
12	Me	H	2-MeIm	Br	0.295	-0.855	-1.77
13	Ph	H	Im	Br	0.275	-0.925	-1.60
14	Me	Cl	2-MeIm	Br	0.255	-0.690	-1.51
15	Ph	H	2-MeIm	Br	0.210	-0.775	-1.58

[a] Potentials are vs. Ag/AgCl in 3 M NaCl, T = 293 K, c = 1 x 10^{-3} M, v = 100 mV/s

[b] Anodic peak potential from the process [Co(II)L] → $[Co(III)L]^+ + e^-$

[c] Cathodic peak potential for the process $[Co(III)L(X)_2]^+ + e^- \rightarrow$ [Co(II)L] + 2 X

[d] Formal potential for the reversible process [Co(II)L] + $e^- \leftrightarrow$ [Co(I)L]

the effect of substitution of the in-plane ligand is a smaller inductive electron withdrawing effect). Even substitution of substituent A by the strong electron withdrawing CF_3 group leads to a positive shift of the potential E_{pc} by only 320 mV (X = py), compared with the unsubstituted parent complex (A = Me).[17c] Substitution with both A = CF_3 and B = Cl should result in a cobalt complex reducible under physiological conditions, and a water soluble Co(II) derivative of this complex may be useful in the targeting of tumor cells.

The entire tumor targeting process can be qualitatively described using a model system which shows the effect of the concentration of pyridine on the electrochemical behavior of the complex [Co(II)acacen]. In the absence of pyridine, the quasireversible Co(II/III) couple is observed at 0.155 V. Upon addition of one equivalent of pyridine, the anodic wave is broadened and oxidation occurs at slightly lower potential, whereas the reduction wave is shifted by more than 700 mV into the negative direction. With increasing pyridine concentration, the anodic peak potential is cathodically shifted, whereas the corresponding cathodic reduction potential remains constant. At high pyridine concentration, the Co(III/II) redox couple becomes quasi-reversible. In the tumor targeting process, the reduction potential of $[Co(L)X_2]^+$ is high when X is a weak axial ligand (in the experiment X = MeCN); reduction of Co(III) should occur in the more reducing environment of tumor cells, but not in healthy cells. However, once the reduced Co(II) complex finds a stronger axial ligand like a histidine (in the model experiment the stronger axial ligand was pyridine), the redox potential should shift negative of the reduction potential within the tumor cell and reoxidize to form a stable Co(III) species. Although the absolute concentration of the stronger axial ligand will never be as large as in the electrochemical experiment, enzyme targeting moieties that localize the cobalt complex near histidines can be attached to the in-plane ligand, significantly raising the local concentration of histidine near the cobalt complex. This is summarized in Figure 1.11.

Targeting of Enzymes with Co(acacen) Derivatives

The synthetic versatility of Schiff base ligands allows the possibility of synthesizing complexes with widely varying properties. In the process of enzyme inhibition, we would like to achieve enzyme specificity and selectivity. One straightforward means of targeting enzymes is the attachment of known specific and selective enzyme inhibitors to the cobalt complex. The known inhibitor would target the desired enzyme, but the cobalt complex would greatly improve the inhibition by irreversibly anchoring the inhibitor to the enzyme. This process is described in a later chapter, which describes the targeting of thrombin. Another possibility would be the binding of the cobalt complex at the active site of an enzyme, and attachment of a known drug that targets a secondary site (Figure 1.12). At this present time, we have synthesized two ligand frameworks that are suitable for the attachment of targeting ligands. Hydroxypropylacacen, which contains a hydroxy group, and acacaciden, which was synthesized by Kevin Hoke and Arnd Böttcher and contains a carboxylic acid moiety, are two ligands which are synthetically versatile and should allow the coupling of a variety of targeting moieties (Figure 1.13).

Figure 1.11. Scheme for Tumor Cell Targeting. In this scheme, the cobalt(III/II) redox couple is at a potential where reduction to cobalt (II) would be unfavorable in healthy cells. However, upon entering tumor cells, reduction to cobalt (II) occurs, and the cobalt complex targets the active site of enzymes (See Figure 1.8). Upon binding to the target histidine, the redox couple shifts so that oxidation to cobalt (III) occurs and the cobalt complex becomes irreversibly bound to the enzyme. The scheme is based upon the addition of pyridine to [Co(II)(acacen)] using cyclic voltammetry in acetonitrile containing 0.1 M TBAP.

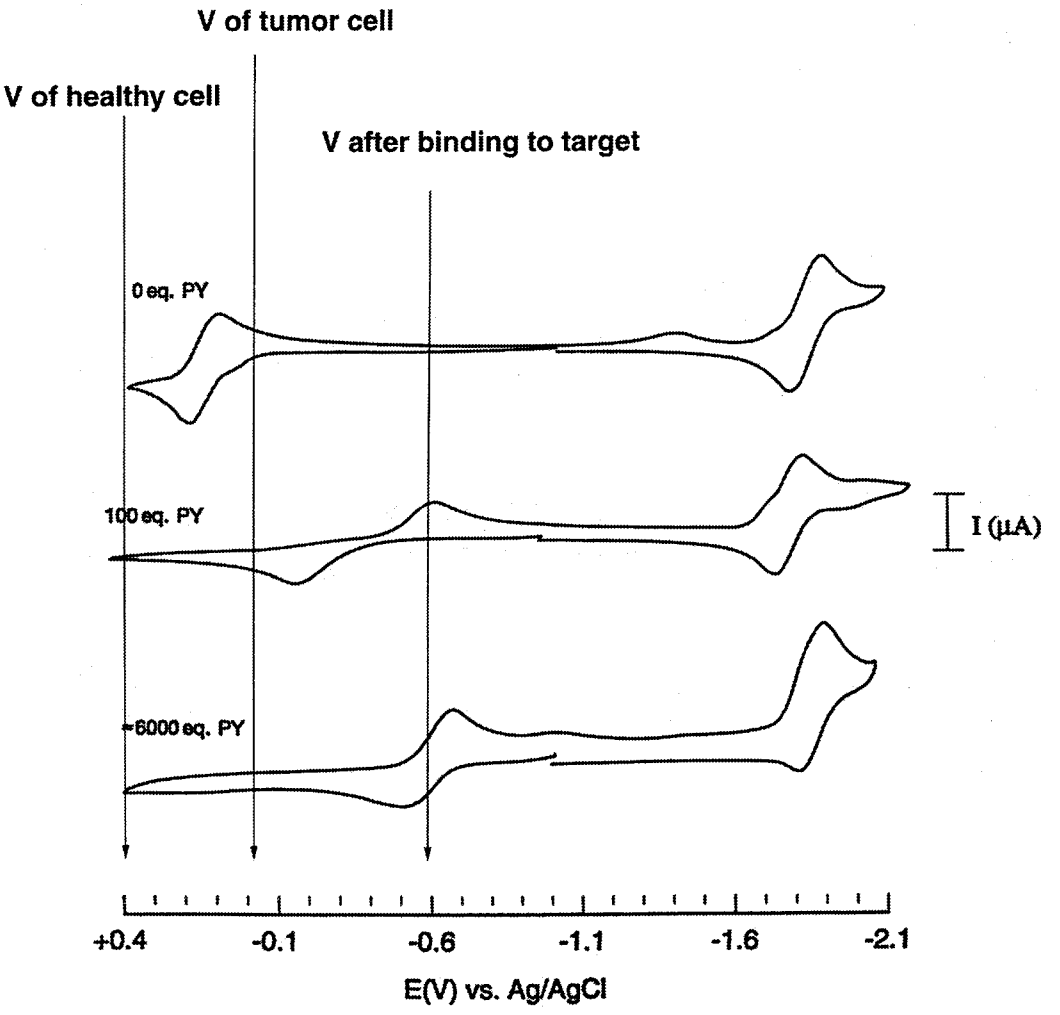

Figure 1.12. Enzyme Targeting Scheme. Two possible targeting mechanisms are outlined: a) the cobalt complex can bind to a histidine near the active site, anchoring an active site-directed inhibitor to the enzyme, and b) the cobalt compound can bind to the enzyme active site, while the attached inhibitor tethers the cobalt complex to the enzyme by binding to a secondary binding site.

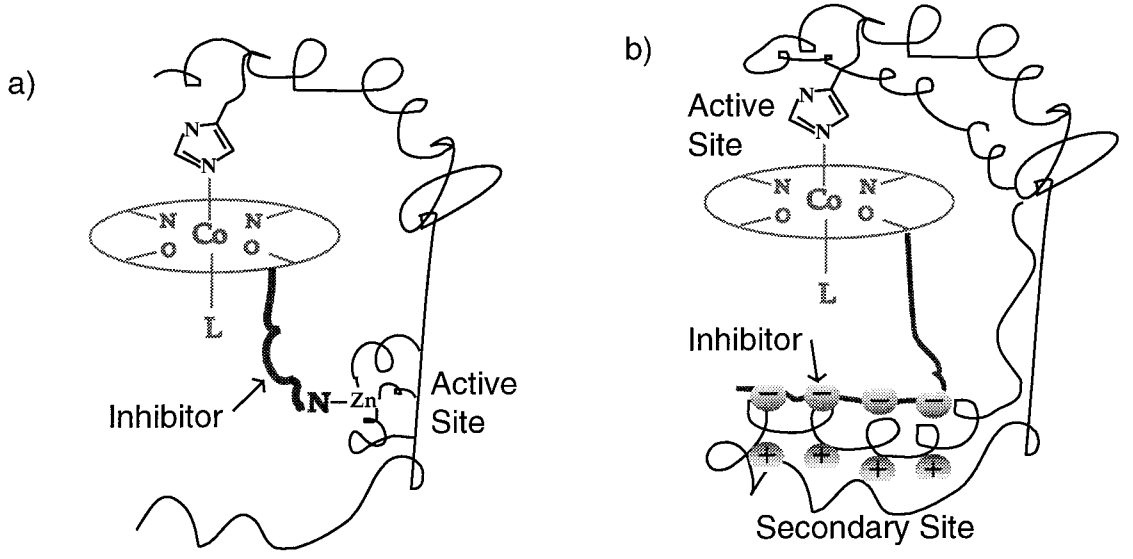

Figure 1.13 Structure of Acacen Derivatives Suitable for the Coupling of Targeting Moieties. a) Ester formation using hydroxypropylacacen would be one means of coupling the ligand to desired groups. b) Peptide coupling of a terminal amine to the carboxylic acid derivative of acacaciden would be a method to link targeting derivatives onto the ligand framework.

a)

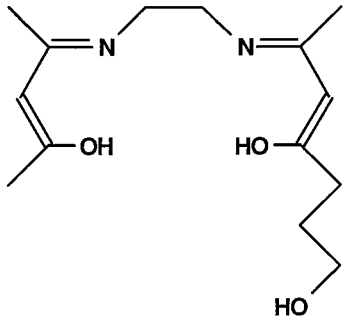

b)

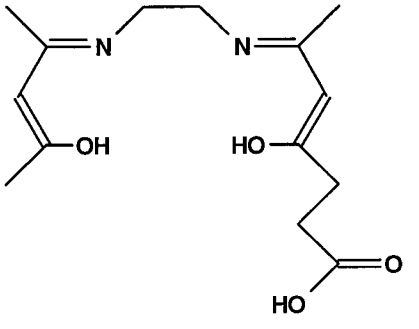

References

1. Stryer, L. (1988) *Biochemistry*, W. H. Freeman and Co., New York.

2. a) Ellis, P.E. and Lyons, J.E. (1990) *Coord. Chem. Rev., 105*, 181. b) Bartoli, J.F., Brigaud, O., Battioni, P., and Mansuy, D. (1991) *J. Chem. Soc. Chem. Commun.*, 440. c) Lyons, J. E. and Ellis, P. E. (1991) *Catal. Lett.., 8*, 45. d) Lyons, J. E., Ellis, P.E., Wagner, R. W., Thompson, R. E., Hughes, M. E., Hodge, J. A., and Gray, H. B. (1992) *Am. Chem. Soc. Div. of Petroleum Chemistry, Symposium, April, 1992.*

3. Martinez, S. E., Smith, J. L., Huang, D., Szczepaniak, A., and Cramer, W. A. (1992) *Research in Photosynthesis;* Murata, N. E., Proceedings in IXth International Congress on Photosynthesis; Kluwer Academic: Dordrecht,Vol. 2, page 495.

4. Shelnutt, J. A., Medforth, C. J., Berber, M. D., Barkigia, K. M., and Smith, K. M. (1991) *J. Am. Chem. Soc., 113*, 4077.

5. Gouterman, M. (1961) *J. Mol. Spectrosc., 6*, 138.

6. Bertini, I., Gray, H. B., Lippard, S. J., and Valentine, J. S. (1994) *Bioinorganic Chemistry*, pp 505-583, University Science Books, Mill Valley, Ca.

7. Sadler, P. J. (1991) *Adv. Inorg. Chem., 36,* 1-48.

8. Devlin, H., Geary, P., Pavanlangston, D., Dori, Z., and Dunkel, E. C. (1993) *Inv. Opth-V, 34*, 1348.

9. (a) Rawlings, N. D. and Barrett, A. J. (1994) *Methods in Enzymology, 244,* 19-61. (b) Rawlings, N. D. and Barrett, A. J. (1994) *Methods in Enzymology, 244*, 461-487. (c) McKerrow, J. H., Sun, E., Rosenthal, P. J., and Bouvier, J. (1993) *Annu. Rev. Microbiol., 47,* 821-853. (d) Chen, W.-T. (1992) *Curr. Opin. Cell Biol., 4,* 802-809. (e)

Davies, J. F., Hostomska, Z., Hostomsky, Z., Jordan, S. R., and Matthews, D. A. (1991) *Science, 252*, 88-95.

10. (a) Langford, C. H. and Gray, H. B. (1966) *Ligand Substitution Processes,* pp 55-101, W. A. Benjamin, Inc., Reading, Mass. (b) Basolo, F. and Johnson, R. C. (1986) *Coordination Chemistry*, pp 97-119, Science Reviews.
11. Fujii, Y. (1972) *Bull. Chem. Soc. Japan, 45,* 3084-3092.
12. Haiek, A., Cwikel, D., Dori, Z., and Gray, H. B., unpublished results.
13. (a) Marcu, G., Várhelyi, C., Fülöp, J., and Itul, D. (1989) *Rev. Roumaine Chim., 34,* 1029. (b) Abdel Salam El Absy, M., Marcu, G., Zsakó, J., and Várhelyi, C. (1982) *Rev. Roumaine Chim., 27*, 917. (c) Costa, G., Mestroni, G., Tauzher, G., and Stefani, L. (1966) *J. Organomet. Chem., 6,* 181.
14. The spectroscopic and electrochemical properties of cobalt (III) schiff base complexes is presented in Böttcher, A., Takeuchi, T., Hardcastle, K. I., Dori, Z., Gray, H. B., and Meade, T. J., in preparation for *Inorg. Chem.*
15. Larsen, E. (1969) *Acta Chem. Scand., 23*, 2158.
16. (a) Sartorelli, A. C. (1988) *Cancer Research, 48*, 775. (b) Brown, J. M. And Koong, A. (1991), *J. Nat. Cancer Inst., 83*, 178.
17. (a) Carter, M. J., Rillema, D. P., and Basolo, F. (1974) *J. Am. Chem. Soc., 96*, 392. (b) Kotocová, A., Sima, J., and Labuda, J. (1993) *Polish J. Chem., 67*, 2077. (c) Kotocová, A., Sima, J., Valigura, D., and Fodran, P. (1987) *Inorg. Chim. Acta, 128*, 11. (d) Rohrbach, D. F., Heineman, W. R., and Deutsch, E. (1979) *Inorg. Chem., 18*, 2536. (e) Reisenhofer, E. and Costa, G. (1981) *Inorg. Chim. Acta, 49,* 121.
18. (a) Averill, D. F. and Broman, R. F. (1978) *Inorg. Chem., 17*, 3389. (b) Costes, J. P., Cros, G., Muratet, F., and Darbieu, M.-H. (1987) *Polyhedron, 6,* 995. (c) Costes, J. P.,

Cors, G., Darbieu, M.-H., and Laurent, J.-P. (1982) *Trans. Met. Chem., 7,* 219. (d) Darbieu, M.-H., Cros, G., de Montauzon, D., and Laurent, J.-P. (1982) *Trans. Met. Chem., 7,* 219. (e) Costa, G., Mestroni, G., Puxeddu, A., and Reisenhofer, E. (1970) *J. Chem. Soc. (A),* 2870.

19. Tait, A. M., Lovecchio, F. V., and Busch, D. H. (1977) *Inorg. Chem., 16,* 2206.

20. pK_a values for the five different axial bases used in this study are (in aqueous solution): py: 5.23; Im: 6.99; N-MeIm: 7.25; 2-Me-Im: 7.86; NH_3: 10.25 as reported in D. D. Perrin, (1972) *Dissociation Constants of Organic Bases in Aqueous Solution,* Butterworths: London, Supplement 1972.

Chapter 2. Electronic Structures of Halogenated Porphyrins

Introduction

It is well established that halogenation leads to dramatic changes in the spectroscopic properties of porphyrins.[1] Both the Soret and Q bands in the absorption spectrum of β-octabromo-tetrakis(pentafluorophenyl)porphyrin ($TFPPBr_8$) are strongly red-shifted relative to the corresponding bands in tetraphenylporphyrin (TPP). In our efforts to understand these and other unusual electronic structural features, we have done theoretical and experimental work on a $ZnTFPPX_8$ (X = H, Cl, Br) model system. Since the geometries of $ZnTFPPX_8$ molecules are very similar to those of β-alkyl-tetraphenylporphyrins,[2] we have attempted to determine the specific influence that the highly distorted porphyrin framework has on the electronic structures of these systems. Our findings have suggested possible reasons for the high activities and oxidative stabilities of the halogenated iron-porphyrin catalysts employed by Lyons and Ellis in the oxygenation of alkanes. For example, β-octabromo[tetrakis(pentafluorophenyl)-porphyrinato]iron(III)chloride catalyzes the room-temperature conversion of isobutane to *tert*-butyl alcohol in the presence of oxygen at a rate of 190 mol-product per mol-catalyst per hour with over 90% selectivity to the alcohol. Remarkably, this activity is unchanged after 74 hours.[3]

The standard model for the interpretation of porphyrin spectra is due to Gouterman (the Four Orbital Model, or FOM).[4] Figure 2.1 shows the Gouterman orbitals for $ZnTFPPBr_8$; there are two nearly degenerate HOMOs (b1 and b2 with a_{2u} and a_{1u} symmetries in D_{4h}) and two nearly degenerate LUMOs (c1 and c2 with e_g symmetry in D_{4h}). The ground-state configuration is $(b1)^2(b2)^2$ and the excited states are given by Eqs. 1 and 2:

Figure 2.1. The Gouterman Four Orbitals for $ZnTFPPBr_8$ from AM1 Calculations.

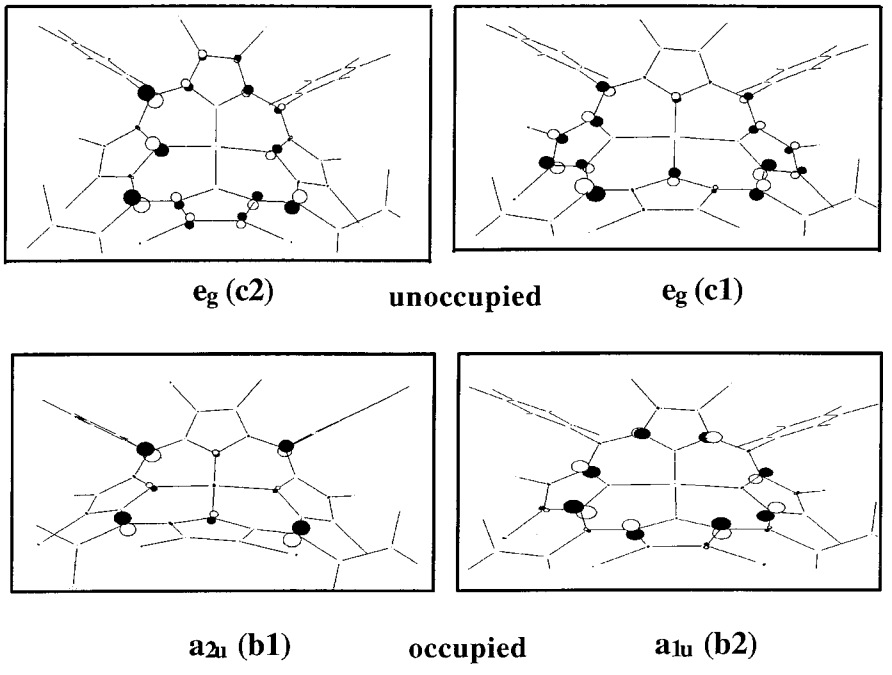

$$\left.\begin{matrix} B_x \\ Q_x \end{matrix}\right\} = [(b1c2) \mp (b2c1)]/(2)^{1/2} \qquad (1)$$

$$\left.\begin{matrix} B_y \\ Q_y \end{matrix}\right\} = [(b1c1) \pm (b2c2)]/(2)^{1/2} \qquad (2)$$

where Q_x, Q_y are the states associated with the visible bands, and B_x, B_y correspond to the Soret bands. This model is used with semiempirical AM1[5] calculations using MOPAC.[6] These calculations include full configuration interaction (CI) within the orbitals of the FOM.

Calculational and Experimental Details

The calculations were performed on a series of halogenated porphyrins: ZnTFPP, ZnTFPPCl_8, and ZnTFPPBr_8.[7] All porphyrins were purified on a silica gel column (150 Å pore size and 75-150 μ particle size). ZnTFPP was eluted using dichloromethane/hexane (1/1 v/v), while ZnTFPPCl_8 and ZnTFPPBr_8 were eluted with dichloromethane/hexane (2/1 v/v). Absorption spectra were measured using a Cary 14 spectrophotometer. The porphyrin solutions were prepared by dissolving approximately 1.25 mg of porphyrin in 50 ml of methylcyclohexane followed by 20:1 solvent: solution dilution. Spectra were obtained at 25 °C.[8]

Results

Examination of Table 2.1 shows that the calculations reproduce the experimental trends. The absorption spectrum shifts to the red as the size of the Cβ substituents increases (H to Cl to Br). Thus, porphyrins with hydrogen at the beta(pyrrolic) positions exhibit the highest-energy transitions, whereas those compounds with bromine in the pyrrolic positions have the lowest-energy transitions.

Table 2.1. Distortion of $CuTFPPX_8$.[a]

Distortion (Å)	X = H	X = Cl	X = Br
N	0.000	0.12	0.15
C_{meso}	0.006	0.13	0.18
$C_{ß}$	0.008	0.80	1.25

[a] From Cu plane, see references 10 and 11.

[b]The hydrogens were optimized using MOPAC.

Table 2.2. Excitation Energies for $ZnTFPPX_8$ from Theory (AM1) and Experiment.

	ZnTFPP λ (nm)	$ZnTFPPCl_8$ λ (nm)	$ZnTFPPBr_8$ λ (nm)
Q (visible)			
Exper	544	575	596
Theory (Q_x)	517	535 (527)[a]	553 (552)[b]
(Q_y)	516	533 (524)[a]	548 (547)[b]
B (Soret)			
Exper	412	442	464
Theory (B_x)	317	329 (324)[a]	345 (343)[b]
(B_y)	317	328 (323)[a]	344 (342)[b]

[a]Using same geometry as $ZnTFPPCl_8$ but with H replacing Cl.

[b]Using same geometry as $ZnTFPPBr_8$ but with H replacing Br.

In order to ascertain the electronic perturbations associated with this size-induced red-shifting, the FOM-MO transition energies were examined (Table 2.2). Note that these are simple MO excitation energies, whereas the theoretical values in Table 2.1 include CI. The results set out in Table 2.2 suggest that the red shifts in the absorption spectra are attributable to a decrease in the one-electron excitation energies. However, it is not clear from these data how the electronic and steric properties of the β-pyrrole substituents individually affect the orbital energies.

In order to estimate the component of the red-shifting that is sterically induced, the X atoms of $ZnTFPPX_8$ molecules were removed and replaced with either X' = Cl, Br, F, or CH_3, while retaining the geometries of the respective compounds (and using the correct C-X' bond distances). The effects of these replacements on MO excitation energies are given in Table 2.3. In each case, there are decreases in the transition energies as the porphyrin distorts. Since the nature of the substituent varies from an electron-donating CH_3 to a highly electron-withdrawing F (while a net decrease in the HOMO-LUMO gap is evident for each substituent), we can conclude that distortion clearly induces red-shifting in porphyrin absorptions. Further examination of Table 2.3 shows that, as the porphyrin saddles, both the HOMO and LUMO energies increase. However, the HOMOs are destabilized more than the LUMOs, leading to red-shifts in the absorption spectra. These findings are consistent with earlier work done on β-alkyl-porphyrins.[2]

A good test of the electronic effect of the substituents can be obtained by maintaining a constant geometry while varying the substituents on the porphyrin skeleton. Calculation of transition energies upon constraint of the macrocycle to the planar ZnTFPP geometry (Table 2.3) yields HOMO-LUMO[9] gaps of -2.40

Table 2.3. Energies from AM1 Calculations.

	ZnTFPP	$ZnTFPPCl_8$		$ZnTFPPBr_8$	
Orbital Energies	ε_i	ε_i	ε_i[a]	ε_i	ε_i[b]
b2	-8.40	-8.87	-8.39	-8.77	-8.39
b1	-8.05	-8.67	-8.07	-8.64	-8.03
c1	-2.71	-3.34	-2.73	-3.36	-2.85
c2	-2.66	-3.30	-2.68	-3.34	-2.81
Excitation Energies	E_{ij}	E_{ij}	E_{ij}[a]	E_{ij}	E_{ij}[b]
b1 → c1	5.35	5.33	5.34	5.28	5.18
b1 → c2	5.39	5.37	5.39	5.30	5.22
b2 → c1	5.69	5.53	5.66	5.42	5.54
b2 → c2	5.74	5.57	5.71	5.44	5.58

[a]Change due to Cl → H at the same geometry.

[b]Change due to Br → H at the same geometry.

(ZnTFPP), -2.45 ($ZnTFPPCl_8$), -2.37 ($ZnTFPPBr_8$), and -2.36 eV ($ZnTFPPMe_8$), which are nearly the same for all of the β substituents. This suggests that a change in electronegativity at the Cβ positions equally stabilizes both the HOMOs and LUMOs, with a correspondingly small effect on the excitation energies. Furthermore, the HOMO-LUMO gaps of $ZnTFPPCl_8$, $ZnTFPPBr_8$, and $ZnTFPPMe_8$ similarly drop with increasing distortion from the planar structure. It also should be noted that although substituent electronic properties have little effect on the transition energies for substitution with X' = H, Cl, Br, and Me, F is an exception; probably because of its powerful electron-withdrawing properties, it significantly perturbs the HOMO-LUMO gap.

The electronic effect of each halogen is to lower the energies of both the HOMOs and LUMOs of $ZnTFPPX_8$. However, the distortion of the porphyrin predominantly raises the energies of the HOMOs, so the net result is a large drop in the LUMO energies and a smaller drop in the HOMO energies upon halogenation of the porphyrin macrocycle. Furthermore, the HOMOs of $ZnTFPPBr_8$ should be destabilized with respect to $ZnTFPPCl_8$ since bromines are slightly less electronegative and add steric bulk to the ring, further distorting the porphyrin structure. Indeed, the finding that the porphyrin LUMO is stabilized more than the HOMO is supported by electrochemical data. The oxidation and reduction potentials using cyclic voltammetry for ZnTFPP are 1.36 and -0.96; the potentials for $ZnTFPPCl_8$ are 1.62 and -0.47, while the potentials for $ZnTFPPBr_8$ are 1.58 and -0.49 V vs. SCE.[10]

Our model of steric and electronic effects should guide the design of novel porphyrins with specific properties. For example, since the spectral red-shift is highly sensitive to distortion of the porphyrin ring, porphyrin geometry can be qualitatively probed by absorption spectroscopy. The greater the red-shifting in the spectra, the greater

the distortion of the porphyrin ring. Furthermore, decoupling of the electronic effects of the substituent from the distortion predicts that a planar porphyrin with electron-withdrawing substituents in β positions would show extremely high oxidation potentials, since the HOMOs are *not* destabilized due to distortion of the ring. For example, saddle-shaped octa-β-halotetrakis(mesityl)porphyrin derivatives are easier to oxidize than the corresponding tetra-β-halogenated derivatives that are not saddle-shaped.[11] The stability with respect to oxidation is an important factor to consider in the design of porphyrin catalysts: lowering the energy of the porphyrin HOMOs should enhance catalyst lifetimes, because this type of electronic stabilization strongly disfavors oxidative destruction of the macrocycle.

References

1. (a) Callot, H. J. (1974) *Bull. Soc. Chim. Fr.*, *8*, 1492. Corrections to the structures have been reported: Crossley, M. J., Burn, P. L., Chew, S. S., Cuttance, F. B., and Newsom, I. A. (1991) *J. Chem. Soc., Chem. Commun.*, 1564. (b) D'Souza, F., Villard, A., Caemelbecke, E. V., Franzen, M., Boschi, T., Tagliatesta, P., and Kadish, K. M. (1993) *Inorg. Chem.*, *32*, 4042. (c) Bhyrappa, P. and Krishnan, V. (1991) *Inorg. Chem.*, *30*, 239. (d) Lyons, J. E., Ellis, P.E., Wagner, R. W., Thompson, R. E., Hughes, M. E., Hodge, J. A., and Gray, H. B. (1992) *Am. Chem. Soc. Div. of Petroleum Chemistry, Symposium, April,* 1992.

2. (a) Barkigia, K. M., Chantranupong, L., Smith, K. M., and Fajer, J. (1988) *J. Am. Chem. Soc.*, *110*, 7566. (b) Barkigia, K. M., Berber, M. D., Fajer, J., Medforth, C. J., Renner, M. W., and Smith, K. M. (1990) *J. Am. Chem. Soc.*, *112*, 8851. (c) Shelnutt, J. A., Medforth, C. J., Berber, B. D., Barkigia, K. M., and Smith, K. M. (1991) *J. Am. Chem. Soc.*, *113*, 4077. (d) Sparks, L. D., Medforth, C. J., Park, M. S., Chamberlain, J. R., Ondrias, M. R., Senge, M. O., Smith, K. M., and Shelnutt, J. A. (1993) *J. Am. Chem. Soc.*, *115*, 581. (e) Barkigia, K. M., Renner, M. W., Furenlid, L. R., Medforth, C. J., Smith, K. M., and Fajer, J. (1993) *J. Am. Chem. Soc.*, *115*, 3627. (f) Senge, M. O. (1992) *J. Photochem. Photobiol. B: Biol.*, *16*, 3.

3. Lyons, J. E. and Ellis, P. E. (1991) *Catal. Lett.*, *8*, 45.

4. Gouterman, M. (1961) *J. Mol. Spectrosc.*, *6*, 138.

5. Dewar, M.J.S., Healy, E. F., Stewart, J. J. P., and Zoebisch, E. G. (1985) *J. Am. Chem. Soc.*, *107*, 3902.

6. Stewart, J. J. P. Program Number 581 (MOPAC) from the Quantum Chemistry

Program Exchange (QCPE), Indiana University, Bloomington, Indiana.

7. (a) The $ZnTFPPX_8$ structures were assumed to be the same as those of the corresponding Cu compounds, where data for X = H,Cl, and Br are available.[7b-d] For X = H and Br, the structures of the Cu and Zn derivatives are closely similar.[7b-e] (b) Schaefer, W. P., Hodge, J. A., Hughes, M. E., Gray, H. B., Lyons, J. E., Ellis, P. E., and Wagner, R. W. (1993) *Acta Cryst. Sec. C.*, *49*, 1342. (c) Henling, L. M., Schaefer, W. P., Hodge, J. A., Hughes, M. E., and Gray, H. B. (1993) *Acta Cryst. Sec. C.*, *49*, 1743. (d) Marsh, R. E., Schaefer, W. P., Hodge, J. A., Hughes, M. E., and Gray, H. B. (1993) *Acta Cryst. Sec. C.*, *49*, 1339. (e) Schaefer, W. P., Henling, L. M., Hodge, J. A., and Grinstaff, M. W., unpublished results. (f) The structure of $NiTFPPBr_8$, which shows similar saddle distortions, has been reported: Mandon, D., Ochesbein, P., Fischer, J., Weiss, R., Jayaraj, K., Austin, R. N., Gold, A., White, P. S., Brigaud, O., Battioni, P., and Mansuy, D. (1992) *Inorg. Chem.*, *31*, 2044. Also, see reference 6e.

8. H_2TFPP obtained from Aldrich was purified using techniques described earlier. (Kaizu, Y., Misu, N., Tsuji, K., Kaneko, Y., and Kobayashi, H. (1985) *Bull. Chem. Soc. Japan*, *58*, 103). $H_2TFPPCl_8$ (Wijesekera, T., Matsumoto, A., Dolphin, D., and Lexa, D. (1990) *Angew. Chem. Int. Ed. Engl.*, *29*, 1028) and $H_2TFPPBr_8$ (Ellis, P.E. and Lyons, J.E. (1990) *Coord. Chem. Rev.*, *105*, 181) were prepared according to literature procedures.

9. The lower Q band energy is a good estimate of the HOMO-LUMO gap.

10. Hodge, J. A., Hill, M. G., and Gray, H. B. (1995) *Inorg. Chem.*, *34*, 809.

11. Ochsenbein, P., Ayougou, K., Mandon, D., Fischer, J., Weiss, R., Austin, R. N., Jayaraj, K., Gold, A., Terner, J., and Fajer, J. (1994) *Angew. Chem., Int. Ed. Engl.*, *33*, 348.

Chapter 3. Ruffling in a Series of Nickel(II) *Meso*-Tetrasubstituted Porphyrins

Introduction

It was found that high resolution X-ray crystal structures of cytochromes *c* show an iron porphyrin cofactor that is distorted from planarity by a significant degree.[1] This heme distortion, primarily consisting of the ruffling distortion, is highly conserved for mitochondrial cytochromes *c* from diverse species and also for other *c*-type cytochromes such as turnip cytochrome *f*.[2] Since nonplanar distortions of porphyrins can significantly alter chemical and photophysical properties of metalloporphyrins, it is possible that ruffling of the heme in cytochrome *c* can modify the redox properties of the heme. This implies that protein-controlled ruffling of the heme is one possible mechanism with which the tertiary structure of the surrounding protein can regulate the heme redox potentials.

It has been demonstrated in previous studies that naturally-occurring iron porphyrins are expected to be planar in the absence of external perturbations.[3] In order to investigate the magnitude of the external perturbation required to cause a nonplanar distortion, several series of highly substituted synthetic porphyrins (that have nonplanar conformations as a consequence of the steric crowding of the substituents at the periphery of the macrocycle) were investigated.[4] In this case, the external perturbation is supplied by the steric crowding of the peripheral substituents. In particular, it was demonstrated that sizable steric interactions at the periphery are necessary to cause nonplanar distortions of porphyrins with metal ions as large as Cu(II) and Fe(III).[3] Thus, the nonplanar distortion of the heme of cytochrome *c* is most likely the result of forces exerted by (1) the covalent linkages between the heme and the protein backbone, (2) the hydrogen bonds between the propionic acid substituents of the heme and amino acids of the protein, and (3) the steric interactions exerted by the protein side chains in contact with the heme.

A good model system for the ruffling distortion is needed so that a detailed study of the effect of ruffling on the properties of the porphyrin can be determined and differentiated from other types of nonplanar distortion. Thus, a series of nickel (II) *meso*-tetrasubstituted porphyrins, Ni**1** to Ni**11a** shown in Figure 3.1, were studied. The substituents are alkyl groups of increasing size, causing increasingly ruffled porphryin frameworks. The conformations of these nickel porphryins were calculated using molecular mechanics force fields similar to one used previously.[1] X-ray crystal structures of some of these nickel porphyrins have been reported and the calculated structures are generally consistent with the X-ray crystallographic results. INDO/s molecular orbital calculations show that many of the spectroscopic properties are primarily a result of conformational differences rather than substituent electronic differences.

Tetrasubstituted porphyrins, with either a single atom or else a nonplanar substituent group attached at the *meso* carbons generally exhibit the ruffling distortion. The reason that the ruffling distortion is favored is that only a small movement of the *meso* substituent out of plane is sufficient to relieve the quasi-equatorial steric interaction between the substituent atom directly bonded to the *meso* carbon and the adjacent pyrrole rings. Free rotation of the tetrahedrally-bonded atoms at the *meso* carbons (e.g., alkyl substituents) removes strain efficiently because the atoms in the β-carbon positions of the substituent do not also have to move out of the plane to reduce crowding.

Calculational Details

Quantum mechanical calculations made use of the INDO/s semiempirical method developed and optimized for spectroscopic predictions by Zerner and coworkers.[5] HyperChem(Hypercube, Inc.) and Argus programs were used for the calculations. The parameter β(d) was varied to give reasonable energies for the d-d transitions for the nickel

Figure 3.1. Nickel(II) *Meso*-Tetrasubstituted Porphyrins.

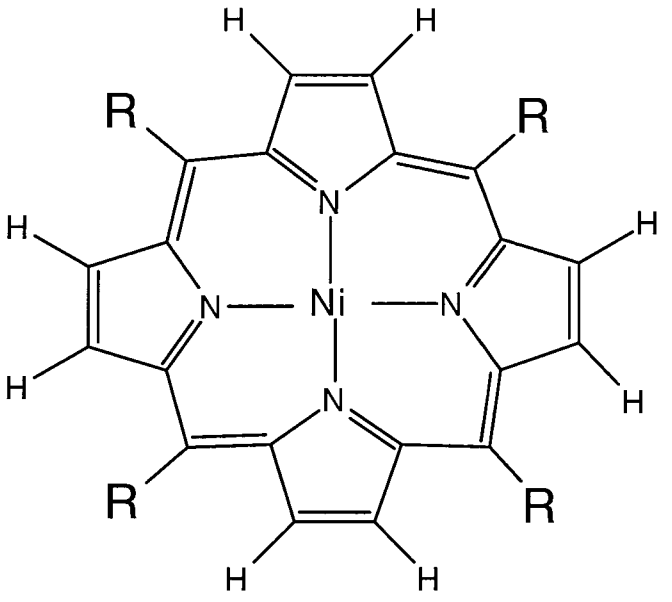

1. TMeP R= —CH_3

2. TEtP R=

3. TPrP R=

4. TPeP R=

5. TiPrP R=

6. TcHP R=

7. TtBuP R=

8. TAdP R=

9. TPP R=

10.TmyP R=

11.TcPrP R=

11a. TcPrP-11a (αβαβ) H_3COOC R=

porphyrins and a value of 32 was chosen. Molecular structures used in the MO calculations are the ones obtained from the classical energy-optimization calculations. The MO calculations are performed on the entire molecule, including the complete substituents, and also, for comparison, on analogs for which the structure of the macrocycle is maintained the same as calculated for the entire molecule, but the *meso*-substituents are replaced by methyl groups.

Results and Discussion

The π-π^* transitions of the macrocycle give rise to the bands in the UV-visible region of the absorption spectrum, including the B (Soret) band near 400 nm and the Q_0 and Q_v bands in the red region of the visible spectrum.[6,7] The UV-visible absorption spectra of the entire series of nickel porphyrins are shown in Figure 3.2 and the peak wavelengths of the bands are listed in Table 1. Both the B and Q bands progressively red shift as the substituent group becomes more bulky. Thus, *meso*-tetrasubstituted porphyrins with simple linear alkane substituents have the B band near 430 nm and the Q_0 and Q_v bands near 540 and 580 nm, respectively. Bulkier substituents like *tert*-butyl and adamantyl give greatly red-shifted spectra with the B band near 470 nm and the Q bands at about 600 and 650 nm. A marked broadening of the bands is noted for the bulkiest substituents (Figure 3.2). This broadening is probably not a result of structural heterogeneity. Also, the intensities of the Q bands increase relative to the B band as the substituents become more bulky; the Q_0 band also gains intensity relative to the Q_v band.

INDO/s calculations were performed using the lowest energy conformations of the nickel tetrasubstituted porphyrins obtained from molecular mechanics calculations. The predicted energies of the singlet π-π^* transitions associated with the B and Q bands are given in Figure 3.3 as a function of the calculated ruffling dihedral angle. The red shifts in

Figure 3.2. UV-visible Absorption Spectra of Nickel *Meso*-Tetrasubstituted Porphryins.

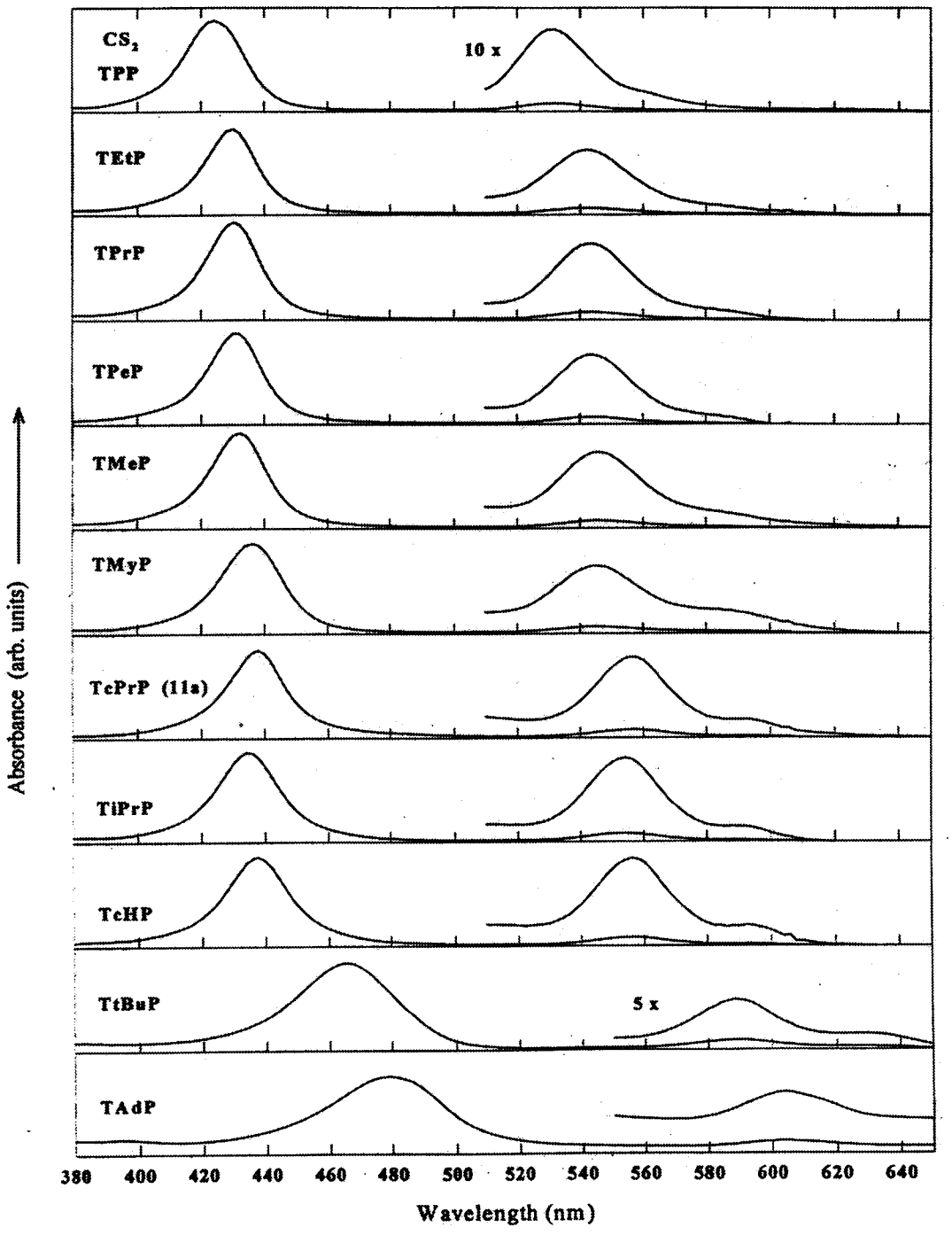

Figure 3.3. Excitation Energy for *Meso*-Tetrasubstituted Nickel (II) Porphryins Versus Dihedral Angle.

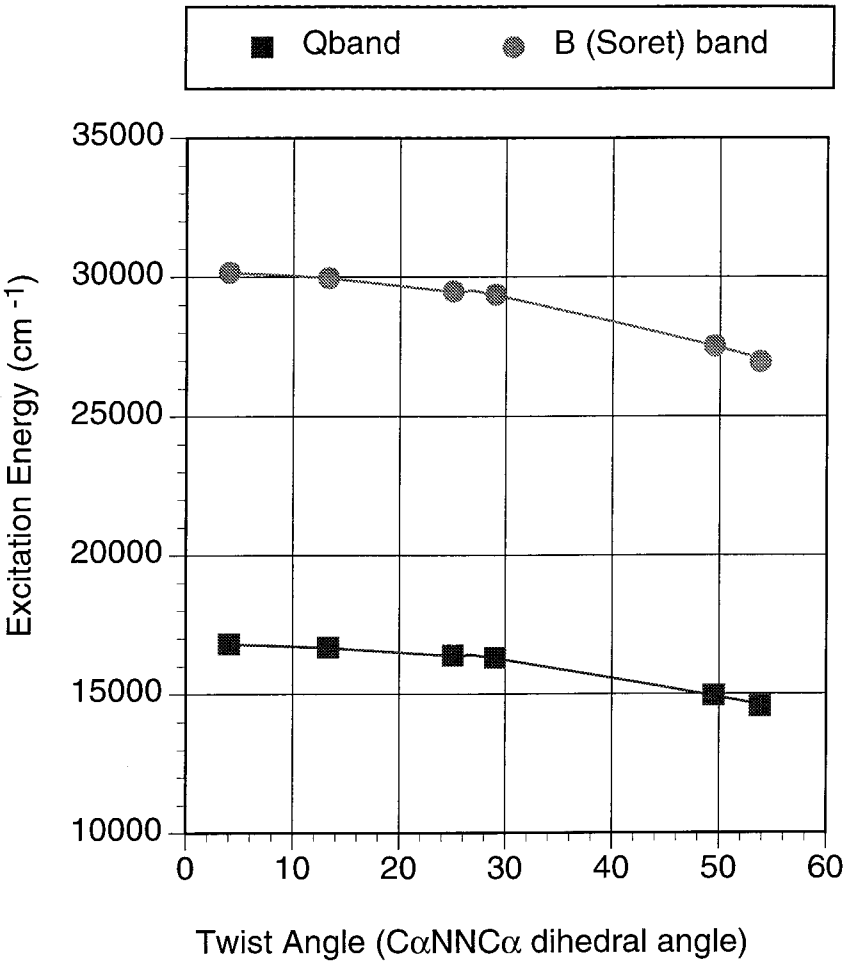

the transition energies with the degree of ruffling are accurately predicted even though the absolute calculated energies are significantly different from the experimentally measured transition energies. The energies of the lowest unoccupied molecular orbitals (LUMOs) and highest occupied molecular orbitals (HOMOs) are plotted in Figure 3.4. The red shifts in the transitions result from the ruffling of the macrocycle (which is proportional to the C_α-C_m torsion angle) and not the small differences in the electronic properties of the substituents. This was demonstrated by carrying out the INDO calculations on the same macrocycle conformations, but with methyl groups replacing the actual substituents. These calculations with the replacements gave nearly the same trends with ruffling as that shown in Figure 3.3.

The excited state configurations in which one of the electrons of the $a_{1u}(\pi)$ or $a_{2u}(\pi)$ orbitals is promoted to one of the degenerate pair of $e_g(\pi^*)$ orbitals give rise to the Q and B states upon mixing by the configuration interaction. The origin of the red shift is a decrease upon ruffling in the separation of the highest filled $a_{1u}(\pi)$ or $a_{2u}(\pi)$ orbitals and the lowest unoccupied $e_g(\pi^*)$ orbitals. The decrease in the separation is primarily a result of a destabilization of the $a_{1u}(\pi)$ or $a_{2u}(\pi)$ orbitals caused by ruffling; the energy of the $e_g(\pi^*)$ orbitals by contrast are relatively unchanged by ruffling.

The extinction coefficient of the Q band is observed to increase relative to the B band. The oscillator strength of the Q band is seen to be relatively constant; however, the oscillator strength of the B band decreased by 39% as the macrocycle ruffles in the series of Ni tetrasubstituted porphyrins. The decrease in the B-band oscillator strength is consistent with the observed increase in the intensity of the Q band relative to the Soret (Figure 3.2). The decrease in the B-band oscillator strength is probably due to the decrease in conjugation with increased ruffling of the macrocycle.

Figure 3.4. Calculated HOMO and LUMO Energies of *Meso*-Tetrasubstituted Ni(II) Porphyrins.

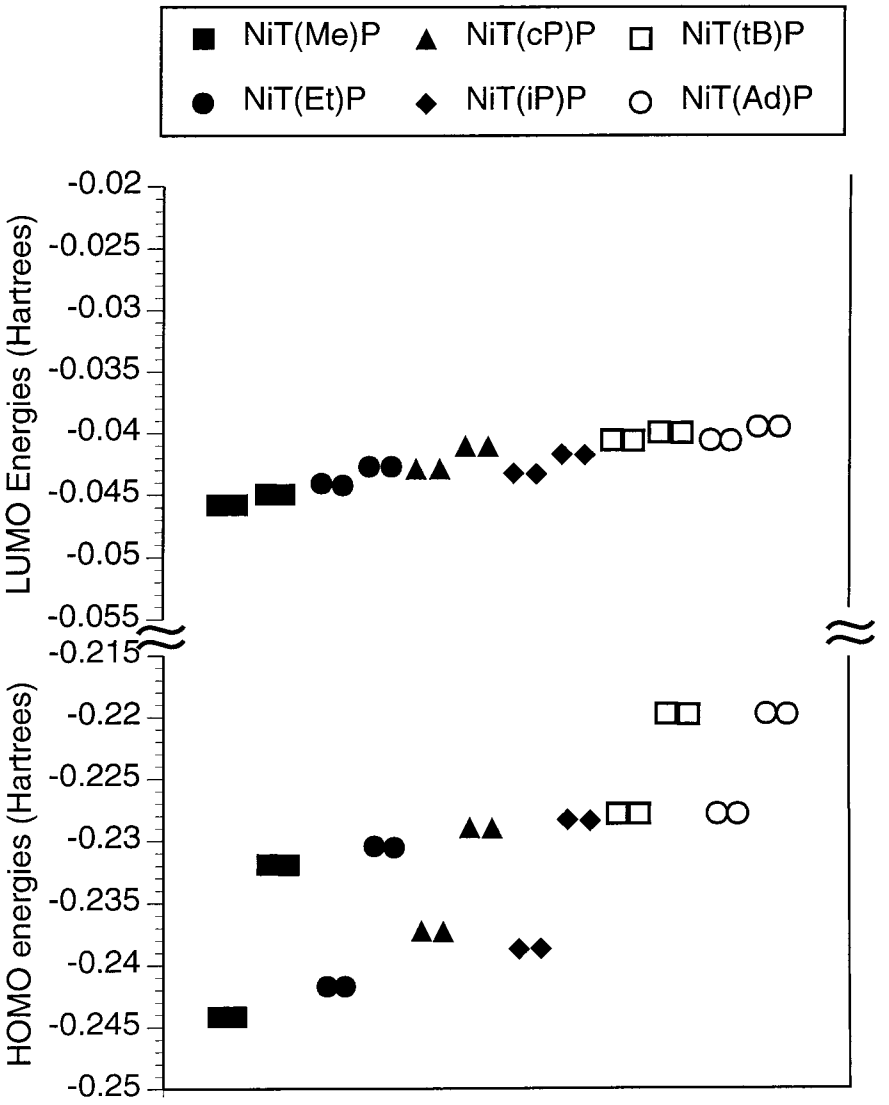

These INDO/s calculations suggest that the ruffling distortion of the macrocycle is the origin of the UV-visible absorption band shifts. Although it is important to find a spectroscopic means of distinguishing between ruffling distortions and other nonplanar distortions, as yet no characteristic spectroscopic features allow one to distinguish between the different conformers. However, the tetrasubstituted porphyrins do provide a useful model system for the investigation of the changes in chemical properties brought about by the ruffling distortion of the heme in cytochrome *c*. The moderate degree of distortion of the heme in cytochrome *c* is roughly equivalent to that occurring for some conformers of nickel tetraethyl porphyrin. Energetically, however, the ruffling of the heme may be more significant because ruffling is more difficult for the Fe(II) and Fe(III) ions which are larger than Ni(II).

These results have important implications for understanding the role of nonplanar distortions in the biological function of proteins like cytochrome *c* that contain nonplanar porphyrins. The primary question to be addressed for cytochrome *c* is what influence ruffling has on the properties of the heme and how changes in these properties influence electron-transfer reactions. Clearly, INDO/s calculations suggest that the reduction potentials of the ring and metal are influenced by ruffling. Thus, the protein environment of the porphyrins can influence the redox properties by controlling the nonplanarity of the macrocycle. Further, changes in metal size clearly affect the relative energies of the planar and the nonplanar conformers; therefore, the oxidation state of the Fe atom can influence protein structure through the energetics of the nonplanar conformers and their interaction with the surrounding protein. Thus, changes in the relative energies of the conformers may influence the equilibrium structure of the protein moiety and ultimately protein-protein binding events during electron transport. Finally, the photophysical properties of related

pigments in the photosynthetic reaction centers could be influenced by photoinduced interconversion between conformers. For example, conformation gating of electron-transfer reactions in the reaction centers may play a role in the initial events of photosynthesis. This has been suggested previously for electronic-induced structural changes in the primary donor.[8] Also, the protein moiety of reaction centers may control electron-transfer rates by stabilizing certain conformers over others.

References

1. Hobbs, J. D. and Shelnutt, J. A. (1995) *J. Protein Chem.*, *14*, 19.

2. Martinez, S., E., Smithe, J. L., Huang, D., Szczepaniak, A., and Cramer, W. A. (1992) *Research in Photosynthesis*, Murata, N., Ed., Proceedings in IXth International Congress on Photosynthesis, Kluwer Academic: Dordrecht, Vol. 2, page 495.

3. Anderson, K. K., Hobbs, J. D., Luo, L., Stanley, K. D., Quirke, J. M. E., and Shelnutt J. A. (1993) *J. Am. Chem. Soc.*, *115*, 12346.

4. Hobbs, J. D., Majumder, S. A., Luo, L., Sickelsmith, G. A., Quirke, J. M. E., Medforth, C. J., Smith, K. M., and Shelnutt J. A. (1994) *J. Am. Chem. Soc.*, *116*, 3261. All molecular mechanics calculations were performed by collaborators W. Jentzen, M. C. Simpson, J. D. Hobbs, X. Song, and J. A. Shelnutt at Sandia National Laboratories.

5. (a) Ridley, J. E. and Zerner, M. C. (1973) *Theor. Chim. Acta*, *32*, 111. (b) Bacon, A. and Zerner, M. C. (1979) *Theor. Chim. Acta*, *53*, 21. (c) Zerner, M. C., Loew, G. H., Kirchner, R. F. and Mueller-Westerhoff, U. T. (1980) *J. Am. Chem. Soc.*, *102*, 589. (d) Edwards, W. D., Weiner, B., and Zerner, M. C. (1988) *J. Phys. Chem.*, *92*, 6188.

6. The near UV and visible spectra were obtained with a 10-mm quartz cell using a Hewlett-Packard HP 8452A diode array spectrophotometer. The absorption spectra were taken in carbon disulfide. These spectra were taken by collaborators W. Jentzen, M. C. Simpson, J. D. Hobbs, X. Song, and J. A. Shelnutt at Sandia National Laboratories.

7. Porphyrins were prepared by collaborators T. Ema, N. Y. Nelson, C. J. Medforth, and K. M. Smith at the University of California, Davis using published procedures (Lindsey, J. S., Schreiman, I. C., Hsu, H. C., Kearney, P. C., and Marguerettaz, A. M.

(1987) J. Org. Chem., 52, 827.)

8. Renner, M. W., Barkigia, K. M., Zhang, Y., Medforth, C. J., Smith, K. M., and Fajer, J. (1994) *J. Am. Chem. Soc., 116*, 8582.

Chapter 4. Interaction of Co(acacen) Derivatives with Carbonic Anhydrase

Introduction

In order to selectively target tumor tissues, it is necessary to have a means of differentiating them from the healthy counterparts. Since tumor cells generally have a low blood supply and high metabolism, the oxygen level in these cells is lower than in normal cells, making reductive reactions more favorable in tumor cells.[1] Thus, one possible way of selectively targeting tumor cells would be to activate a drug only in the reducing environment of a tumor cell. The reduction of octahedral Co(III) compounds to Co(II) compounds is one promising means of exploiting the reducing environment of tumor cells. While cobalt(III) compounds are kinetically inert to ligand substitution, reduction to cobalt(II) results in significant labilization of the ligands.[2] One method of exploiting this labilization upon reduction to cobalt(II) is the use of toxic nitrogen mustard axial ligands that would be selectively released upon entering the hypoxic tumor cells.[3] However, the synthesis of these complexes requires the preparation of Co(III) complexes that undergo relatively rapid substitution in the Co(III) oxidation state, since the nitrogen mustards are unstable in their free base form.[2] This results in high toxicity in healthy cells.

Another means of inducing cell death would be the inhibition of an enzyme that is crucial to the cellular life cycle. Studies with Co(III)acacen derivatives described later in this thesis have shown that these cobalt complexes can inhibit enzymes, raising the possibility that these cobalt complexes could cause cell death. Indeed, cytotoxicity studies[4] have shown that [Co(III)acacen$(NH_3)_2$]Cl, which exchanges ligands relatively rapidly, causes cell death and/or cell arrest within *Xenopus* blastulae. However, Co(III) complexes containing slowly exchanging ligands like imidazole (Im) such as [Co(III)acacen$(imidazole)_2$]Cl have relatively low cytotoxicity. This data suggests that the toxicity towards cells is directly related to the kinetics of ligand exchange. Facilitating this

ligand exchange process may further increase the toxicity of these cobalt complexes.

Reduction of the Co(III) complex to the corresponding Co(II) complex is one means of greatly increasing the ligand exchange process in these Schiff base acacen complexes.[5] If enzyme inhibition is the mechanism of the cytotoxicity, then this inhibition process may be enhanced upon reduction to Co(II). This increased rate in the substitution of axial ligands effectively frees up two coordination sites and greatly reduces the steric bulk of the complex, since [Co(II)acacen] is essentially planar. Furthermore, the [Co(II)acacen] complex becomes much more hydrophobic and may readily target the lipophilic interior of enzymes due to the loss of charge. {[Co(III)(acacen)$(NH_3)_2$]$^+$ is positively charged, whereas the corresponding [Co(II)(acacen)] is neutral.} These differences in the properties of the cobalt (III) versus cobalt (II) complexes should allow cobalt (II) complexes to inhibit enzymes where the corresponding Co(III) complexes cannot.

If it is possible to target enzymes with Co(II) acacen derivatives where Co(III) acacen derivatives have no effect, then the reduction of Co(III) complexes to Co(II) complexes may serve as a redox trigger for the activation of enzyme inhibitors within tumor cells. If the potential of the Co(III/II) redox couple were in a region where reduction to the Co(II) complex occurs only in tumor cells and not in healthy cells, then these cobalt complexes would be activated only upon entering the tumor cell. In this chapter the inhibition of carbonic anhydrase by a Co(acacen) derivative in the Co(II) and *not* the Co(III) oxidation state is described. The demonstration that Co(II)acacen derivatives exhibit inhibitory activity that the corresponding Co(III) complexes do not possess is an important step in the development of cobalt compounds that may selectively target tumor cells.

Carbonic anhydrase (CA) is a zinc containing enzyme that catalyzes the reversible hydration of carbon dioxide at nearly a diffusion controlled rate.[6] The catalytically essential zinc ion is bound to a distorted tetrahedron of three histidine residues and a water molecule at the base of a narrow 15 Å cleft. In addition to the histidines that serve as zinc ligands, there is a free histidine (HIS64) found at the mouth of the enzyme active site. Copper or mercury binding to HIS64 results in partial inhibition of catalytic activity.[7] In addition, mutagenesis of HIS64 to alanine results in significant loss of catalytic activity with respect to the native enzyme unless imidazole containing buffers are used.[8] These studies showed that HIS64 in native carbonic anhydrase II functions as a proton-shuttle group, providing a pathway for the transfer of protons between the active site and buffer molecules in solution. Since HIS64 binding by metals was found to inhibit CA, this enzyme could serve as a model target for inhibition by cobalt acacen derivatives, which have a high binding affinity for nitrogenous donors. In addition to the utility of CA as a model target, there is great pharmaceutical interest in CA inhibitors, since the inhibition of CA has been effective in the treatment of glaucoma.[9]

This study focuses on the inhibition of bovine carbonic anhydrase II,[10] which is more easily obtained than the human isozyme. Although there is no crystal structure for the bovine enzyme, the primary sequence[11] is very similar to that of the human isozyme, which has been crystallographically characterized.[12]

Materials and Methods

Bovine carbonic anhydrase II (EC 4.2.1.1) was purchased from Calbiochem. All other chemicals were of the highest quality available.

Synthesis of Hydroxypropyl Acacen. To 200 mL of deoxygenated CH_2Cl_2 was added 10 mL of acetyl acetone (Aldrich) (acac, 0.0974 mol) and cannulated into a 250 mL

addition funnel, which was attached to a 500 mL 3-neck roundbottom flask containing 100 mL of deoxygenated CH_2Cl_2 (EM Science) and 32.6 mL ethylenediamine (Sigma) (en, 0.488 mol). The solution containing the acac was added dropwise to the en solution. The reaction mixture was extracted with two 50 mL portions of 0.2 NaPi, pH 5.5. The organic layer was separated and placed in a -20 °C freezer overnight. The resulting solution was filtered through fluted filter paper (VWR Scientific) and the solvent was removed *in vacuo*. The compound was further purified using flash silica gel chromatography using 95:5:0.5 (v:v:v) CH_2Cl_2:MeOH:Et_3N as the eluant (EM Science, EM Science, Aldrich). The resulting monoacacen was characterized by NMR (300 MHz, D_2O): δ = 1.97 (s, CH_3), δ = 2.03 (s, CH_3), δ = 2.92 (t, CH_2), δ = 3.33 (t, CH_2), δ = 5.02 (s, CH).

Monoacacen (0.5 g, 3.5 x 10^{-3} mol) was added to one equivalent of 1-hydroxy-4,6-heptanedione, which was synthesized as described previously.[13] The reaction was allowed to proceed for 4 hours and the solvent was removed *in vacuo*. The sample was purified using flash silica gel chromatography using 93:7 (v:v) CH_2Cl_2:MeOH as the eluant. The resulting hydroxypropyl acacen was characterized by NMR (300 MHz, D_2O): δ = 1.74 (m, CH_2), δ = 1.83 (s, CH_3), δ = 1.86 (s, CH_3), δ = 1.93 (s, CH_3), δ = 2.33 (t, CH_2), δ = 3.36 (m, CH_2—CH_2), δ = 3.56 (t, CH_2), δ = 4.93 (s, CH), δ = 4.96 (s, CH).

Synthesis of Co(II)hydroxypropyl Acacen. Hydroxypropyl acacen (0.25 g, 9.4 x 10^{-4} mol) was dissolved in 2 mL of deoxygenated methanol in an inert atmosphere glove box. To this solution was added Co(II)$(CH_3COO^-)_2(H_2O)_4$ (0.2338 g, 9.4 X 10^{-4} mol). The mixture was allowed to stir for an additional 30 minutes. The solvent was removed *in vacuo* and the compound was used without further purification.

Synthesis of [Co(III)hydroxypropyl Acacen$(NH_3)_2$]$^+CH_3COO^-$. Hydroxypropyl acacen (hpr) was reacted with Co(II)$(CH_3COO^-)_2(H_2O)_4$ as described earlier. However,

before removing the solvent *in vacuo*, anhydrous ammonia gas was bubbled through the reaction mixture and subsequently exposed to air. The solvent was removed *in vacuo*, and the product was purified using an alumina column with neat methanol as the eluant. The sample was characterized by NMR (300 MHz, D_2O): δ = 1.84 (m, CH_2), δ = 2.05 (s, CH_3), δ = 2.22 (s, CH_3), δ = 2.23 (s, CH_3), δ = 2.36 (t, CH_2), δ = 3.52 (s, CH_2—CH_2), δ = 3.58 (t, CH_2), δ = 5.11 (s, CH), δ = 5.14 (s, CH) and mass spectrometry (ESI), MW expected 359.33 g/mol, found 359 g/mol.

Synthesis of Acacen. To 20 mL of ethanol was added 20 mL of acac (0.0973 mol). To this solution was added 6.5 mL of ethylenediamine (0.0973 mol) using an addition funnel. The solution was placed in a refrigerator at 4 °C overnight, and the crystals were triturated three times with anhydrous dietylether (m.p. = 110.1-111.1).

Synthesis of [Co(III)acacen(NH_3)$_2$]Cl. Cobalt acetate (249.08 g) was dissolved in 1.75 liters of methanol and the solution was filtered through Whatman paper no 1. The ligand was suspended in 150mL methanol. Nitrogen dried by passage through a silica gel desiccant column was bubbled over the reagents for 15 minutes. The cobalt acetate solution was added dropwise (1/2 hour) and the orange-brown solution was left to react at room temperature under nitrogen for 2 hours. The flask was opened, and anhydrous ammonia gas (Matheson) was bubbled into the solution. After filtration on a sintered glass buchner, the mixture was concentrated on a rotary evaporator. A solution containing one equivalent of sodium chloride dissolved in a minimum amount of water is added; the solution is then poured into a wide vessel, and left to crystallize slowly. The resulting brown crystalline powder was filtered, washed with methanol, and dried.

Affinity Chromatography. The affinity chromatography of carbonic anhydrase was carried out as described by Johansen.[14] Briefly, a benzenesulfonamide inhibitor of carbonic

anhydrase is coupled to sepharose 4B using a glycine-tyrosine spacer. CA was bound to the column equilibrated with 0.05 M Tris-sulfate pH 7.5, and eluted with 0.2 M potassium thiocyanate in 0.05 M Tris-sulfate pH 6.5. The excess thiocyanate is removed from the solution using a Centriprep protein concentrator (Amicon) and subsequent gel filtration chromatography using a PD-10 column (Pharmacia) equilibrated with 0.05 M Tris-sulfate pH 7.5.

Preparation of Apocarbonic Anhydrase. Apocarbonic anhydrase was prepared using the method described by Hunt *et al.*[15] CA (10 mg) was dissolved in 15 mL of 0.2 M NaPi pH 7.0, containing 0.1 M pyridine-2,6-dicarboxylic acid (referred to as "phosphate buffer") and placed in a Centriprep protein concentrator (Amicon). The solution was concentrated and refilled with phosphate buffer four times. Upon completion, the excess phosphate buffer from the concentrated sample was removed using gel filtration chromatography using a PD-10 column that was washed with phosphate buffer and equilibrated with zinc-free buffer (0.05 M Tris-HCl, pH 8).

Enzyme Assays. The activity of carbonic anhydrase was determined by monitoring the enzyme-catalyzed hydrolysis of *p*-nitrophenyl acetate.[16] *p*-Nitrophenyl acetate (*p*-NPA) was recrystallized from anhydrous diethyl ether and used without further purification. Acetonitrile (Fluka), used to prepare stock solutions of *p*-NPA, was used without further purification. Assays were initiated by adding 0.1 mL of 5 x 10^{-4} M *p*-NPA in acetonitrile to a 0.9 mL of 0.05 M Tris, pH 8 solution containing 1.555 x 10^{-6} M CA. The hydrolysis of *p*-NPA was followed spectrophotometrically by monitoring the appearance of the *p*-nitrophenolate anion at 400 nm.

Incubation of CA with [Co(III)(acacen)$(NH_3)_2$]Cl and [Co(III)(hpr)$(NH_3)_2$]OAc. CA (20 mg, 6.7 x 10^{-7} mol) was dissolved in 0.5 mL Tris buffer (pH 8, 0.05 M). To this

solution was added 30 mg of [Co(hpr)$(NH_3)_2$]OAc (30 mg, 7.6 x 10^{-5} mol) dissolved in 0.5 mL of H_2O. This solution was incubated for 48 hours. The excess cobalt complex was separated from the protein using a PD-10 gel filtration column equilibrated with Tris buffer (pH 8, 0.05 M). This enzyme, which was incubated with the Co(III) complex, retained 100% of its activity. CA (15 mg, 5 x 10^{-7} mol) was dissolved in 1.5 mL Tris buffer (pH 8, 0.05 M). To this solution was added [Co(acacen)$(NH_3)_2$]Cl (17.7 mg, 5 x 10^{-5} mol) dissolved in 0.5 mL of H_2O. The excess cobalt complex was separated from the protein using a PD-10 gel filtration column equilibrated with Tris buffer (ph 8, 0.05 M). This enzyme, which was incubated with the Co(III) complex, retained 100% of its activity.

Incubation of CA with Co(II)hpr. Two samples of CA (30 mg, 1 x 10^{-6} mol) were dissolved in 3 mL of degassed Tris buffer (pH 8, 0.05 M). To one of the samples was added Co(II)hydroxypropyl acacen (30 mg, 9 x 10^{-5} mol). The other sample of CA served as the control. The solutions were incubated under inert atmosphere (glove box) and a 1 mL aliquot was removed from each sample after 48 and 96 hours of incubation. The protein was then exposed to air and the excess Co(II)hydroxypropyl acacen separated from the protein using a PD-10 gel filtration column (Pharmacia) equilibrated with Tris buffer (Ph 8, 0.05 M). The enzymatic activity of the samples were determined, and the inhibition is described in Table 4.1.

Incubation of ApoCA with [Co(acacen)$(NH_3)_2$]Cl. ApoCA (3.33 x 10^{-8} mol) in 0.5 mL of 0.05 M Tris-sulfate, pH 7.5 (Tris-sulfate buffer) was incubated with 0, 1, 10, and 25 mole equivalents of Co(acacen)$(NH_3)_2$Cl dissolved in the Tris-sulfate buffer. After incubation of the samples overnight at 25 °C, 2 enzyme equivalents of zinc are added to the solution and allowed to incubate for 24 hours. The resulting solutions were purified by

Table 4.1. Inhibition of CA with [Co(II)hydroxypropyl-acacen].

Time of Incubation	Percent Inhibition of CA
48 hours	33.8%
96 hours	43.2%

affinity chromatography, and the enzyme was assayed for activity. The results are tabulated in Table 4.2.

Results and Discussion

In this work, the primary goal was to obtain an understanding of the interaction of Co(II)acacen derivatives with enzymes in comparison to the corresponding Co(III) complexes. However, since the unsubstituted [Co(II)acacen(H_2O)$_2$] complex[17] is neutral in charge and insoluble in water, the synthesis of a water soluble Co(II)acacen derivative was necessary in order to characterize the interaction of these Co(II) compounds with enzymes without the use of organic solvents, which could interfere with protein stability. Since the hydrophobic character of the Co(II) complexes may help target the lipophilic interior of enzymes, the synthesis of a neutral water soluble cobalt(II)hydroxypropylacacen (hpr) complex was devised in Figure 4.1.

Incubation of bovine carbonic anhydrase II (BCAII) with Co(II)hpr resulted in significant loss of activity versus the control as shown in Table 5.1. Since the activity loss upon incubation with the Co(II) complex was only partial, it was not clear whether a fraction of the enzyme was completely inhibited and another fraction was completely active, or whether all of the BCAII sample was partially inactivated. One means of separating active enzyme from inactive enzyme is the use of affinity chromatography.[7] A carbonic anhydrase inhibitor is tethered to a solid sepharose support and packed into a column. If the enzyme active site is accessible, then the inhibitor will bind to the enzyme, and the enzyme will be retained on the column. However, if the enzyme is completely inactivated, then the inhibitor will not bind to the protein, and the enzyme will flow through the column unimpeded.

Table 4.2. Inhibition of BCAII after Incubation with Apo-BCAII and Reincorporation of Zinc.

Equivalents of Cobalt Complex Added	Percent Inhibition
1	4.9%
10	49.3%
25	65.4%

Figure 4.1. Synthetic Scheme for the Synthesis of Water Soluble Co(II)(acacen) Derivatives. a) The first step is the synthesis of monofunctionalized acacen using excess ethylenediamine with dilute 2,4-pentanedione. b) The second step involves the reaction with a hydroxy functionalized dione (1-hydroxy-4,6-heptanedione). c) The metallation of the ligand under anaerobic conditions results in the formation of a water soluble Co(II) complex.

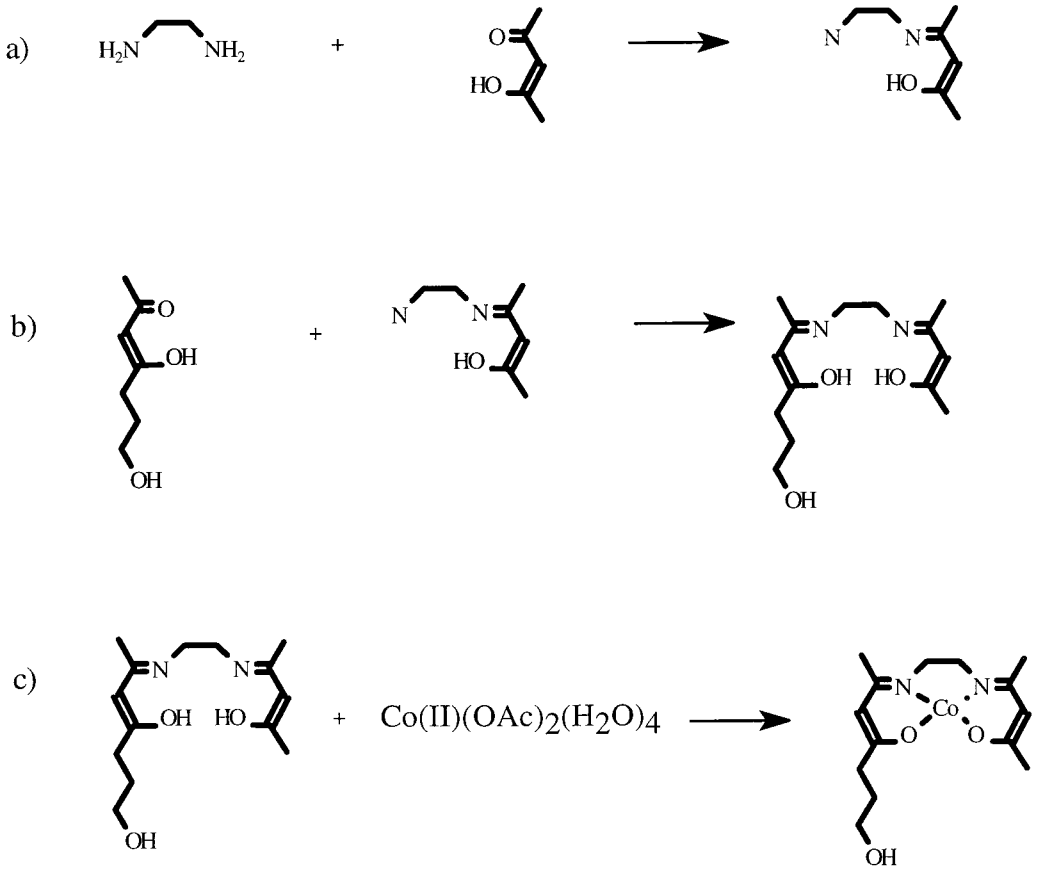

When the enzyme that was partially inactivated by Co(II)hpr was placed upon the affinity column, the BCAII was retained on the column (Figure 4.2). Since the inhibitor that is tethered to the affinity column normally interacts with the active site zinc, this suggests that zinc is retained in the enzyme and the active site of all the enzyme molecules is still accessible to external substrates. Control experiments have shown that the cobalt complex does not bind to the column, and cobalt bound enzyme lacking zinc does not bind to the affinity column. These experiments suggest that BCAII is partially inhibited by the Co(II) complex; however, the exact mechanism of inhibition is unclear. One possibility is the Co(II) complex binds to HIS64 at the mouth of the enzyme, which restricts the access of the enzyme substrate to the active site, but does not completely block it. Another possibility is the Co(II)hpr binds to internal histidines, altering the conformation of the enzyme and rendering the catalysis less effective (Figure 4.3).

When [Co(III)hpr$(NH_3)_2$]OAc is incubated with BCAII, there is no loss of enzyme activity. The inability of the Co(III) species at inhibiting BCAII may be due to the loss in hydrophobicity of the compound due to the positive charge added upon oxidation of Co(II) to Co(III) and the greater steric bulk of the Co(III)hpr complex. While Co(II)hpr is essentially planar due to rapidly exchanging axial ligands, axial ligand exchange with the Co(III) complex is much slower. The presence of the axial ligands on the cobalt(III) complex may prevent the inhibition of BCA by restricting the access to and binding to histidines.

If the Co(III) complex is prevented from binding to key histidines due to its excessive steric bulk, then one possible method of accessing these key histidines is by increasing the flexibility of the enzyme. One means of increasing the flexibility of the enzyme is removal of the zinc from the active site. Although the removal of the zinc

Figure 4.2. Affinity Chromatography Elution Profile after Incubation of Co(II)hpr with BCAII. Most of the enzyme was retained on the column, since the large majority of the protein eluted in fractions 22-30 rather than within fractions 5-10. Approximately 10mg of enzyme was injected onto a column containing 10 mL of packing.

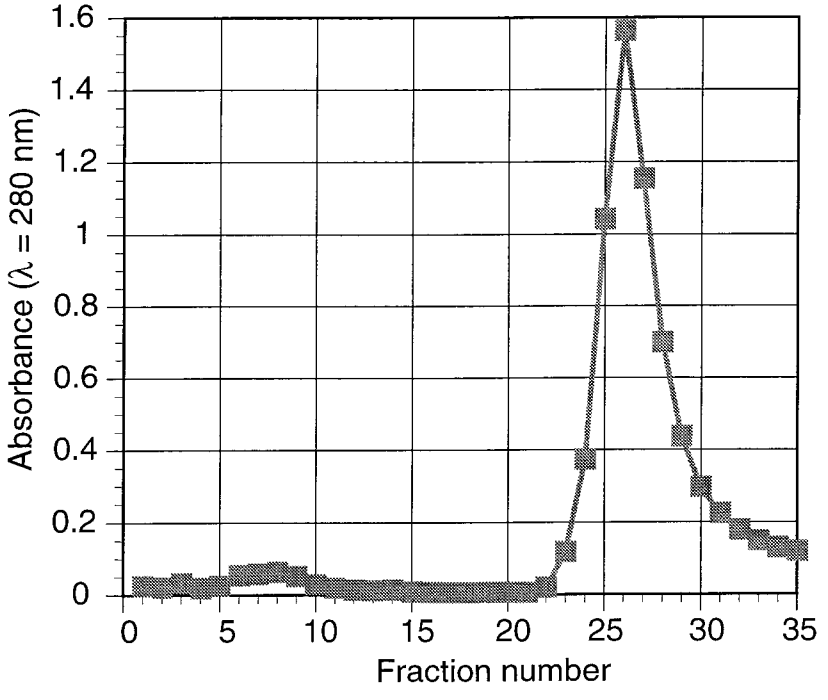

Figure 4.3. Possible Mechanisms of BCAII Inhibition by Co(II)hpr. a) The substrate access to the active site is normally unhindered. b) Upon interaction of the enzyme with the cobalt complex, there is binding of the compound to an internal histidine, causing a conformational change, rendering inhibition less effective. c) The cobalt complex binds to a histidine at the mouth of the active site, blocking access of the substrate, resulting in inhibition of the enzyme.

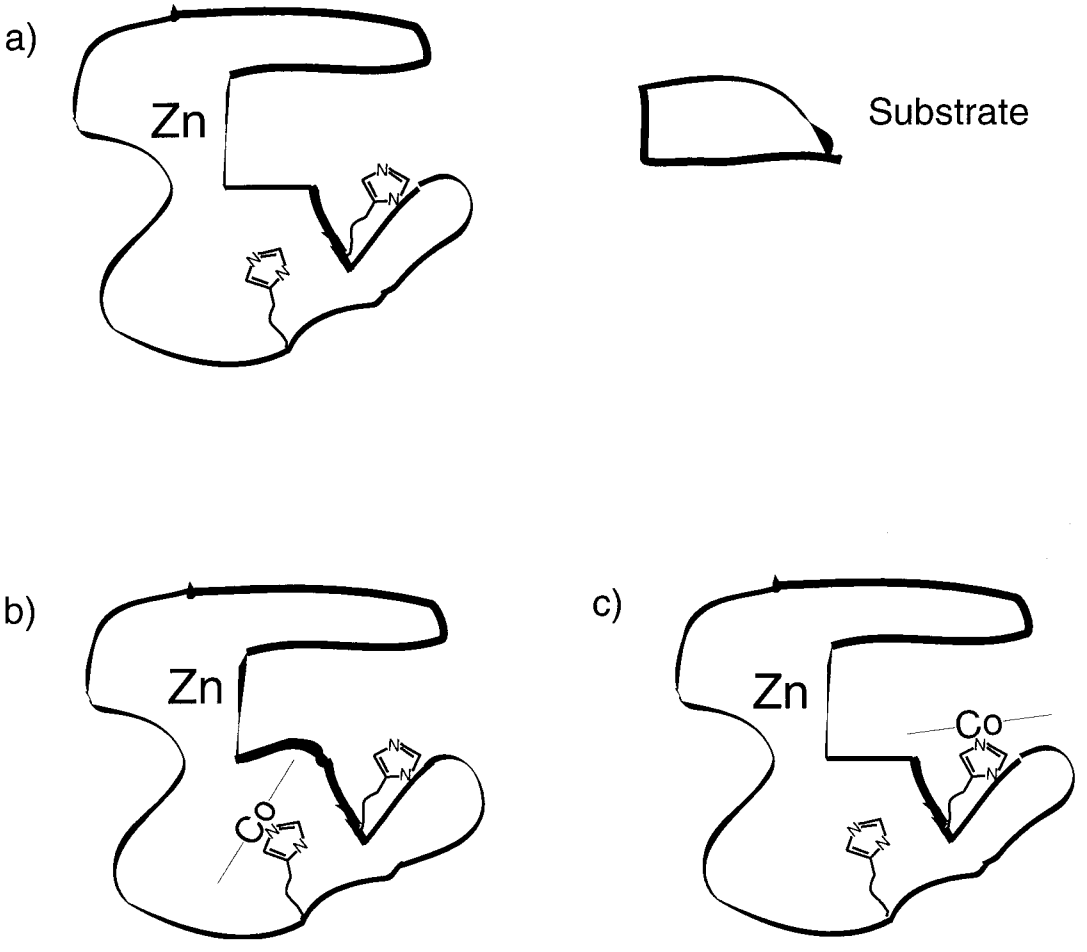

abolishes all catalytic activity, the zinc can be replaced after incubation with the Co(III) chelate. Another interesting possibility is that the cobalt complex will bind to the zinc-binding histidines, preventing the reincorporation of the zinc at the active site. After incubation of the Co(III) complex with apo-BCAII, two enzyme equivalents of zinc were added to the solution. When this solution was placed upon an affinity column, the enzyme bound to the column (Figure 5.4), which suggests the zinc reincorporated into the active site. Enzymatic assays showed partial inhibition of BCAII, with the degree of inhibition rising with increasing concentration of cobalt complex in the incubation.

Since the cobalt(III) complex cannot inhibit native BCAII, but can inhibit BCAII after binding to apo-BCAII and reincorporation of the zinc, this suggests that the cobalt compound is targeting a binding site that is inaccessible in the more structurally rigid native enzyme, but becomes accessible in the more flexible apo-enzyme. Since Co(II)hpr can inhibit the native enzyme, the less sterically restricted Co(II) complexes can access and target enzymes sites that Co(III) complexes cannot. One shortcoming of this work, however, is the lack of structural characterization of the inhibited species. Trypsin digests and cyanogen bromide cleavage of the protein framework resulted in the loss of cobalt binding to the enzyme due to the labilization of the ligand exchange process. One possible means of delineating the histidines targeted by the cobalt complex is to use site-directed mutagenesis to remove non-essential histidines and characterize the effect of the cobalt complexes upon these mutant enzymes. Another possibility is characterizing the crystal structure of the cobalt complexes bound to the enzyme. This possibility is under investigation in a collaboration with Professor David Christianson and graduate student Laura Scolnick at the University of Pennsylvania.

Figure 4.4. Affinity Chromatography Elution Profile Following the Reincorporation of Zinc after Incubation of 25 Equivalents of [Co(III)(acacen)(NH_3)$_2$]Cl with Apo-BCAII. Most of the enzyme was retained on the column, since the large majority of the protein eluted in fractions 12-17 rather than within fractions 4-5. Approximately 2.5 mg of enzyme was injected onto a column containing 3 mL of packing.

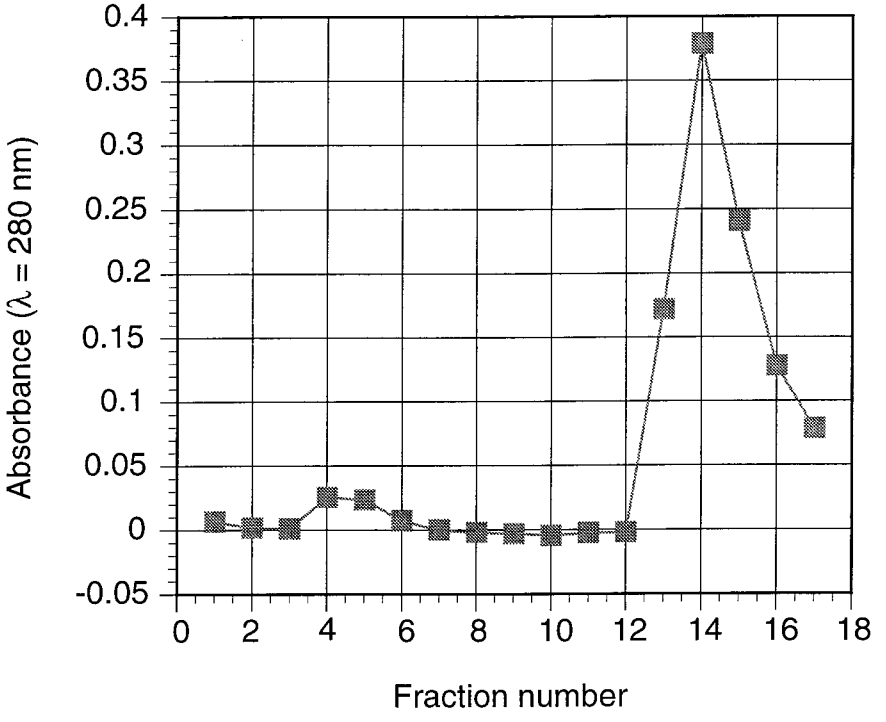

The cobalt(II) complexes in their present form are not viable as inhibitors due to their sensitivity to oxygen and their slow inhibition kinetics. However, the synthesis of electron-deficient ligand frameworks is being investigated (see Chapter 1), and cobalt complexes which may exhibit redox chemistry within biologically relevant conditions may be synthesized shortly. The inhibition kinetics of Co(II)hpr may be slow due to the lack of an accessible electron acceptor near the site of binding. However, in biologically relevant systems, the redox process may be mediated by glutathione buffers, which are present in high concentrations within cells. In the following chapter, the work with another target enzyme thermolysin is described. This target was chosen in order to get a better understanding of the mechanism of enzyme inhibition by Co(III)(acacen) derivatives.

References

1. (a) Sartorelli, A. C. (1988) *Cancer Research, 48*, 775. (b) Brown, J. M. and Koong, A. (1991), *J. Nat. Cancer Inst., 83*, 178.

2. Basolo, F. and Johnson, R. C. (1986) *Coordination Chemistry*, pp 97-119, Science Reviews.

3. Ware, D. C., Palmer, B. D., Wilson, W. R., and Denny, W. A. (1993) *J. Med. Chem., 36,* 1839-1846.

4. Louie, A. and Meade, T. J., unpublished results.

5. Böttcher, A., Takeuchi, T., Low, D. W., Hardcastle, K. I., Dori, Z., Gray, H. B., and Meade, T. J., in preparation for *Inorg. Chem.*

6. (a) R. P. Davis (1961) *The Enzymes, 5*, P. D. Boyer, Ed., Academic Press, New York, 545. (b) Maren, T. H. (1967) *Physiological Reviews, 47,* 595-781. (c) Silverman, D. N., Lindskog, S. (1988) *Acc. Chem. Res., 21,* 30-36. (d) Christianson, D. W. (1991) *Adv. Protein. Chem., 42,* 281-355.

7. (a)Tu, C., Wynns, G. C., and Silverman, D. N. (1981) *J. Biol. Chem. 256*, 9466-9470. (b) Eriksson, A. E., Kylsten, P. M., Jones, T. A., and Liljas, A. (1988) *Proteins: Struct. Funct. Gen. 4*, 283-293.

8. Tu, C., Silverman, D. N., Forsman, C., Jonsson, B.-H., and Lindskog, S. (1989) *Biochemistry, 28,* 7913-7918.

9. Maren, T. H. In *Carbonic Anhydrase: From Biochemistry and Genetics to Physiology and Clinic Medicine;* Botre, F., Gros, G., Storey, B. T., Eds.; VCH Publishers: New York, (1991), pages 186-207 and references therein.

10. (a) Nyman, P.-O. And Lindskog, S. (1964) *Biochim. Biophys. Acta, 85*, 141-151. (b)

Lindskog, S. (1960) *Biochim. Biophys. Acta, 39*, 218-226.

11. Sciaky, M., Limozin, N., Filippi-Foveau, D., Gulian, J.-M., and Laurent-Tabusse, G. (1976) *Biochimie, 58,* 1071-1082.

12. (a) Liljas, A., Kannan, K. K., Bergstén, P.-C., Waara-I., Fridborg, K., Strandberg, B., Carlbom, U., Järup, L., Lövgren, S., and Petef, M. (1972) *Nature New Biol., 235*, 131-137. (b) Eriksson, A. E., Jones, T. A., and Liljas, A. (1988) *Proteins Struct. Funct. Genet., 4,* 274. (c) Nair, S. K. And Christianson, D. W. (1991) *J. Am. Chem. Soc., 113*, 1991.

13. Detty, M. R. (1979) *J. Org. Chem., 44*, 2073-2077.

14. Johansen, J.T. (1976) *Carlsberg Res. Commun. 41*, 73-80.

15. Hunt, J. B., Rhee, M.-J., and Storm, C. B. (1977) *Anal. Biochem. 79*, 614-617.

16. Pocker, Y. and Stone, J. T. (1967) *Biochem. 6,* 668-678.

17. Morgan, G. and Smith, J. (1925) *J. Chem. Soc.,* 2030.

Chapter 5. Inhibition of Enzymes with Co(III) Schiff Base Derivatives

Inhibition of Thermolysin with $[Co(III)(acacen)L_2]^+$

Introduction

The discovery that cobalt(III) chelate complexes are efficient inhibitors of the herpes simplex virus has sparked considerable interest in this well studied chelate complex.[1] When the inhibition of viral replication was examined, it was found that these cobalt compounds inhibited the late stages of viral particle formation, leaving empty capsids lacking in DNA. This raises the possibility that these cobalt complexes are inhibiting an enzyme crucial for the maturation of viral particles. A possible target for these cobalt complexes is the serine protease that is encoded within the viral genome and is essential for proper capsid formation.[2] Although it may be feasible to analyze the effects of the cobalt complexes with this viral protease, the enzyme is not readily available and is difficult to work with due to its low catalytic activity.[3] However, if the source of the antiviral activity is indeed through enzymatic inhibition, then these cobalt complexes may be widely applicable towards a variety of enzymatic targets.

One possible mechanism of enzyme inhibition is covalent binding of the cobalt complex to an active site residue, resulting in the loss of enzymatic activity. Previous studies have shown that $[Co(acacen)(NH_3)_2]^+$ binds to apomyoglobin and metmyoglobin at a stoichiometry of 6:1; NMR and UV-visible spectroscopic data suggest that this binding occurs to enzyme histidines.[4] Since these cobalt chelate complexes have a binding affinity for histidines, one possible mechanism of enzyme inhibition is the exchange of weaker nitrogenous ligands such as amines, for the stronger imidazole moiety on enzyme histidine residues. There are a number of protein families that have histidine residues as part of the active site and include serine proteases, cysteine proteases, and RNases; many enzymes within these families have therapeutic interest.[5] However, for the purposes of

characterizing and understanding the mechanism of inhibition in this initial study, thermolysin was chosen as the model target enzyme because it is stable, well characterized, and readily available.

Thermolysin is a 34.6-kDa, zinc-containing neutral metalloendoprotease isolated from *Bacillus thermoproteolyticus*. The enzyme has been extensively characterized: its amino acid sequence[6] and three dimensional structure[7] are known. The enzyme has received a great deal of attention because it serves as an excellent model for pharmacologically and biologically interesting members of this class.[8] In addition, studies have shown that chemical modification of the histidine at the active site results in inactivation of the enzyme.[9] Thus, binding of the cobalt complex to active site histidines will result in loss of enzymatic activity.

Materials and Methods

Thermolysin (recrystallized 3 times from DMSO) was obtained from Calbiochem and initially dissolved in 0.1 M Tris (Sigma), 2.5 M NaBr (Aldrich), and 10 mM $CaCl_2$ (Aldrich), pH 7.2. This solution was further purified using gel filtration chromatography on an FPLC instrument using a Superdex 75 column (Pharmacia) equilibrated with 0.1 M Tris, 0.1 M NaBr, 0.01 M $CaCl_2$, pH 7.2 (henceforth described as "tris run buffer"). This stock solution was stored at 4 °C; and the enzyme concentration was determined by using $E_{1\%}^{280} = 17.65$[10] and a molecular weight[11] of 34,600 g/mol. UV-visible spectroscopy was performed using a Hewlett Packard HP8452A diode array spectrophotometer equipped with a Hewlett Packard HP89090A Peltier temperature control accessory. N-[3-(2-Furyl)acryloyl]glycly-L-leucinamide (FAGLA) (Sigma) was used as thermolysin substrate. A stock solution of FAGLA (4.0 mM) was prepared by dissolving the substrate in dimethylformamide (EM Science) (DMF) and diluting it with buffer to a final

concentration of 0.1 M Tris, 0.1 M NaBr and 10 mM $CaCl_2$, pH 7.0 (final concentration of DMF, 2.5%). Phosphoramidon (N-(α-L-rhamnopyranosyloxyphospho)-L-leucyl-L-tryptophan) was obtained from Calbiochem, and all other chemical reagents were of the highest quality available.

Synthesis of N,N'-ethylenebis(acetylacetoneimine) [acacen]. To 500 mL of ethanol was added 500 mL of 2,4-pentanedione (Aldrich) (acac). To this solution was added dropwise 162.5 mL of ethylenediamine using an addition funnel. The solution was stirred for 1 hr at 60 °C after the addition of ethylenediamine (Sigma) was completed. The ligand was crystallized from solution at 4 °C, filtered, and triturated 3x with anhydrous diethyl ether (EM Science), yielding a white solid, MP 110.1-111.1.

Synthesis of [Co(III)(acacen)(L)$_2$]Cl (L=2-Me-Imidazole, Imidazole, NH_3). The synthesis of Co(III)(acacen)L_2 complexes has been reported previously in the literature.[12] The synthesis of [Co(III)(acacen)$(NH_3)_2$]Cl is described here, and the other complexes were synthesized in an analogous fashion. Cobalt acetate (EM Science) (249.08 g) was dissolved in 1.75 liters of methanol (EM Science) and the solution was filtered through Whatman paper number 1. The ligand was suspended in 150 mL methanol. Nitrogen, dried by passage through a silica gel desiccant column, was bubbled over the reagents for 15 minutes. The cobalt acetate solution was added dropwise (1/2 hour) and the orange-brown solution was left to react at room temperature under nitrogen for 2 hours. The flask was opened to air, and when L = Imidazole or 2-MeIm, 2 equivalents of the ligand (Aldrich) were added to the solution. When L = NH_3, anhydrous ammonia gas (Matheson) was bubbled into the solution. After filtration on a sintered glass buchner, the mixture was concentrated on a rotary evaporator. A solution containing one equivalent of sodium chloride dissolved in a minimum amount of water was added and the solution was

poured into a wide vessel, and left to crystallize slowly. The resulting brown crystalline powder was filtered, washed with methanol, and dried.

Enzyme Assays. All steady-state enzyme assays were performed at 25°C using the spectrophotometric method of Feder and Schuck.[13] For all assays, the concentration of enzyme and substrate was 50 nM and 2.0 mM respectively. The peptidase activities of thermolysin were determined by following the decrease in absorption at 346 due to the enzymatic hydrolysis of FAGLA. Initial velocities were determined for ≤ 10% of the reaction.

Treatment of Thermolysin with [Co(acacen)(L)$_2$]Cl. Stock solution of thermolysin was mixed with the cobalt complex dissolved in tris run buffer to yield a final enzyme concentration of 10 μM and the cobalt concentration varying from 0.2 mM to 5 mM. These solutions were incubated at 25° C for several hours along with a control lacking cobalt complex. Periodically 5 μL aliquots of these solutions were assayed for residual enzyme activity by their addition to a spectrophotometric cuvette containing 495 μL of run buffer and 500 μL of the FAGLA stock solution and following the absorption decrease at 346 nm.

pH Dependence of the Inactivation of Thermolysin. The buffers used were: MES (pH 5.4) and Tris (pH 7.2, 8.6); all buffers were 0.1 M and contained 0.1 M NaBr and 0.01 M $CaCl_2$. Thermolysin (10 mM) was incubated at 25° C in the appropriate buffer with [Co(acacen)$(NH_3)_2$]Cl (2.5 mM). Periodically 5 μL aliquots were taken and assayed for residual enzyme activity.

Active Site Protection of Thermolysin. Thermolysin (10 μM, tris run buffer , pH 7.2) was incubated at 25 °C with Co(acacen)$(NH_3)_2$Cl (5 mM) in the presence and absence of the inhibitor phosphoramidon (50 μM), which has a reported K_I of 32 nM at

pH 7.5.[14] Phosphoramidon binds to thermolysin at the active site, and this enzyme-inhibitor complex has been crystallographically characterized.[15] After incubation with the cobalt complex overnight, the enzyme was separated from any phosphoramidon and cobalt complex that is not covalently attached to the enzyme using gel filtration chromatography on an FPLC instrument using a Superdex 75 column (Pharmacia) equilibrated with 0.1 M Tris, 5 mM $CaCl_2$, pH 9. The resulting solution was transferred into tris run buffer using a PD-10 column (Pharmacia), and characterized spectrophotometrically.

Model Studies for the Qualitative Evaluation of Ligand Exchange Rates. The conversion of $[Co(acacen)(NH_3)_2]^+$ to $[Co(acacen)(Im)_2]^+$ can be evaluated spectrophotometrically by monitoring the increase in absorption at 420 nm. After a rapid initial rise in absorbance (< 10 s), the subsequent increase in absorption (over several hours) fits a pseudo-first order rate law, showing an exponential rise to a maximum absorbance value. Although the entire ligand substitution process is complex and is under further investigation, the present study reveals that the kinetics of the slow component of the ligand substitution process is relevant to enzyme inhibition, since inhibition occurs within this longer time range. For pH 5.4, the experiments were performed in 0.1 M MES buffer, and for pH 7.2 and 8.6, the determinations were performed in 0.1 M Tris buffer; all solutions also contained 0.1 M NaBr, 0.01 M $CaCl_2$, 2.5 mM Im, and 0.25 mM $[Co(acacen)(NH_3)_2]Cl$. These pH dependence studies were performed at 25 °C. For the temperature studies, solutions contained 0.1 M NaBr, 0.01 M $CaCl_2$, 0.1 M imidazole, and 1.34 mM $[Co(acacen)(NH_3)_2]^+$. These studies were performed at both 25 °C and 37 °C.

Analysis of $[Co(acacen)L_2]Cl$:Enzyme Binding Ratios. The cobalt complex:enzyme binding ratios can be determined using UV-visible spectroscopy. The concentration of the cobalt complex in the solution is evaluated by measuring the

absorbance at 338 nm using an extinction coefficient of 6673 M^{-1} cm^{-1}, which is the extinction coefficient for [Co(III)(acacen)Im_2]Cl. The absorbance of the cobalt complex at 280 nm is calculated using interpolation from known absorbances based upon standards of [Co(III)(acacen)Im_2]Cl. (The absorbance of the cobalt complex at 280 nm does not follow Beer's law due to overlapping absorbance bands). Finally, the protein absorbance at 280 nm can be determined by subtraction of the cobalt complex absorbance at 280 nm. The protein concentration is calculated using $E_{1\%}^{280} = 17.65$[9] and a molecular weight of 34,600 g/mol.[10] This method was found to accurate to within ± 5%.

Atomic Absorption Measurements. Water was glass-distilled and passed through a primary deionization unit and a 0.2 μm postfilter cartridge (Barnstead). The solution was polished through a mixed-bed resin (Sigma). Plastic containers used for pipet tips, and eppendorf tubes were acid-cleaned first by rinsing with 1:40 nitric acid/water (vol/vol) and then by rinsing three times with zinc-free water. Samples were transferred into zinc-free water using a PD-10 column (Pharmacia) which was initially washed with 50 mL of 50 mM Tris, 2.5 mM 1,10-phenanthroline, pH 7.2, and then equilibrated with 50 mL of zinc free water. The resulting solutions were diluted 1:1 with Ultrex II concentrated nitric acid (J. T. Baker), and then heated at 60 °C for 6 hours. Atomic absorption measurements were taken on a Varian (AA-875) graphite furnace atomic absorption spectrophotometer.

Results and Discussion

Kinetics of Inactivation. The concentration dependent irreversible inhibition of thermolysin with [Co(acacen)$(NH_3)_2$]Cl is shown in Figure 5.1. If binding of the cobalt complex to thermolysin is the mechanism of enzyme inhibition, then this requires some form of ligand substitution process since the stable form of [Co(acacen)L_2]$^+$ is a six

Figure 5.1. Concentration Dependent Inhibition of Thermolysin with [Co(III)(acacen)(NH_3)$_2$]Cl. The concentration of the Co(III) inhibitor is shown in the figure legend.

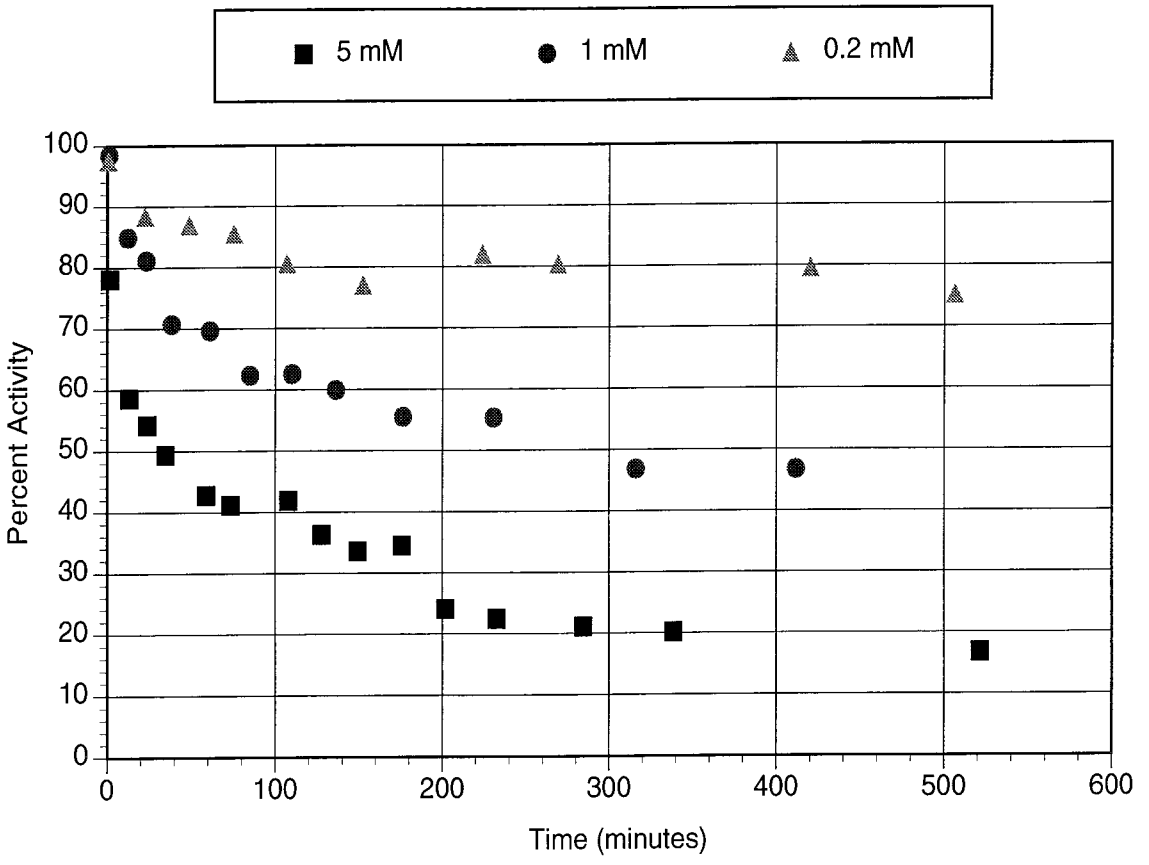

coordinate pseudo-octahedral geometry.[16] Substitution reactions are generally classified as having dissociative or associative mechanism. For the dissociative mechanism, the rate determining step is the loss of a ligand, forming a transient five coordinate complex, followed by rapid binding of the incoming ligand. For the associative mechanism, the rate determining step is the association of the incoming ligand, forming a seven-coordinate species, with rapid loss of the leaving group to form the six-coordinate product. The associative mechanism is unfavored in octahedral complexes due to the steric crowding about the coordination sphere and lack of suitable orbitals for the bonding of incoming ligands. Although a mechanism where the association of the incoming ligand is the rate limiting step cannot be ruled out, the majority of the data for the ligand exchange of octahedral Co(III) complexes in aqueous solution suggest that ligand dissociation is the most likely mechanism for ligand substitution:[17]

$$Co(acacen)L_2^+ \xrightarrow{slow} Co(acacen)L^+ + L \xrightarrow{E} Co(acacen)(L)(E)^+$$

If ligand loss is the rate limiting step in enzyme inhibition, then factors that increase the rate of axial ligand loss from the cobalt complex should increase the rate of enzyme inhibition. Ligand loss can be accelerated with the use of weaker donors such as ammonia (NH_3) or by generating unfavorable steric interactions between the axial ligand and acacen. The use of sterically restricted ligands increases the rate of ligand substitution by reducing the activation energy of ligand dissociation by relieving steric strain in the transition state.[16a] When the ligand is imidazole or a histidine residue, ligand exchange should be slow and unfavorable. The irreversible inactivation of thermolysin upon incubation with $[Co(III)(acacen)L_2]^+$, where L = imidazole (Im), NH_3, and 2-MeIm is shown in Figure 5.2.

Figure 5.2. Ligand Dependent Inhibition of Thermolysin. When the ligand is imidazole (Im), ligand substitution processes are slow, resulting in little or no loss of enzyme activity. In contrast, when the axial ligand is the more labile ammonia (NH_3) or 2-methylimidazole (2-MeIm), inhibition is observed.

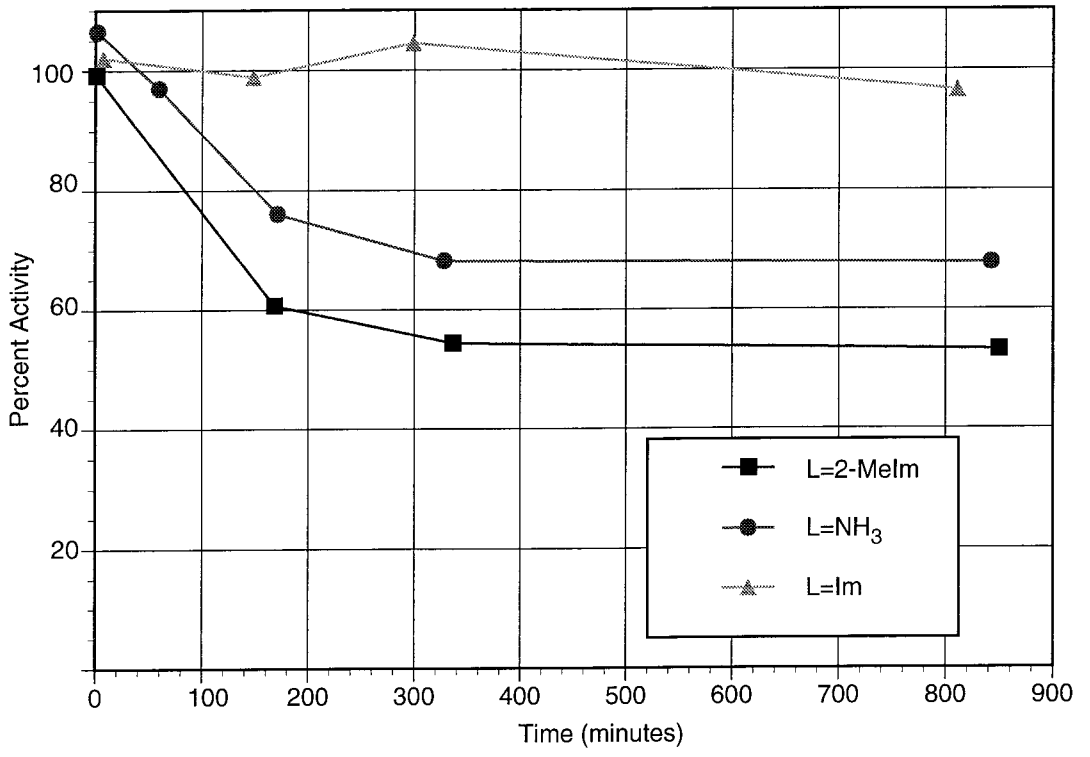

When Im is the axial ligand, there is little or no loss of enzymatic activity observed. This suggests that axial ligation of an imidazole ring results in the formation of a kinetically inert cobalt complex. This is a very important finding because the proposed mechanism suggests that binding to enzyme histidines results in a stable irreversibly bound complex. However, when NH_3 or the sterically bulky 2-MeIm are initially bound to the cobalt complex as axial ligands, incubation with thermolysin results in enzymatic inhibition. These data support the mechanism where a weak axial ligand bound to the cobalt complex exchanges with the imidazole ring of an enzyme histidine residue, resulting in the loss of enzymatic activity.

Temperature Dependence of Inhibition. Increasing the temperature at which the cobalt complex is incubated with thermolysin increases the rate of enzyme inhibition. In an effort to understand the basis of this rate increase, the temperature dependence of the rate of ligand exchange was carried out in a model system. Incubation of $[Co(acacen)(NH_3)_2]^+$ in a solution containing excess imidazole results in the formation of $[Co(acacen)Im_2]^+$; this conversion was spectrophotometrically monitored at 420 nm, and the observed rate was found to fit a first order rate law. Increasing the temperature of incubation in the model system resulted in a significant increase in the rate of formation of the bisimidazole cobalt complex from a rate of 1.4×10^{-2} s^{-1} to 7.5×10^{-2} s^{-1}. These experiments, shown in Figure 5.3, suggest that the increase in the rate of thermolysin inhibition at higher temperatures is at least partially attributable to an increase in the rate of ligand substitution of the cobalt complex.

pH Dependence of Ligand Exchange. The inhibition of thermolysin upon incubation with $Co(acacen)(NH_3)_2Cl$ was studied for the pH range of 5.4 to 8.6. The loss of enzyme activity was found to be slightly accelerated at lower pH values and decelerated

Figure 5.3. Temperature Dependence of the Rate of Enzyme Inhibition and the Rate of Ligand Exchange in a Model System. Left: The rate of enzyme inhibition increases when the temperature of incubation of [Co(acacen)$(NH_3)_2$]Cl with thermolysin is raised from 25 °C to 37 °C. The concentration of cobalt complex is 1.35 mM, and the concentration of thermolysin in the incubation solution is 1 x 10^{-5} M. Right: The rate of formation of [Co(acacen)$(Im)_2$]Cl upon incubation of [Co(acacen)$(NH_3)_2$]Cl in the presence of 0.1 M imidazole increases significantly when the temperature is raised from 25 °C to 37 °C. These experiments suggest that ligand exchange processes may be involved in the rate determining step of enzyme inhibition.

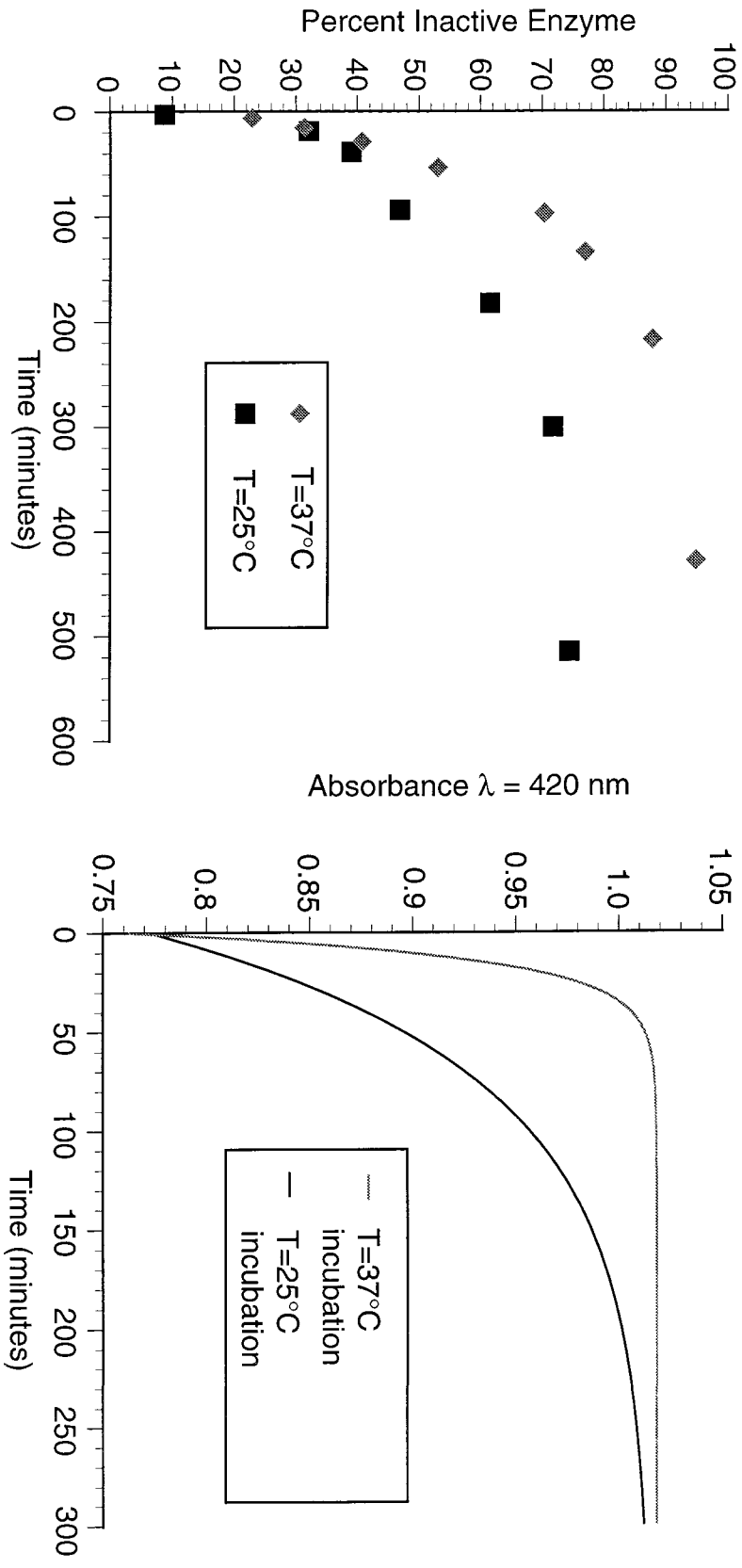
Percent Inactive Enzyme
100
90
80
70
60
50
40
30
20
10
0
0
100
200
300
400
500
600
Time (minutes)
T=37°C
T=25°C
Absorbance λ = 420 nm
1.05
1.0
0.95
0.9
0.85
0.8
0.75
0
50
100
150
200
250
300
Time (minutes)
T=37°C incubation
T=25°C incubation

at higher pH values (Figure 5.4). Since histidine would be protonated at lower pH and deprotonated at higher pH, binding of the cobalt complex to the histidine is disfavored at low pH and favored at higher pH. However, the loss of enzyme activity is increased at lower pH, suggesting that the rate determining step in the inhibition of thermolysin is *not* binding to the histidine residue. Model studies which monitored the exchange of amines with imidazoles showed an increase in the rate of ligand exchange at lower pH values, and a slight decrease in the rate of ligand exchange at higher pH. The observed rate increased from 2.92×10^{-4} s^{-1} to 3.40×10^{-4} s^{-1} to 4.82×10^{-4} s^{-1} when the pH of the experiment was decreased from 8.6 to 7.2 to 5.4. The finding that the slow step in the ligand exchange rate correlates with the enzyme inhibition kinetics further supports the hypothesis that ligand substitution kinetics rather than binding to histidines governs the rate of enzyme inhibition.

Active Site Protection. If binding of the cobalt complex to the active site HIS231 is the mechanism of enzymatic inhibition, then preventing the binding of the cobalt complex to the active site should prevent the loss of enzymatic activity. When thermolysin was treated with the strong competitive inhibitor phosphoramidon (K_I = 32 nM) in the presence of 5 mM [Co(acacen)$(NH_3)_2$]Cl, there was no detectable loss of enzyme activity due to irreversible inactivation by the cobalt complex. Spectroscopic characterization of this enzyme reveals the binding of two cobalt complexes. That inhibition is prevented by phosphoramidon, which binds at the active site of thermolysin, suggests that Co(acacen)$(NH_3)_2$Cl inactivates the enzyme by binding to the active site of the enzyme.

Characterization of Inhibited Thermolysin. After 12 hours of incubation of 10 μM thermolysin with 5 mM Co(acacen)$(NH_3)_2$Cl at room temperature, the excess cobalt

Figure 5.4. pH Dependance of Thermolysin Inhibition with [Co(III)(acacen)$(NH_3)_2$]Cl

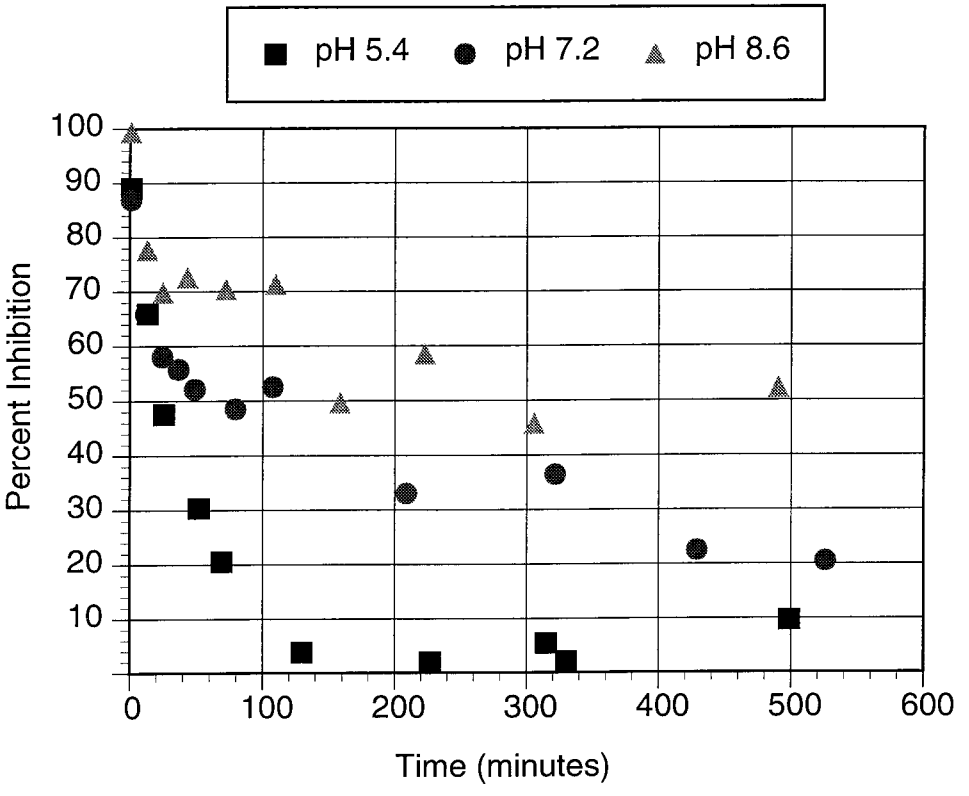

complex was removed using FPLC through a Superdex 75 column (Pharmacia) equilibrated with 0.1 M Tris, 0.1 M NaBr, 0.01 M $CaCl_2$, pH 7.2. Two peaks were found in the chromatogram. The first peak, which eluted after 11.5 mL of buffer, has no residual activity. After dialysis of this first fraction, UV-visible spectroscopy reveals the binding of three cobalt complexes for each enzyme molecule. These cobalt complexes remain bound to the enzyme for a period of several weeks, and no recovery of enzyme activity is observed. Reinjection of this fraction onto the FPLC column shows no change in the elution profile. The second peak, which eluted after 13.5 mL of buffer, has approximately 75% of the original enzyme activity, and shows the binding of approximately 2.5 cobalt complexes for each enzyme molecule. The retention time of peak two on the gel filtration column is identical to the native enzyme. If the second fraction is concentrated using centricon concentrator (Amicon), allowed to stand overnight at room temperature, and is reinjected into the FPLC, then only one major peak is found with the elution time of peak two. This peak has complete (100%) activity and no bound cobalt complexes.

Similarly, concentration and reinjection of the peak obtained after incubation of thermolysin with phosphoramidon and cobalt complex (described in the "Active Site Protection" section) resulted in complete loss of cobalt binding to the enzyme. The FPLC traces from the gel filtration of thermolysin, thermolysin after incubation with phosphoramidon, thermolysin after incubation with phosphoramidon and $[Co(acacen)(NH_3)_2]Cl$, and thermolysin after incubation with $[Co(acacen)(NH_3)_2]Cl$ is shown in Figure 5.5.

Peak one in Figure 5.5 elutes earlier from the gel filtration column than the native enzyme, suggesting that there must be perturbations from the native structure in the protein found in the first peak, since faster elution from a gel filtration column suggests an

Figure 5.5. Elution Profiles of Thermolysin Samples from FPLC on a Superdex 75 Gel Filtration Column. a) Native thermolysin b) Thermolysin + Phosphoramidon c) Thermolysin + Phosphoramidon + [Co(III)(acacen)$(NH_3)_2$]Cl d) Thermolysin + [Co(III)(acacen)$(NH_3)_2$]Cl

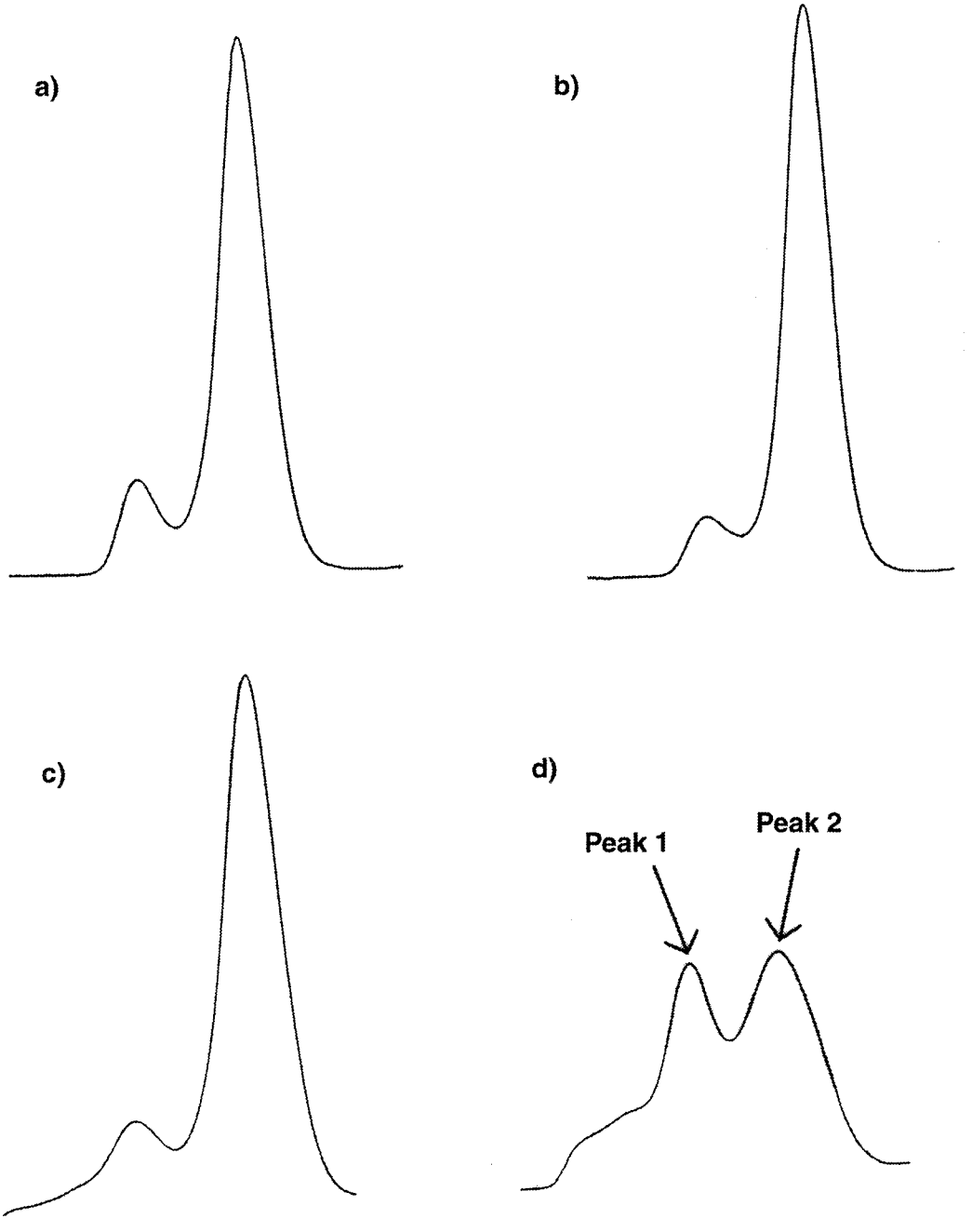
a)
b)
c)
d)
Peak 1
Peak 2

increase in the size of peak one with respect to the native enzyme. Simple modeling of the thermolysin active site using a known enzyme crystal structure[18] suggests that the proposed inhibited enzyme, $[Co(acacen)(NH_3)(HIS213\text{-}E)]^+$, would be a sterically constricted structure due to interactions of the acacen ligand with the zinc atom bound at the active site.

Two possible outcomes from these destabilizing interactions are the loss of zinc from the enzyme, or the dissociation of the cobalt complex from the active site of the enzyme. Atomic absorption measurements of peak one from the FPLC purification of thermolysin did not detect the presence of zinc within the sample. The loss of zinc from the enzyme may allow greater flexibility of the enzyme structure and may help accommodate the bound cobalt complexes by releasing steric strain and possibly providing a second axial ligand to stabilize the binding of the cobalt complex to the enzyme. One possible reason for the eventual loss of cobalt complexes from fraction two of the FPLC may be the lack of a suitable second enzyme-derived axial ligand for the cobalt complex, whereas the enzyme lacking zinc may allow enough flexibility to accommodate the cobalt complexes with a suitable second axial ligand.

Circular dichroism (CD) of peak one from the FPLC shows no apparent change in the secondary structure of the enzyme compared with the native enzyme (Figure 5.6). In contrast, the near-UV CD spectra show changes in tertiary structure attributable to perturbations in tyrosine or tryptophan residues of the enzyme (Figure 5.7). The increase in molar ellipticity suggests that some of the tyrosine (or tryptophan) residues within the protein may have acquired greater mobility due to changes in the packing environment. These small perturbations in the structure due to loss of zinc and the binding of three

Figure 5.6. CD Spectra of Thermolysin and Cobalt(III)-Modified Thermolysin.

Fraction 1 is the first peak from the FPLC purification of Thermolysin + [Co(III)(acacen)$(NH_3)_2$]Cl in Figure 5.5. The control is native thermolysin.

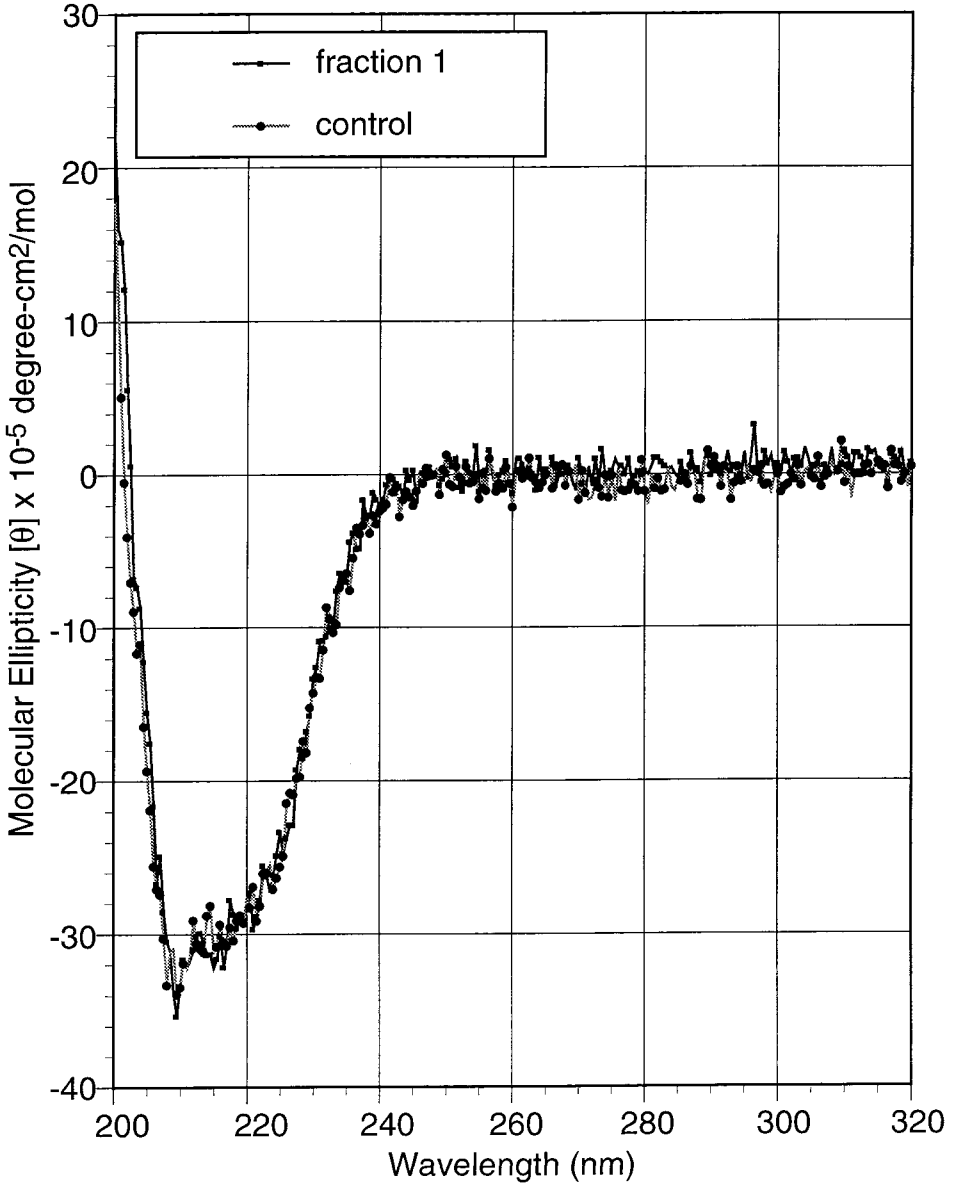

Figure 5.7. Near-UV CD Spectra of Thermolysin and Cobalt(III)-Modified Thermolysin. Fraction 1 is the first peak from the FPLC purification of Thermolysin + [Co(III)(acacen)(NH_3)$_2$]Cl in Figure 5.5. The control is native thermolysin.

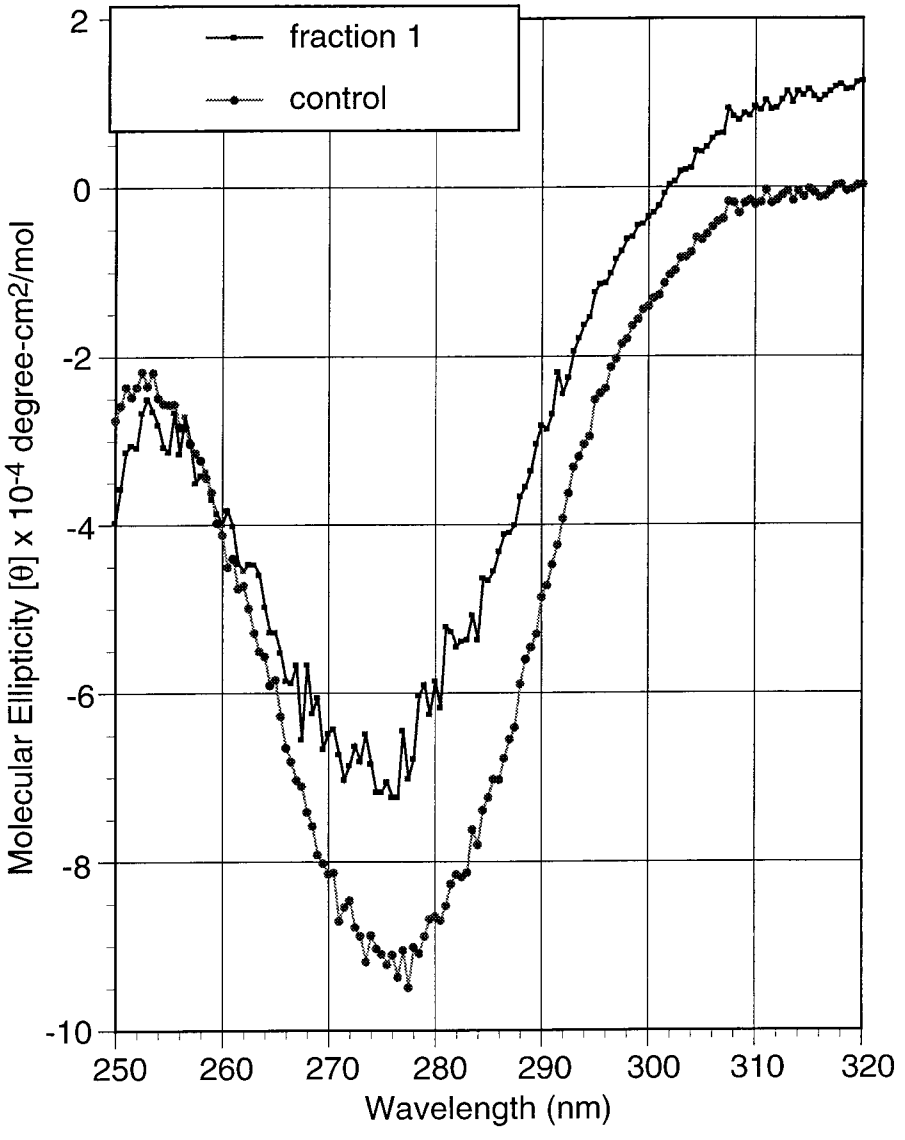

equivalents of cobalt complex may increase the overall size of the enzyme and decrease the elution time of fraction one in comparison to the native enzyme in the FPLC runs.

Further characterization of the inhibited enzyme were attempted using trypsin digests and cyanogen bromide cleavage of the enzyme in 70% formic acid. However, these experiments failed due to the loss of cobalt binding from the enzyme. In the case of trypsin digests, the high temperature required for enzyme denaturation resulted in loss of the cobalt from the enzyme. This is not surprising, since there is a great increase in the rate of ligand exchange upon increasing the temperature as shown in Figure 5.3. Isolation of cobalt bound peptide fragments from cyanogen bromide digestion probably failed due to the acid labilization of ligand exchange, as observed in the model studies of pH dependance of ligand exchange.

Cobalt:Enzyme Binding Ratios. Spectrophotometric characterization of the completely inhibited thermolysin species (Peak 1 in Figure 5.5) showed the binding of three cobalt complexes to thermolysin. Characterization of the thermolysin after incubation with both phosphoramidon and the cobalt complex showed the initial binding of two cobalt complexes. Since protection of the enzyme active site prevented the binding of one equivalent of cobalt complex *and* protected the activity of the enzyme, this suggests that the enzyme was inhibited by the binding of one cobalt chelate to the active site of the enzyme. Although the exact location of binding was not elucidated, the likely target for the binding is HIS231 at the active site.

Model of Enzyme Inhibition. The model of enzyme inhibition is proposed to be as follows:

$$[Co(acacen)L_2]^+ + E\text{-}Zn \underset{k_2}{\overset{k_1, -L}{\rightleftharpoons}} [Co(acacen)L]^+ + E\text{-}Zn \underset{k_4}{\overset{k_3}{\rightleftharpoons}}$$

$$[Co(acacen)L]^+ \bullet E\text{-}Zn \underset{k_6}{\overset{k_5}{\rightleftharpoons}} [Co(acacen)L]^+ - E\text{-}Zn$$

The first step in the reaction scheme is the loss of an axial ligand so the cobalt becomes coordinatively unsaturated. This rate k_1 is proposed to be slow and rate limiting in the reaction scheme. The ligand exchange as the rate limiting step is supported by the temperature, axial ligand, and pH dependance of ligand exchange. This loss of ligand is followed by the formation of the enzyme-inhibitor complex which forms a slowly reversible cobalt complex bound enzyme species. The spectrophotometric binding results and the active site protection studies strongly suggest that the inhibition is a result of the binding of the cobalt complex to the active site of thermolysin. The formation of $[Co(acacen)L]^+$–E-Zn is proposed to be the fast component of the inhibition profile (Figure 1). However, a small amount of activity still persists in the sample due to the slight reversibility of the inhibitor bound enzyme species (i.e., k_6 is slow but observable in the assay). This residual activity decreases as the inhibitor bound enzyme slowly converts into a stable, irreversible, inhibitor-bound enzyme species that lacks zinc.

This slow loss of zinc (k_7 in the scheme below), which is supported by atomic absorption experiments, can be attributed as the slow component of the inhibition profile shown in Figure 5.1:

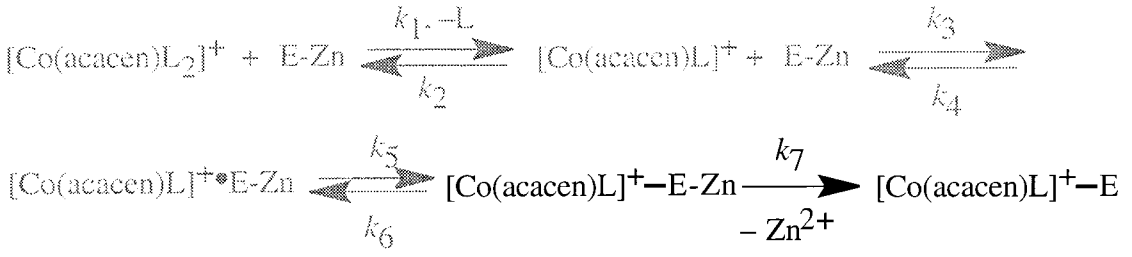

These initial studies show that cobalt schiff base complexes can irreversibly inhibit thermolysin by targeting the enzyme active site, and this activity towards enzymes may be generalized to a large variety of enzymes containing active site histidines. Current studies are focused on demonstrating the ability to gain affinity and selectivity towards enzymes by linking enzyme specific targeting groups to the periphery of the schiff base ligand.

Inhibition of Thrombin with Co(III)(acacen) Derivatives

Introduction

Thrombin is a protease that has received attention because of its central role in the blood coagulation cascade.[19] Thrombin converts fibrinogen into fibrin, which forms the blood clot. In addition, it is involved in the activation of other blood coagulation factors such as V, VIII, XIII, and protein C. Thrombin activity is thought to play a role in the reocclusion of coronary arteries after thrombolytic therapy following a heart attack,[20] demonstrating the need for more potent and specific inhibitors of thrombin.

Thrombin is a trypsin-like serine protease containing the catalytically essential histidine, serine, and aspartate triad at the active site of the enzyme. Many compounds have been reported to inhibit thrombin by using small inhibitors directed at this active site, such as derivatives of a tripeptide, D-Phe-Pro-Arg, which have excellent potency and selectivity toward thrombin.[21] Other selective inhibitors of thrombin have been directed toward both the active site of thrombin and at an additional fibrinogen recognition exo site (FRE) of the enzyme.[22] The paradigm for this mode of inhibition is hirudin, which is a 65 amino acid protein produced by the leech *Hirudo medicinalis*. Hirudin binds very tightly to thrombin with a $K_d \approx 10^{-14}$ M,[23] with the C-terminal amino acid fragment (residues 55-65) binding to the FRE,[24] while the N-terminal fragment blocks the catalytic active site.

Cobalt(III) acacen derivatives have been shown to inhibit enzymes containing histidines at the active site of the enzyme. Since thrombin contains an active site histidine, these cobalt complexes may serve as a novel means of inhibiting thrombin and may be developed into therapeutic agents. The first step in developing potential drugs is the development of compounds with specificity and selectivity towards target enzymes. In this

study we demonstrate this principle by rationally designing and synthesizing novel thrombin active site-directed cobalt(III) acacen derivatives.

Materials and Methods

Human α-thrombin (3037 NIH units/mg) and substrate Spectrozyme TH (H-D-hexahydrotyrosyl-L-alanyl-L-arginine-*p*-nitroanilide-diacetate salt) were purchased from American Diagnostica. All other reagents were of the highest quality available and purchased from Sigma unless otherwise noted.

Preparation of Thrombin Stock Solutions. Thrombin (1 mL of 30 μM enzyme in 0.75 M sodium chloride solution) was divided into 100 μL aliquots and diluted to 10 mL using aqueous 0.75 M NaCl. These 10 mL samples were divided into 1 mL aliquots and stored frozen at -80 °C until used. Samples should not be stored at -20 °C, which is close to the eutectic point for the thrombin-salt mixture, since freeze-thaw cycling may damage the enzyme.

Peptide Synthesis. Peptide NH_2-Gly-Gly-Gly-D-Phe-Pro-Arg-$CONH_2$ was prepared by the Beckman Institute Biopolymer Synthesis Group (Caltech) on *p*-methylbenzhydrylamine (MBHA) resin using N-*tert*-butyloxycarbonyl (Boc) amino acid derivatives for Merrifield solid-phase synthesis on an ABI Model 430A peptide synthesizer. The terminal Boc protecting group was removed with triflouoroacetic acid (TFA). Side chain protecting groups and the peptide-resin bond were cleaved under HF conditions (90% HF, 5% *p*-cresol, 5% *p*-thiocresol). After removal of HF under vacuum, the peptide/resin mixture was washed on a fritted funnel with ether. The peptide was then dissolved in 10% aqueous acetic acid and filtered through, leaving the resin behind. The crude peptide solution was subjected to gel filtration on anion exchange resin AG 1-X2 to remove the scavengers. The peptide was further purified by reversed-phase HPLC on a

Vydac C8 column using a 30-min. linear gradient of 6 - 26% acetonitrile/water/0.1% TFA with a 2.0 mL/min. flow rate. The peptide was characterized by NMR (300 MHz, D_2O): δ = 1.68-2.01 (m, 6 H, γ-Pro, γ-Arg, β-Arg), δ = 2.25 (m, 2 H, β-Pro), δ = 2.96 (m, 2 H, β-Phe), δ = 3.20 (t, 2 H, δ-Arg), δ = 3.53 (m, 2 H, δ-Pro), δ = 3.84 (s, 4 H, α-Gly), δ = 3.97 (s, 2 H, α-Gly), δ = 4.29 (m, 1 H, α-Arg), δ = 4.41 (m, 1 H, α-Pro), δ = 4.54 (m, 1 H, α-Phe), δ = 7.3-7.5 (m, 5 H, Phe). Observed m/Z^+ was 589 as expected.

Enzyme Assays. Enzyme-catalyzed hydrolysis rates were measured spectrophotometrically using a Hewlett Packard HP8452A diode array spectrophotometer equipped with a Hewlett Packard HP89090A peltier temperature control accessory. The peptidase activities of thrombin were determined by following the decrease in absorption at 406 nm due to the enzymatic hydrolysis of Spectrozyme TH. Initial velocities were determined for $\leq$ 10% of the reaction. All assays were performed in 10 mM Tris, 10 mM HEPES, 0.1% polyethylene glycol, 0.5 M NaCl, pH 7.8 (run buffer) using 3.07 x 10^{-9} M thrombin and substrate concentrations ranging from 1 μM to 50 μM, depending upon the experiment.

Treatment of Thrombin with Co(III)acacen Derivatives. Stock solution of thrombin was mixed with the cobalt complex dissolved in run buffer to yield a final enzyme concentration of 3.10 x 10^{-9} M and the cobalt concentration varying from 100 μM to 1 μM concentrations, and a total volume of 992 μL. These solutions were incubated at 25° C for several hours along with a control lacking cobalt complex. Periodically a vial was assayed for residual enzyme activity by the addition of the sample to a spectrophotometric cuvette and subsequent addition of 8 μL of 5 mM Spectrozyme TH to initiate the reaction. This showed the reversible and irreversible interactions of the cobalt complex with thrombin. In order to determine the irreversible interaction of the enzyme

with the cobalt compounds, stock solution of thrombin was mixed with the cobalt complex dissolved in run buffer to yield a final enzyme concentration of 1.54 x 10^{-7} M thrombin and the cobalt concentration varying from 50 μM to 500 μM. These samples were incubated at 25° C for several hours along with a control lacking cobalt complex. Periodically 20-μL aliquots of these solutions were assayed for residual enzyme activity by their addition to a spectrophotometric cuvette containing 972 μL of run buffer and 8 μL of 5 mM Spectrozyme TH solution.

Determination of K_I of $NH_2GGGdFPR\text{-}CONH_2$. The K_i value for the peptide was determined by plotting v_0/v_i versus [I] plots ($v_0/v_i = [I]/K_I(1 + [S]/K_m) + 1$) using a K_m value of 2.45 x 10^{-6} M for Spectrozyme TH.[25] The determinations were performed using three different concentrations of Spectrozyme (10 μM, 40 μM, and 100 μM) and peptide concentrations ranging from 1 mM to 20 mM.

Synthesis of "Aciden." This synthesis of aciden, the synthesis of acacaciden, and the synthesis of [Co(III)acacaciden$(NH_3)_2$] were developed and performed by Kevin Hoke and later by Arnd Böttcher. (See Figure 5.10 for a synthetic scheme.) To a solution of one equivalent of 4,6-dioxoheptanoic acid (Aldrich) in CH_2Cl_2 (EM Science) was added one equivalent of ethylenediamine (Aldrich) in CH_2Cl_2 and the insoluble 1:1 condensation product immediately precipitated. The product was collected and dried *in vacuo*. The resulting aciden was characterized by NMR (300 MHz, D_2O): δ = 2.03 (s, CH_3), δ = 2.38-2.47 (m, CH_2-CH_2), δ = 3.12 (t, CH_2), δ = 3.58 (t, CH_2), δ = 5.21 (s, CH). MP = 140 °C.

Synthesis of "Acacaciden." One equivalent of aciden was powdered and slurried in methanol (Fluka). One equivalent of triethylamine and 2 - 2.5 equivalents of acac were added. The mixture was allowed to stir overnight to give a yellow solution. The reaction mixture was evaporated to dryness to obtain the crude product as an orange oil. Further

purification was accomplished using silica gel flash chromatography using a 5% to 25% gradient of MeOH in CH_2Cl_2 with 0.5% TEA to guard against hydrolysis of imine bonds in acidic solution. The solvent was removed *in vacuo* and the solid was recrystallized from EtOH to give a beige solid. The resulting acacaciden was characterized by NMR (300 MHz, $CDCl_3$): δ = 1.87 (s, CH_3), δ = 1.92 (s, CH_3), δ = 1.97 (s, CH_3), δ = 2.57 (s, CH_2-CH_2), δ = 3.43 (s, CH_2-CH_2), δ = 4.97 (s, CH), δ = 4.99 (s, CH), δ = 10.80 (s, OH), δ = 10.85 (s, OH). Observed m/Z^+ was 282 as expected.

Synthesis of [Co(III)acacaciden(NH_3)$_2$]. One equivalent of acacaciden was degassed *in vacuo* and placed under argon. Dry, degassed methanol was transferred into the flask via cannula. One equivalent of cobaltous acetate was dissolved in the degassed methanol and the resulting purple solution was added via cannula to the clear solution of the ligand. An immediate color change from purple to orange was observed as the reaction was stirred under argon for 2 hours. Ammonia gas was bubbled into the solution and the flask was opened to air. The reaction was stirred with ammonia for four hours. The reddish solution was filtered and concentrated. The reaction mixture was purified over cation exchange (G-25, Pharmacia) using aqueous ammonium acetate, followed by removal of the volatile buffer to give a light brown powder. Cobalt bromide and cobalt chloride were also used in the synthesis, and the compound was recrystallized instead of purified with cation exchange. The resulting *[Co(III)acacaciden(NH_3)$_2$]* was characterized by NMR (300 MHz, D_2O): δ = 2.07 (s, CH_3), δ = 2.15 (s, CH_3), δ = 2.24 (s, CH_3), δ = 2.54 (m, CH_2-CH_2), δ = 3.59 (s, CH_2-CH_2). The vinyl protons were obscured by the solvent peak. Observed m/Z^+ was 373 as expected.

Coupling of NH_2GGGdFPR-$CONH_2$ to Acacaciden. The peptide coupling reaction and NMR characterization was performed by Kevin Hoke. [Co(III)acacaciden(NH_3)$_2$]

was dissolved in 0.1 M HEPES buffer, pH 8 at 5 °C. One equivalent of peptide dissolved in the same buffer was added. Five equivalents of 1-(3-dimethylaminopropyl)-3-ethylcarbodiimide (EDC) were added directly to the solution. Four hours later, another 5 equivalents were added. The reaction was stirred overnight at 5 °C, then lyophilized to give a reddish brown product. The crude material was purified over cation exchange resin (G-25, Pharmacia), eluting with ammonium acetate. One major product and a minor product were collected, but only the major product was further purified and characterized by NMR. This major product was purified on HPLC using a Vydac C18 column with 0-30% acetonitrile gradient over 70 minutes, with 50 mM ammonium acetate pH 6.5 as the aqueous component. The peptide was characterized by NMR (300MHz, D_2O): δ = 1.63-1.8 (m, 4H, γ-Pro, γ-Arg, β-Arg) (2 H partially obscured by acetate from HPLC buffer), δ = 2.05 (shoulder, CH_3 (ligand)), δ = 2.15 (s, 3 H, CH_3), δ = 2.23 (s, 3 H, CH_3), δ = 2.35 (m, 2 H, β-Pro), δ = 2.61-2.75 (m, 4 H, CH_2-CH_2), δ = 2.86 (m, 2H, β-Phe), δ = 3.19 (m, 2H, δ-Arg), δ = 3.58-3.60 (m, 4 H, CH_2-CH_2), δ = 3.65 (m, 2 H, δ-Pro), δ = 3.92-3.94 (m, 6 H, α-Gly), δ = 4.26 (m, 1 H, α-Arg), α-Pro, α-Phe not observed, δ = 7.26-7.37 (m, 5 H, Phe).

Synthesis of Symmetric [Co(III)(acacen)(L_2)] Derivatives. See the thermolysin section for synthesis of these complexes. In the case of the trifluoroacacen, the compound was synthesized using the same procedure as acacen, but 1,1,1-trifluoro-2,4,-pentanedione was used instead of 2,4-pentanedione (acac). Similarly, in the case of Cl-acacen, 3-chloro-2,4-pentanedione was used instead of acac.

Results and Discussion

In earlier studies with thermolysin, it was found that the enzyme is inhibited with [Co(III)(acacen)(NH_3)$_2$]Cl concentrations on the order of 1 mM. The inhibition kinetics

toward thermolysin is comprised of an initial rapid decrease in the enzyme activity, followed by a slower decrease in the loss of enzyme activity. It was proposed that binding to the thermolysin active site was sterically restricted, and the second slower decrease in enzyme activity resulted from the loss of zinc from the active site of the enzyme. In contrast with thermolysin, there is rapid irreversible loss of enzyme activity in the inhibition of thrombin with [Co(III)(acacen)$(NH_3)_2$]Cl (Figure 5.8).

This increase in the rate of enzyme inhibition may result from greater access of the cobalt complex to the active site of thrombin compared with thermolysin. Thermolysin has an affinity for hydrophobic residues, whereas thrombin cleaves after positively charged residues like lysine and arginine.[26] Since [Co(III)(acacen)$(NH_3)_2$]$^+$ is positively charged, binding to the thrombin active site should be favored over the thermolysin active site due to the coulombic attraction to the aspartate in the thrombin active site. In addition, the histidine at the active site of thermolysin is protonated at pH 7; this histidine is thought to stabilize the oxyanion created in the transition state of peptide bond breaking. In contrast, the thrombin histidine serves as a general base in the catalytic triad found in all serine proteases. The positive charge on the protonated histidine of thermolysin would repel the positively charged cobalt complex, making the formation of an initial enzyme-inhibitor complex unfavorable compared with complex formation to the neutral histidine in the thrombin active site. These combined factors probably serve to increase the affinity for the thrombin active site over the thermolysin active site and significantly increase the rate of enzyme inhibition.

In addition to the increased rate of binding of [Co(acacen)$(NH_3)_2$]Cl with respect to thermolysin, similar rate increases are seen when the ligand is 2-MeIm, while the inhibition when imidazole is the ligand is still not observed (Figure 5.9). The rate of

Figure 5.8. Irreversible Inhibition of Thrombin with [Co(III)(acacen)$(NH_3)_2$]Cl.

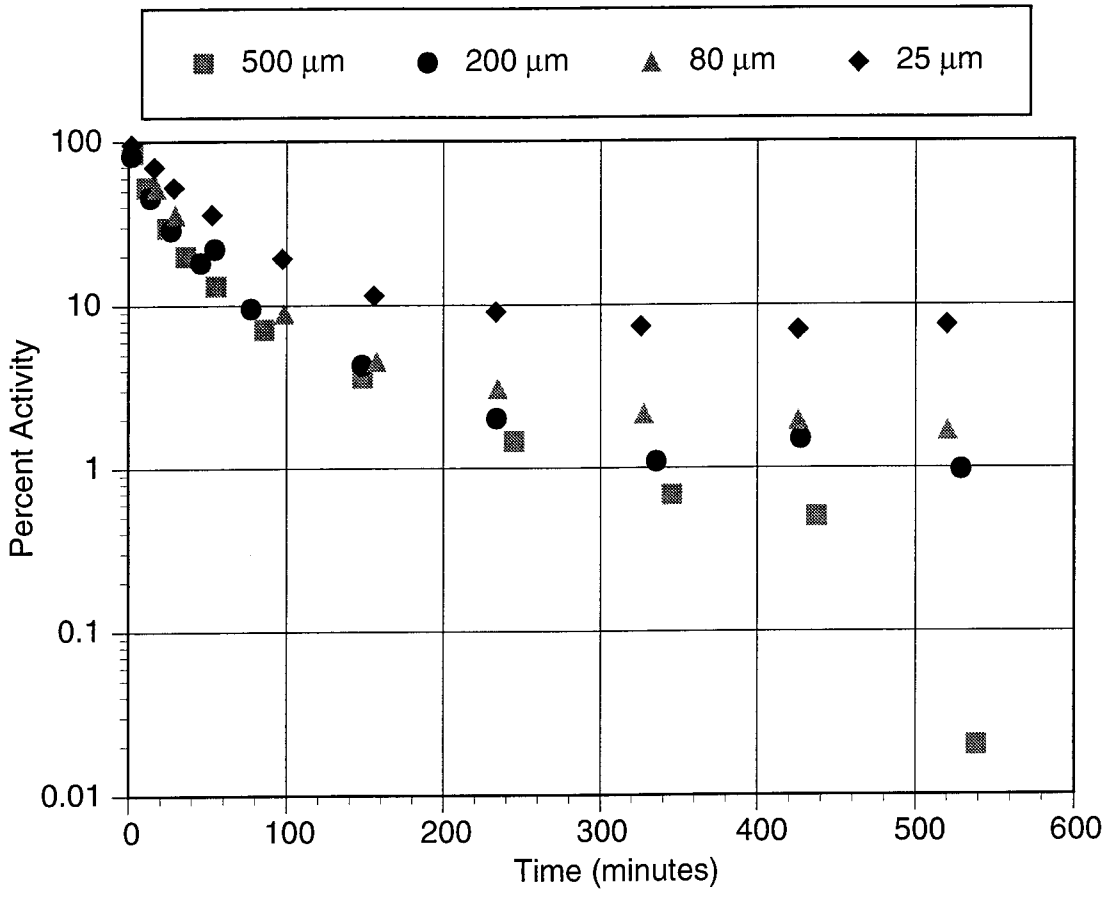

Figure 5.9. Inhibition of Thrombin with 500μM $[Co(acacen)(L)_2]^+$: Dependence of Inhibition upon the Axial Ligand.

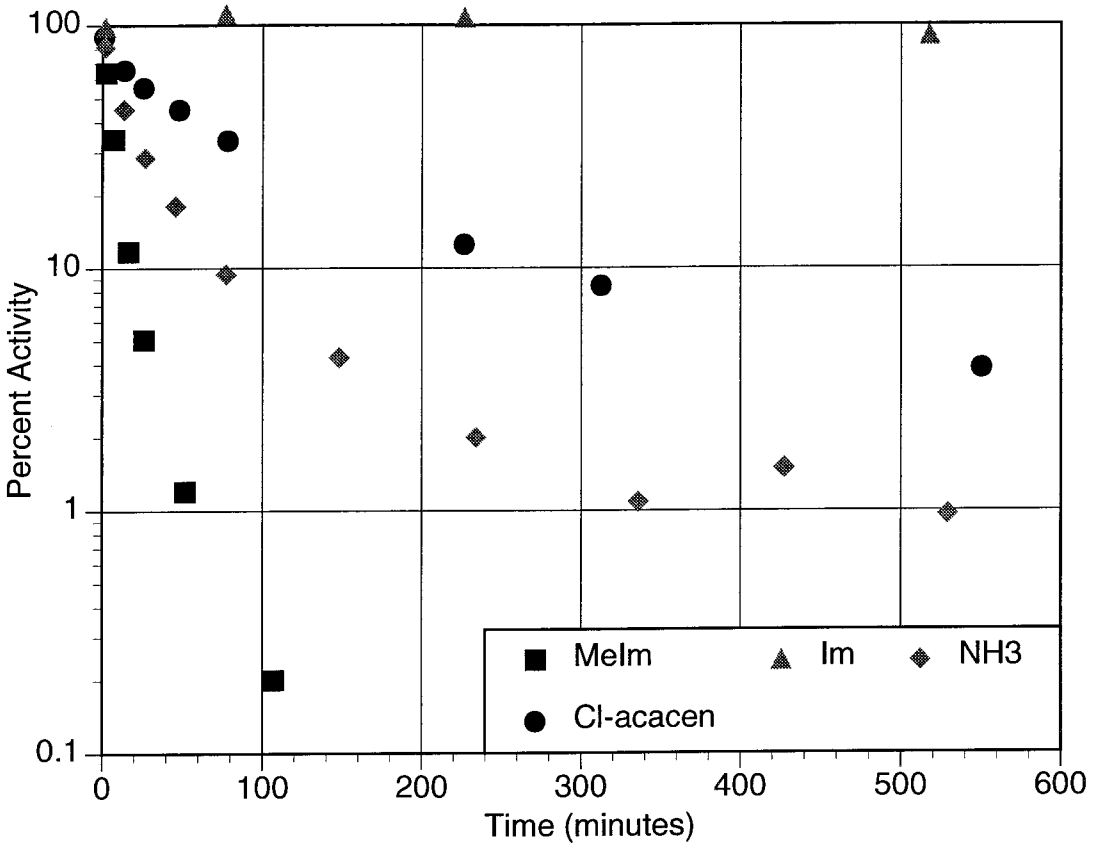

inhibition with 2-MeIm as ligand is very rapid, with almost complete inhibition of thrombin observed after 100 minutes of incubation time. The other factor investigated here is the effect of substitution about the periphery of the ligand. Substitution of the vinylic hydrogen with chlorine increases the size of the overall complex and also decreases the overall electron density due to the electron withdrawing nature of the chlorine atom. This change results in a slight decrease in inhibition for [Co(III)(Cl-acacen)$(NH_3)_2$]Cl. The loss in inhibition may be a result of electronic or steric effects since the chlorine is significantly bulkier than the hydrogen it replaced.

More compelling is the result obtained for the incubation with [Co(III)(trifluroacacen)$(NH_3)_2$]Cl. The difference between trifluro-acacen and acacen is the replacement of two methyl groups with trifluromethyl groups (Figure 5.10). Incubation of 500 μM [Co(III)(trifluroacacen)$(NH_3)_2$]Cl with thrombin and thermolysin resulted in no loss of enzymatic activity. Since the size of the trifluoromethyl group is similar in size to the methyl group, the loss of inhibition is most likely due to the electronic effect of substitution rather than steric effects. Model ligand exchange studies were performed, and incubation of [Co(III)(trifluoroacacen)$(NH_3)_2$]Cl with imidazole results in no change of UV-vis spectra and no formation of [Co(III)(trifluoroacacen)$(Im)_2]^+$. This suggests that the lack of inhibition is due to the slow rate of ligand substitution in the trifluroacacen species.

There should be a decrease in the rate of ligand exchange as the metal center becomes more electropositive because the transition state involving the loss of ligand becomes increasingly unfavorable as the cobalt becomes electron poor. However, this factor alone may not account for a complete loss of ligand exchange. One experimental observation in the ligand substitution process is the presence of rapid component in the

Figure 5.10. Structure of [Co(III)trifluoroacacen(NH_3)$_2$]$^+$. A change of two methyl groups in [Co(III)(acacen)(NH_3)$_2$]$^+$, a), results in [Co(III)trifluoroacacen(NH_3)$_2$]$^+$, b). This small change results in a major difference in anti-enzymatic activity.

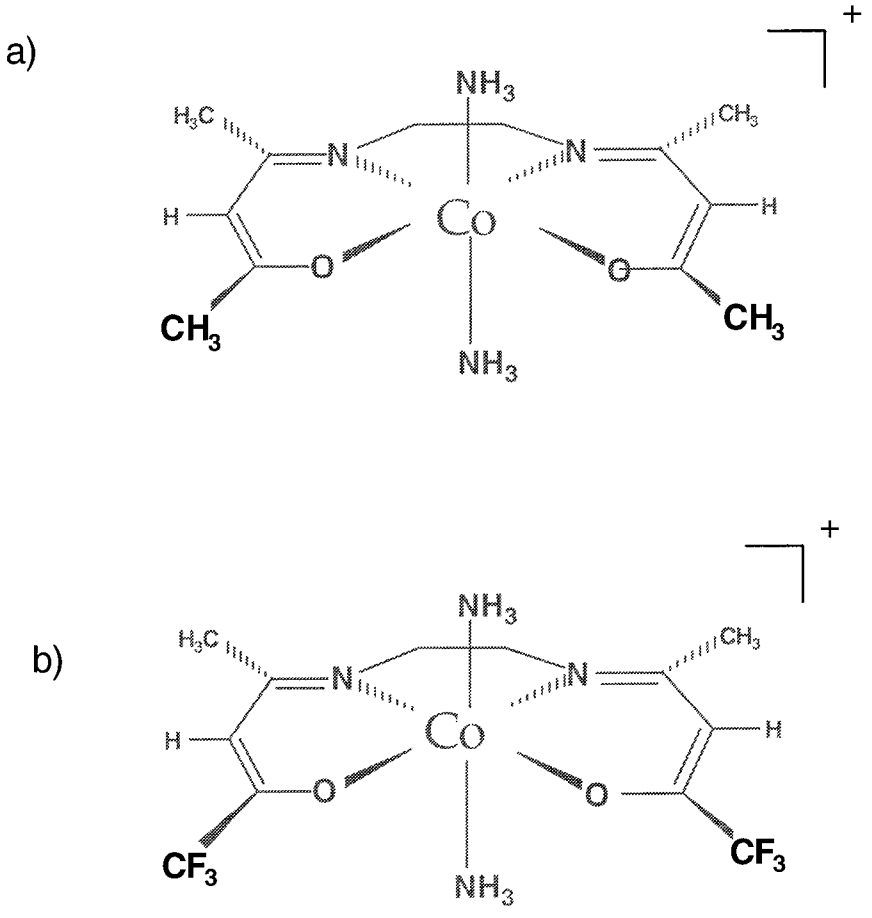

kinetics as [Co(III)(acacen)$(NH_3)_2$]Cl is mixed with excess imidazole (as mentioned in the thermolysin section). Since the substitution of amines or ammonia with other ligands is usually a slow process with Co(III) compounds, a mechanism other than the simple dissociation of axial amines may be occurring. One possibility is the dissociation of the equatorial oxygen from the ligand, followed by substitution at the equatorial site. The slower step in the exchange process may be the subsequent dissociation of the axial ligand, with rearrangement to form an axially substituted species. Further experiments will need to be performed in order to understand the ligand substitution mechanism in greater detail.

Thrombin "Targeting" with Peptide Coupled Co(III) Acacen Derivatives.

Although the inhibition thrombin is much more effective with [Co(III)(acacen)$(NH_3)_2$]$^+$ compared with thermolysin, the inhibition is far from the range of therapeutic utility. Anti-thrombolytic drugs would require nanomolar affinites or less for thrombin. Furthermore, these cobalt derivatives have little selectivity in binding to thrombin compared with the numerous proteins found in the bloodstream; the cobalt compounds should bind to any accessible histidine. Thus, the next steps in the development of cobalt Schiff base drugs would be to improve the affinity and selectivity for target enzymes. It should be pointed out that the immediate goal is not to produce therapeutics, but to delineate what factors may increase the affinity towards target enzymes.

One means of gaining affinity for thrombin would be to use known inhibitiors to direct the cobalt complex to the active site. The most potent and most selective inhibitors use peptides containing the sequence D-Phe-Pro-Arg.[20] Thus, a logical means of targeting the thrombin active site would be to link a peptide containing this D-Phe-Pro-Arg sequence to the cobalt complex. The peptide chosen was NH_2-GGG-d-FPR-CO-NH_2,[27] which

contains a glycine linker followed by the active site directed sequence. The glycine linker was added to give flexiblity to the peptide. The simplest means of linking the peptide to the cobalt complex would be the coupling of the terminal amine using standard peptide chemistry; since coupling to a carboxylic acid would be required, the C-terminal amide form of the peptide was used. Since a cobalt(III)acacen derivative containing a carboxylic acid ("acidacacen") was not known, a novel synthetic scheme was developed and applied by Kevin Hoke (Figure 5.11). The corresponding cobalt derivative was synthesized and the peptide was coupled as described in the experimental section.

Inhibition of Thrombin with Peptides, Co(III) Complexes, and Peptide Coupled Co(III) Complexes. In order to evaluate the effect of peptide coupling on the inhibitory activity toward thrombin, it is necessary to assess the activity of each component (i.e., the peptide and cobalt complex) before coupling. The peptide, NH_2-GGG-d-FPR-CO-NH_2, is a reversible inhibitor, and the K_I can be determined by plotting the initial reaction velocity in absence of inhibitor (V_0) divided by the velocity in the presence of inhibitor (V) versus the inhibitor concentration. This will yield a straight line, with $1/K_I$ = (slope)(1 + $\{(1/K_m)[S]\}$), where K_m = Michaelis constant of the substrate = 2.45 μmol/L[28] and [S] represents the concentration of the substrate. This plot is shown in Figure 5.12.

Surprisingly, [Co(III)acacaciden$(NH_3)_2$] does not inhibit thrombin, although it does inhibit thermolysin. This lack of inhibition may be due to repulsion from the active site of thrombin at the arginine binding pocket, where there is a negatively charged aspartate. Other carboxylic acid containing Co(III) complexes also did not inhibit thrombin, while other Co(III) complexes containing phenyl groups did inhibit thrombin.[29] This data suggests that the lack of inhibition is a result of the negatively charged carboxylic acid

Figure 5.11. Synthetic Scheme for the Synthesis of "Acacaciden."

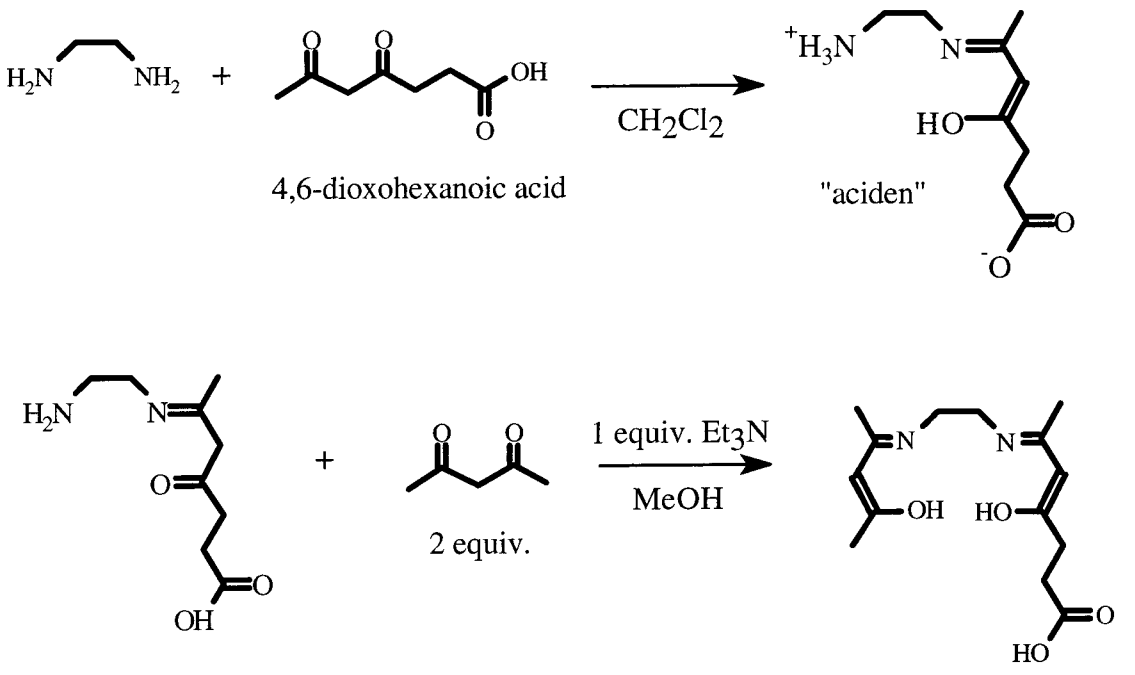

Figure 5.12. Determination of the K_I of NH_2-GGG-d-FPR-CO-NH_2. The K_I was found to be 290 μM ± 23 μM.

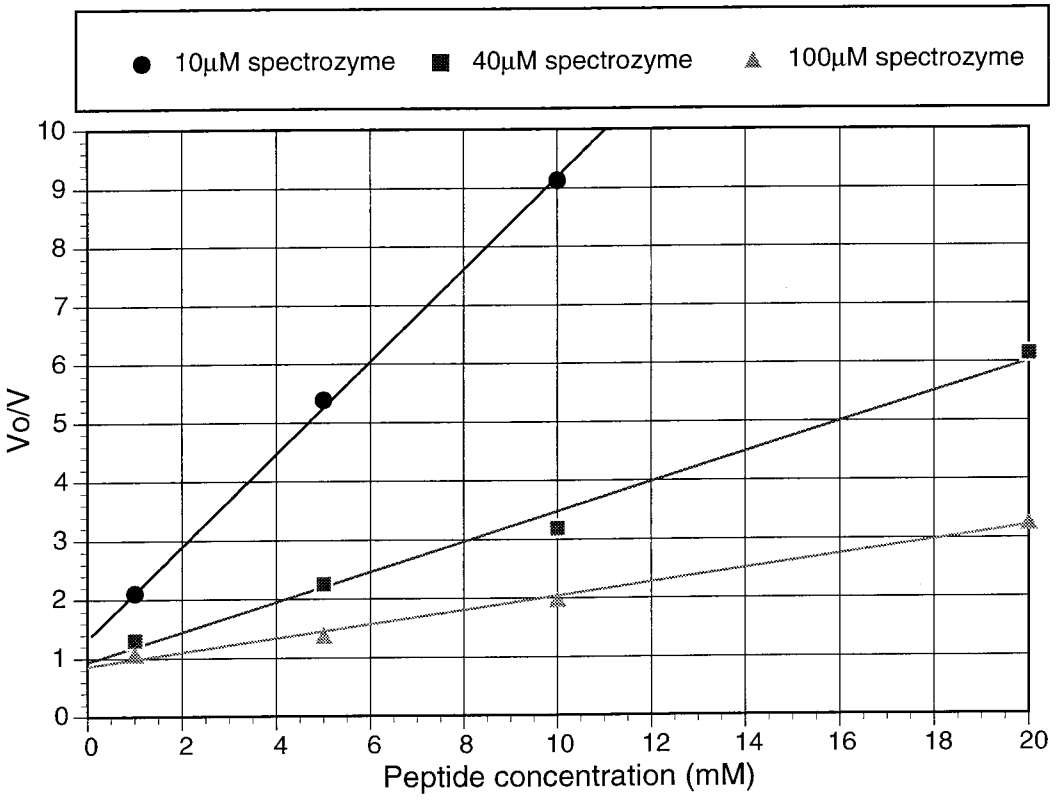

group rather than the increased size of the cobalt complex with respect to the unmodified acacen derivative. For the purposes of comparison, the peptide-coupled Co(III)acacen derivative also can be compared with Co(III)acacen for potency of inhibition.

The inhibition of thrombin with peptide NH_2-GGG-d-FPR-CO-NH_2, [Co(III)(acacaciden)$(NH_3)_2$], [Co(III)(acacen)$(NH_3)_2$]Cl, and the peptide coupled (pepcp) [Co(III)(pepcp-acacaciden)$(NH_3)_2$] is shown in Figure 5.13. In these plots, the sum of the reversible and irreversible components of inhibition is assayed. It can be seen that the peptide coupled cobalt complex is at least an order of magnitude more effective at inhibiting thrombin than the cobalt acacen compound. The other striking feature of the inhibition profile is the extremely rapid inhibition timescale for the peptide coupled complex. Although it takes nearly 1200 minutes for the cobalt acacen complex to inhibit 60% of thrombin activity, the peptide-coupled cobalt compound reaches that level almost instantaneously.

In order to further characterize the inhibition of the peptide-coupled cobalt complex, the irreversible inhibition profile was evaluated (Figure 5.14)[30]. In contrast to the irreversible inhibition of thrombin with [Co(III)(acacen)$(NH_3)_2$]Cl (Figure 5.8), the inhibition with [Co(III)(pepcp-acacaciden)$(NH_3)_2$] initally begins at a low level. This suggests that there is rapid association of the peptide coupled compound with thrombin followed by further irreversible loss of activity upon incubation. It is not clear what the role of the peptide is in the inhibition process. Molecular modeling would suggest that the peptide would bind to the active site, leaving the cobalt complex many ångstrøms away from the target histidine. However, it should be noted that the initial peptide is only a weak inhibitor with K_I = 290 μM, which means it may rapidly associate and dissociate from the thrombin active site. This association and dissociation process may give the cobalt chelate

Figure 5.13. The Inhibition of Thrombin with Peptide NH_2-GGG-d-FPR-CO-NH_2, [Co(III)(acacaciden)$(NH_3)_2$], [Co(III)(acacen)$(NH_3)_2$]Cl, and the Peptide Coupled (pepcp) [Co(III)(pepcp-acacaciden)$(NH_3)_2$].

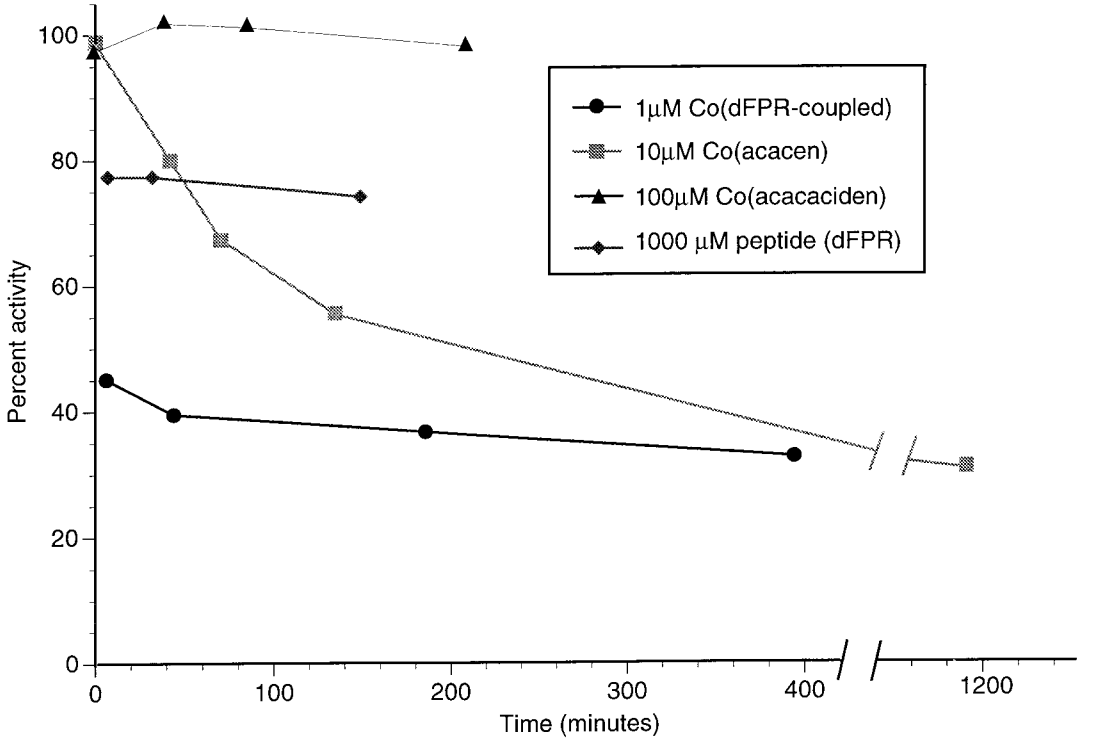

Figure 5.14. Irreversible Inhibition of Thrombin with 1 μM [Co(III)(pepcp-acacaciden)$(NH_3)_2$].

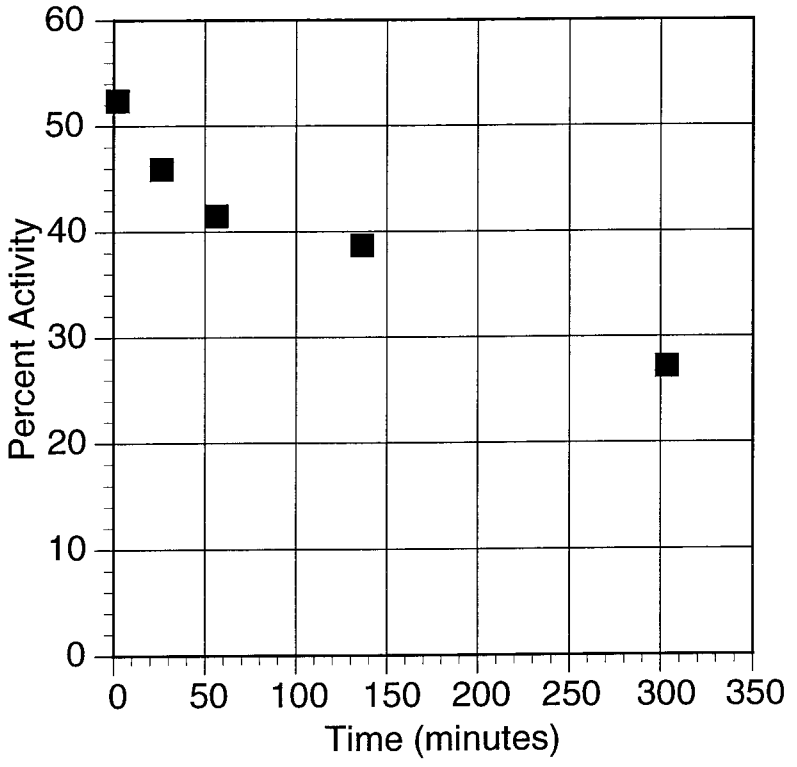

complex resonance time near the active site, and incubation results in irreversible binding to the active site histidine. One other possibility is the peptide serves as a hydrophobic driving force, directing the cobalt complex toward the hydrophobic interior of the enzyme. This possibility will be tested using cobalt complexes coupled to peptides that are not directed toward the active site of thrombin.

Overall, the inhibition of thrombin with peptide-coupled cobalt chelate complexes is very promising. These peptide-coupled compounds show potent inhibition of thrombin at concentrations an order of magnitude below that of the unmodified cobalt acacen complexes. Furthermore, the rate of inhibition is improved tremendously. The peptide-coupled cobalt complexes irreversibly inhibit thrombin immediately upon mixing while the uncoupled cobalt complexes reach a similar level of inhibition only upon incubation for hundreds of minutes. Further understanding of the nature of this inhibition may yield new generations of cobalt complexes with more selectivity and affinity towards thrombin, and similar techniques should be applicable for the targeting of other enzymes with active site histidines such as the AIDS related RNase H.[31]

References

1. (a) Devlin, H., Geary, P., Pavanlangston, D., Dori, Z., and Dunkel, E. C. (1993) *Inv. Ophth-V, 34*, 1348. (b) Asbell, P. A., Epstein, S. P., Wallace, J., Epstein, D., Stewart, C. C., and Burger, R. M. (1995) *J. Invest. Ophthalmol.*, submitted.

2. DiIanni, C. L., Stevens, J. T., Bolgar, M., O'Boyle, D. R., Weinheimer, S. P., and Colonno, R. J. (1994), *J. Biol. Chem.* **269**, 12672-12676.

3. Darke, P. L., Chen, E., Hall, D. L., Sardana, M. K., Veloski, C. A., LaFemina, R. L., Shafer, J. A., and Kuo, L. C. (1994) *J. Biol. Chem.* **269**, 18708-18711.

4. Haiek, A., Cwikel, D., Dori, Z., and Gray, H. B., unpublished results.

5. (a) Rawlings, N. D. and Barrett, A. J. (1994) *Methods in Enzymology, 244,* 19-61. (b) Rawlings, N. D. and Barrett, A. J. (1994) *Methods in Enzymology, 244*, 461-487. (c) McKerrow, J. H., Sun, E., Rosenthal, P. J., and Bouvier, J. (1993) *Annu. Rev. Microbiol., 47,* 821-853. (d) Chen, W.-T. (1992) *Curr. Opin. Cell Biol., 4,* 802-809. (e) Davies, J. F., Hostomska, Z., Hostomsky, Z., Jordan, S. R., and Matthews, D. A. (1991) *Science, 252*, 88-95.

6. Titiani, K., Hermodson, M. A., Ericddon, L. H., Walsh, K. A., and Neurath, H. (1972) *Nature (London), New Biol. 238*, 35-37.

7. (a) Holden, H. M., Matthews, B. W. (1988) *J. Biol. Chem. 263*, 3256-3265. (b) Monzingo, A. F. and Matthews, B. W. (1984) *Biochemistry 23*, 5724-5729. (c) Tronrud, D. E., Monzingo, A. F., and Matthews, B. W. (1986) *Eur. J. Biochem. 157*, 261-268. (d) Tronrud, D. E., Holden, H. M., and Matthews, B. W. (1987) *Science 235*, 571-574.

8. (a) Cushman, D. W. and Ondetti, M. A. (1981) *Top. Mol. Pharmacol.*, 127-168. (b)

Maycock, A. L., DeSousa, D. M., Payne, L. G., ten Broeke, J., Wu, M. T., and Patchett, A. A. (1981) *Biochem. Biophys. Res. Commun. 102*, 964-969. (c) Hangauer, D. G., Monzingo, A. F., and Matthews, B. W. (1984) *Biochemistry 23*, 5730-5741. (d) Hersh, L. B. and Morihara, K. (1986) *J. Biol. Chem. 261*, 6433-6437. (e) Matthews, B. W. (1988) *Acc. Chem. Res., 21,* 333-340.

9. Burstein, Y., Walsh, K. A., and Neurath, H. (1974) *Biochemistry* **13**, 205-210.

10. Ohta, Y., Ogura, Y., and Wada, A. (1966) *J. Biol. Chem., 241*, 5919-5925.

11. Titani, K., Hermodson, M. A., Ericsson, L. H., Walsh, K. A., and Neurath, H. (1972) *Biochemistry, 13*, 2427-2435.

12. For example, see (a) Morgan, G. and Smith, J. (1925) *J. Chem. Soc.,* 2030. (b) Costa, G., Mestroni, G., Tauzher, G., and Stefani, L. (1966) *J. Organomet. Chem., 6,* 181.

13. Feder, J. and Schuck, J. M. (1970) *Biochemistry 9*, 2784-2791.

14. Kitagishi, K. and Hiromi, K. (1984) *J. Biochem. 95*, 529-534.

15. Weaver, L. H., Kester, W. R., and Matthews, B. W. (1977) *J. Mol. Biol. 114*, 119-132.

16. Böttcher, A., Takeuchi, T., Hardcastle, K. I., Dori, Z., Gray, H. B., and Meade, T. J., in preparation for *Inorg. Chem.*

17. (a) Langford, C. H. and Gray, H. B. (1966) *Ligand Substitution Processes,* pp 55-101, W. A. Benjamin, Inc., Reading, Mass. (b) Basolo, F. and Johnson, R. C. (1986) *Coordination Chemistry*, pp 97-119, Science Reviews.

18. Holmes, M. A. and Matthews, B. W. (1982) *J. Mol. Biol., 160*, 623.

19. (a) Mann, K. G. (1987) *Trends Biochem. Sci. 12,* 229-233. (b) Shuman, M. A. (1986) *Ann. N. Y. Acad. Sci. 485,* 228-239. (c) Bode, W., Huber, R., Rydel, T. J., and Tulinsky, A. (1992) *Thrombin: Structure and Function,* Berliner, L. J., ed., pp 3-51,

Plenum, New York.

20. Agnelli, G., Pascucci, C., Cosmi, B., and Nenci, G. G. (1991) *Thromb. Haemostasis 66*, 592-597.

21.(a) Bajusz, S., Barabas, E., Tolnay, P., Szell, E., and Bagdy, D. (1978) *Int. J. Pept. Protein Res. 12,* 217-221. (b) Kettner, C., and Shaw, E. (1979) *Thromb. Res. 14,* 969-973. (c) Claeson, G., Elgendy, S., Cheng, L., Chino, N., Goodwin, C. A., Scully, M. F., and Deadman, J. (1993) *The Design of Synthetic Inhibitors of Thrombin,* Claeson, G., Scully, M. F., Kakkar, V. V., and Deadman, J., eds., Plenum Press, New York.

22. Rydel, T. J., Tulinsky, A., Bode, W., and Huber, R. (1991) *J. Mol. Biol. 221*, 583-601.

23. Stone, S. R. and Hofsteenge, J. (1986) *Biochemistry 25*, 4622-4628.

24. Skrzypczak-Jankun, E., Carperos, V. E., Ravichandran, K. G., Tulinsky, A., Westbrook, M., and Maraganore, J. M. (1991) *J. Mol. Biol. 221*, 1379-1393.

25. Sonder, S. A. and Fenton, J. W. II. (1986) *Clin. Chem. 32*, 934-937.

26. Powers, J. C. and Kam, C.-M. (1992) *Thrombin: Structure and Function,* Berliner, L. J., ed., pp 117-158, Plenum, New York.

27. G = glycine, F = phenylalanine, P = proline, R = arginine, and d refers to the *dextro* isomer of phenylalanine.

28. Sonder, S. A. and Fenton, J. W. (1986) *Clin. Chem., 32*, 934-937.

29. Takeuchi, T. and Böttcher, A., unpublished results.

30. Preliminary data taken with Arnd Böttcher.

31. Davies, J. F., Hostomska, Z., Hostomsky, Z., Jordan, S. R., and Matthews, D. A. (1991) *Science, 252*, 88-95.